POLITECNICO DI MILANO

DEPARTMENT OF ELECTRONICS, INFORMATIONS AND BIOENGINEERING

DOCTORAL PROGRAM IN BIOENGINEERING

Multimodal neuroimaging techniques:

towards the integration of structural and functional connectivity

XXX Cycle

2014-2017

Doctoral dissertation by:

Elisa Scaccianoce

Supervisor:
Prof. Giuseppe Baselli

Co-Supervisor:
Ing. Maria Marcella Laganà
Ing.Flavio Dell'Acqua

Tutor:
Prof. Maria Gabriella Signorini

Chair of the doctoral program:
Prof. Andrea Aliverti

Contents

Summary

Background and aim

The present doctoral thesis is inserted in the neuroimaging research field, as it aims to study the brain connectivity through advanced magnetic resonance imaging (MRI) techniques, which allow to non-invasively investigate brain coordination both from a functional and structural perspective. Specifically, diffusion weighted imaging (DWI) is used to explore white matter (WM) fiber connections by means of both deterministic and probabilistic tractography; functional magnetic resonance imaging, both task-driven and in resting condition (i.e., fMRI and rsfMRI), provides information about cortical activation patterns in gray matter (GM) elicited by specific brain functioning.

Currently, growing interest is gaining the possibility to study brain connectivity as a whole, namely combining functional and structural information in a unique framework to shed lights onto the complexity of the mechanisms that governs the brain functions. However, open challenges related to methodological and technical aspects still remain open to intense research, such as the structural interface between WM and GM at their boundary, the different models describing the richer and richer DWI datasets acquired to reconstruct virtual fibers (alias, streamlines) and the treatment of artifacts, the scale and approach to functional GM parcellation, and many others.

In this work we first dealt with WM-GM combination by integrating structural and functional information in two different ways: i) using deterministic tractography and task-driven functional magnetic resonance imaging (fMRI) (method also tested in a clinical neurorehabilitation context); ii) using probabilistic tractography and resting-state functional magnetic resonance imaging (rsfMRI). Then we addressed the issue of detecting and possibly correcting artifacts in high angular resolution diffusion images (HARDI) by proposing two pipelines: iii) at single subject level, to identify and remove artifacts in HARDI data-set relevant to punctual corruption of given slices and given diffusion directions; iv) in group studies,

performing a quality control over the population dataset in order to detect and exclude subjects with poor reconstructions of the selected tracts.

Methods

Integration of tractographic approaches and functional magnetic resonance imaging modalities

In the first study (i) we integrated deterministic tractography and task-driven fMRI on twenty-five healthy subjects (HSs).

After diffusion tensor (DT) estimate, deterministic tractography was performed with the brute-force approach (Conturo et al. 1999), interpolated streamline algorithm, FA < 0.20 and angle between two subsequent directions > 35° as stopping criteria (Preti et al. 2014). Left arcuate fascicle (AF) and left cingulum bundle (CB) were reconstructed with TrackVis v.0.5.1 (www.trackvis.org) as the main bundles involved in the considered verbal fluency task.

Functional scans were collected asking subjects to perform a paced-overt verbal fluency task. The active cortical areas elicited by the categorical-fluency (versus control condition) were identified at single level by statistical analysis (first level, general linear model) (GLM; Friston et al. 1994), introducing movement parameters as covariates. A contrast of parameter estimates (COPE) image was obtained for each subject and then non-linearly registered to the MNI space to be merged in a group analysis (second level, one sample t-test) to estimate the main effect of the task.

Before integrating these structural and functional information (namely the bundles and the active cortical areas) both at single and group level, two operations were performed as follows:

- both the AF and the CB of each subject were extended into gray matter for 10 mm to reach the most proximal cortical regions. Both extremities of every streamline were extended by using an in-house

Matlab script (Matlab R2010a, MathWorks, http://www.mathworks.it/products/matlab) following the direction of the vector connecting the coordinates of the two last voxels. Finally, each extended tract was masked with a GM atlas (Hui et al., 2005) to select only those parts reaching the cortex.

- from the center of gravity (COG) of each cluster obtained by group-fMRI analysis, 11-mm-radius spheres were drawn to restrict the analysis to the specific cortical areas identified by the cluster peaks and also to take into account the inter-subject variability (Drobyshevsky et al. 2006).

At single level, the AF and CB projections of each subject were intersected with group fMRI activation spheres; the topographic location (i.e., which Brodmann areas were involved) and the extension, in terms of mm^3, were evaluated. The median value and confidence interval at 95% (CI 95%) of the connection volumes between the projections of AF and CB at single level and spheres from fMRI activation were finally computed.

At group level, the group projections of AF and CB were obtained by averaging the single subject projections among all the HSs. These averaged volumes were then thresholded at 0.6 (Mori et al., 2009; Aslan et al. 2009), to limit the random error due to noise and partial volume effects (Hua et al. 2009). The group projections were intersected with the group fMRI activations; then, the volumes of connection were mapped and measured, and the relative weight of each BA was also calculated and expressed both as absolute values and relative percentages (i.e., how much the specific Brodmann area overlapped with the connection). The Dice coefficient (Dice 1945) was computed to test the physiological inter-individual variability of GM-projected bundles, considering the tract projections of every single subject compared to the group projections for both AF and CB. Finally, the Dice coefficient was also calculated for the volumes generated by the overlap between the DTI projections and the group fMRI activations to account for their similarity.

Method (i) pipeline is summarized in Figure A.
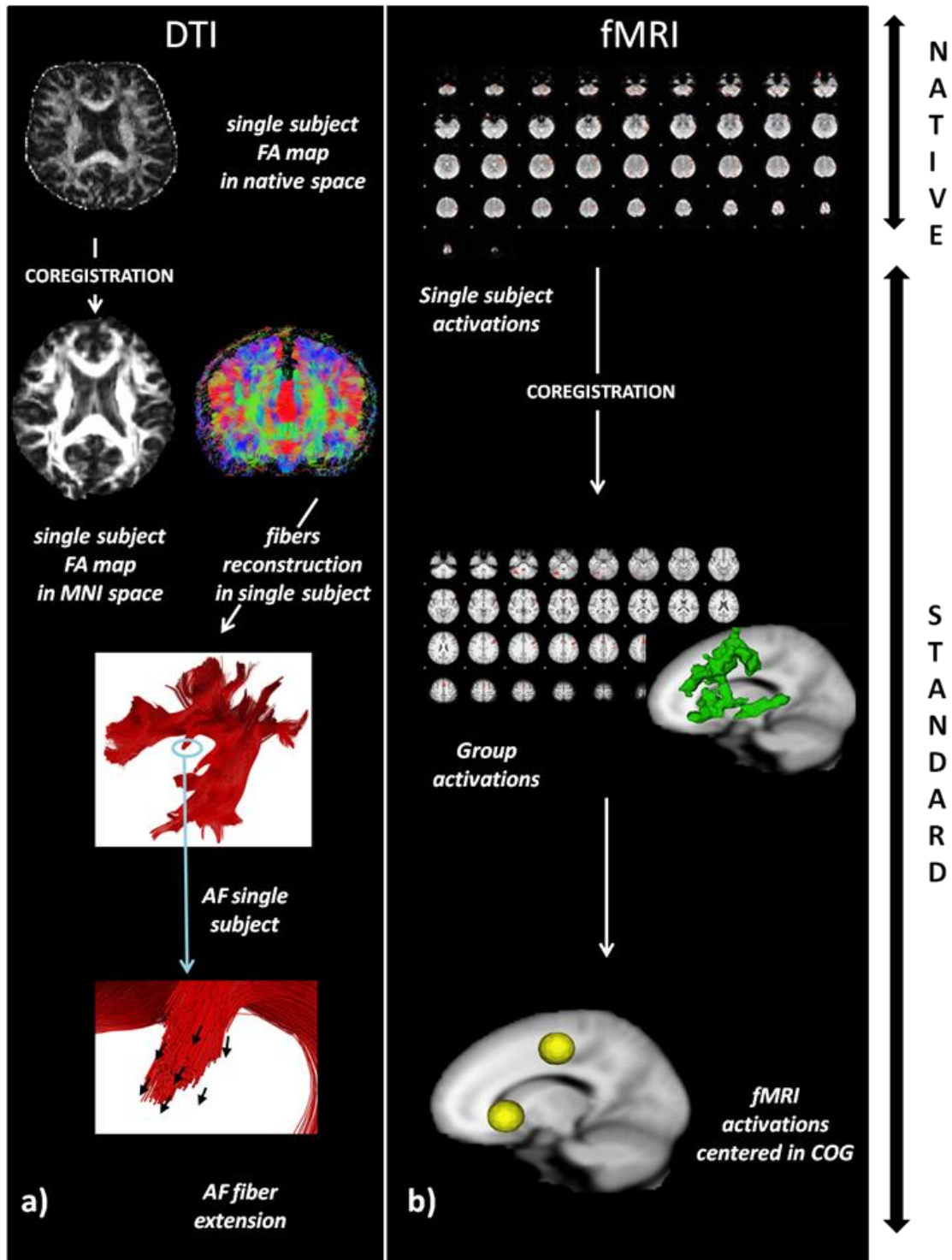
Figure A *Pipeline of DW images (panel a) and fMRI images (panel b) to perform the structural-functional data integration– Scaccianoce et al., 2016*

As a case study, the method was tested in a 65-year-old man who sustained an ischemic stroke (3 months prior) in the left middle cerebral artery territory. DTI-fMRI integration was performed at the single subject level, focusing on the arcuate fasciculus (AF), and was prospectively evaluated at T0 (admission), T1 (discharge after 1 month rehabilitation), and T2 (follow-up, after further three months).

In the second study (ii) we integrated rsfMRI and probabilistic tractography and correlated functional connectivity (FC) indexes and structural connectivity (SC) ones of nineteen HS datasets.

For the functional data, single subject independent component analysis (ICA) was performed by MELODIC (Multivariate Exploratory Linear Optimized Decomposition into Independent Components, Filippini et al., 2009; Beckmann et al., 2009). RSNs were identified by spatial group ICA (MELODIC, Beckmann et al., 2005) with dimensionality set to 30 (Soddu et al., 2016, Elman et al., 2014, Meyer et al., 2013) and the DMN, the LLN and the RLN were visually selected according to the RSN templates provided by Smith and colleagues (2009). The three chosen RSNs were divided into atomically separated clusters of voxels (Costantini et al., 2016) that were used as regions of interest (ROIs) both for functional and structural connectivity analyses. Using the dual regression approach (Beckmann et al., 2009; Filippini et al., 2009) subject-specific spatial maps and time series associated to each ROI belonging to DMN, LLN and RLN were extracted. FC was assessed by two indexes between time series of each pair of ROIs belonging to the DMN, RLN and LLN: the full linear correlation (FCfull), as Pearson's correlation coefficient, and the partial linear correlation (FCpar), computed by correlating the time series associated to A and B and regressing out the time series associated to all the other ROIs, were estimated at both single and group level.

Regarding diffusion data, probabilistic tractography (Probabilistic Tracking with crossing fibres [PROBTRACX] –Behrens et al, 2007) was performed between the pairs of extracted ROIs in the DMN, LLN and RLN considered as seed and target regions. To correct the asymmetry of the method (Cao et al., 2013), namely the different result obtained if setting either ROI A or B as seed and target region, the following approach was used: probabilistic tracts were created setting A as seed and B as target and

viceversa to produce a unique product tract between each pair of ROIs. The number of voxels above threshold of the product tract was defined as the SC index for each pair of ROIs (Khalsa et al.,2014) at both single and group level.

For each pair of ROIs in all the considered RSNs, the relationships between FCfull and SC and between FCpar and SC were evaluated using Spearman's correlations, due to the non-Gaussianity of the considered data samples. Method (ii) pipeline is summarized in Figure B.
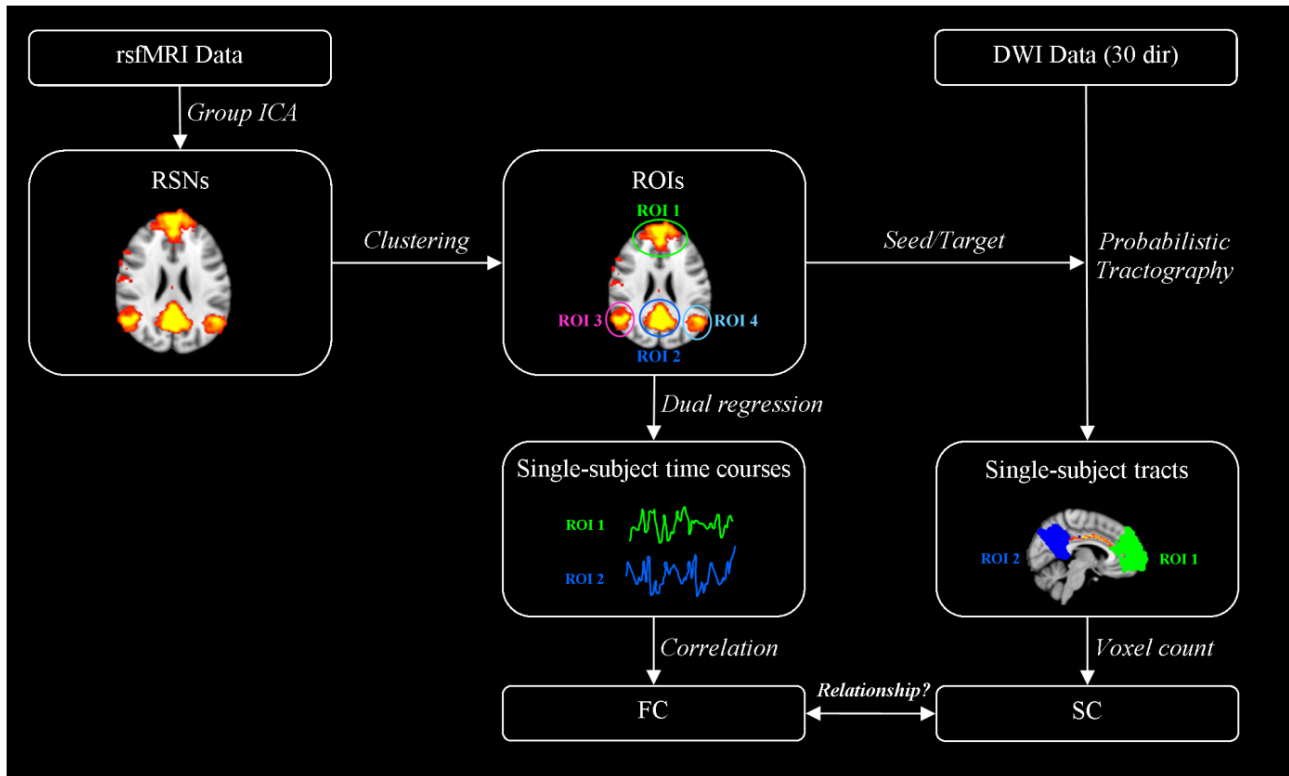
Figure B *Method pipeline. Independent component analysis (ICA) performed on resting state functional MRI (rsfMRI) data to extrapolate resting state networks (RSNs). RSNs were split into their constitutive regions of interest (ROIs) and used to extract time series to evaluate functional connectivity (FC) indexes, defined as the full (FCfull) and partial (FCpar) correlation coefficients between them. The same ROIs were used as seed and target regions to perform probabilistic tractography. The number of voxels of the processed probabilistic tract volume was defined as structural connectivity (SC) index. The purpose of this method was to explore the relationship existing between FC and SC within the RSNs*

Quality control in High Angular Resolution Diffusion Imaging (HARDI)

In the third study (iii) HARDI data from fifteen HSs were acquired in a single shell using a 3T GE HDx system (General Electric, Milwaukee, WI, USA) with a b-value equal to 3000 s/mm2 and 60 diffusion-weighted directions and 7 non-diffusion weighted volumes. By a custom written Matlab code, for each subject, HARDI data were fitted by spherical harmonics of order 8 (SH8) to model complex fiber configuration such as the crossing fibers (Decoteaux et al., 2009). Then, a binary outlier mask was created by identifying as outliers all slices corresponding to a specific diffusion direction with a mean residual value above an automatic threshold obtained for each slice across all diffusion directions. Corrupted slices were regenerated using new SH coefficients obtained by SH decomposition performed this time without outlier directions. SH at order 6 was used when regenerating slices of corrupted directions, while SH at order 8 was applied to the rest of the data. Finally, spherical deconvolution (SD) was run to estimate fiber orientation distribution (FOD) peaks.

In the fourth study (iv) HARDI data were acquired from eleven HSs in a single shell using a 3T GE HDx system (General Electric, Milwaukee, WI, USA) with a b-value equal to 3000 s/mm2 and 60 diffusion-weighted directions and 7 non-diffusion weighted volumes. DT model was then applied to process the data using Explore DTI (Leemans et al, 2009). The dissections of right anterior and posterior segment of the arcuate fasciculus (i.e., aAF and pAF) and the right inferior fronto-occipital fasciculus (IFOF) were performed using Trackvis (trackvis.org). aAF and pAF were selected since a visual inspection identified signal loss in the superior occipital part of the brain of 2 subjects, while IFOF was selected as control tract. The visual identification of artifacts by two expert viewers was considered the gold standard to assess the performance of our method. SH decomposition of order 2, 4 and 6 (hereafter indicated as SH2, SH4, and SH6, respectively) was obtained by a custom written Matlab code (Matlab R2010a, MathWorks, http://www.mathworks.it/products/matlab). The residual, defined as difference between the fitted and the measured signals, was computed vs. the DT and the SH4, SH6, and SH8 models (Figure C). The maximum

residual value was selected for each voxel through all the DW directions, to generate maximum residual maps for each subject. Then, fractional anisotropy (FA), mean diffusivity (MD), DT and SH maximum residuals (all orders) were mapped along the chosen tracts. Finally, a threshold for the identification of outliers was calculated across subjects for each metric.
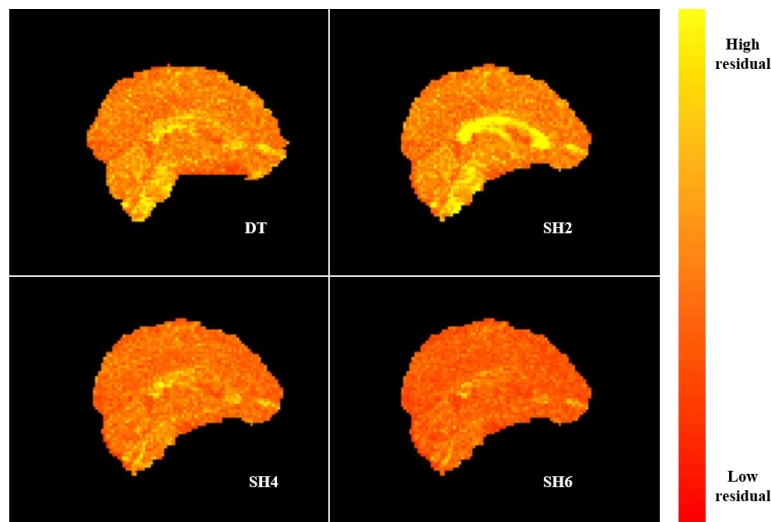
Figure C Maximum residual maps of a single subject with no corrupted images obtained as differences between the actual signal and (from top left image) diffusion tensor model (DT), spherical harmonics of order 2, 4 and 6 (SH2, SH4, SH6) model. Lighter color (i.e., yellow) suggests a higher residual value

Results

Integration of tractographic approaches and functional magnetic resonance imaging modalities

The main results of integrating deterministic tractography and task-driven fMRI of study (i) are summarized hereunder. Focusing on the 4 regions that are typically considered part of the language network, namely BA 6 (dorsal premotor cortex), BA 8 (prefrontal dorsolateral cortex), BA 24/32 (anterior cingulate cortex), BA 44/45 (Broca's area) (Lubrano et al., 2014; Valk 2011; Golistanerad et al., 2015; Friederici 2017), we found

that most of the connections related to CB falls into the BA 24/32, in both single and group analysis, while the connections related to the AF showed a different percentage distribution at single level, compared to the group one, even though the volume in mm^3 of the dorsal premotor cortex (BA 6) has similar extension both at single and group level.

The application of the above-mentioned approach to the stroke patient (Figure D) revealed an increased WM-GM connection in BA 6 at T1 compared to T0, which improvement persisted at T2. Furthermore, at both T1 and T2 a connection located in BA 44/45 that was not revealed at T0 was observed.

The principal results concerning the integration between probabilistic tractography and rsFMRI of study (ii) were related to the correlation of the FC and SC indexes computed between each pair of activation areas obtained by clustering the RSNs (Figure E). Specifically Focusing on FC_{full}-SC correlation, a non-significant value was found within the DMN (r=0.01, p=0.916). On the other hand, a positive significant FC_{full}-SC correlation was observed within the RLN (r=0.214, p=0.022) and the LLN (r=0.489, p<0.0001). The FC_{par}-SC correlation analysis led to similar values of FC_{full}-SC ones in the RLN (r=0.228, p=0.015) and in the LLN (r=0.466, p<0.0001). Within the DMN, even if still not-significant, the FC_{par}-SC correlation was found to be higher than the FC_{full}-SC one (r=-0.015, p=0.878).
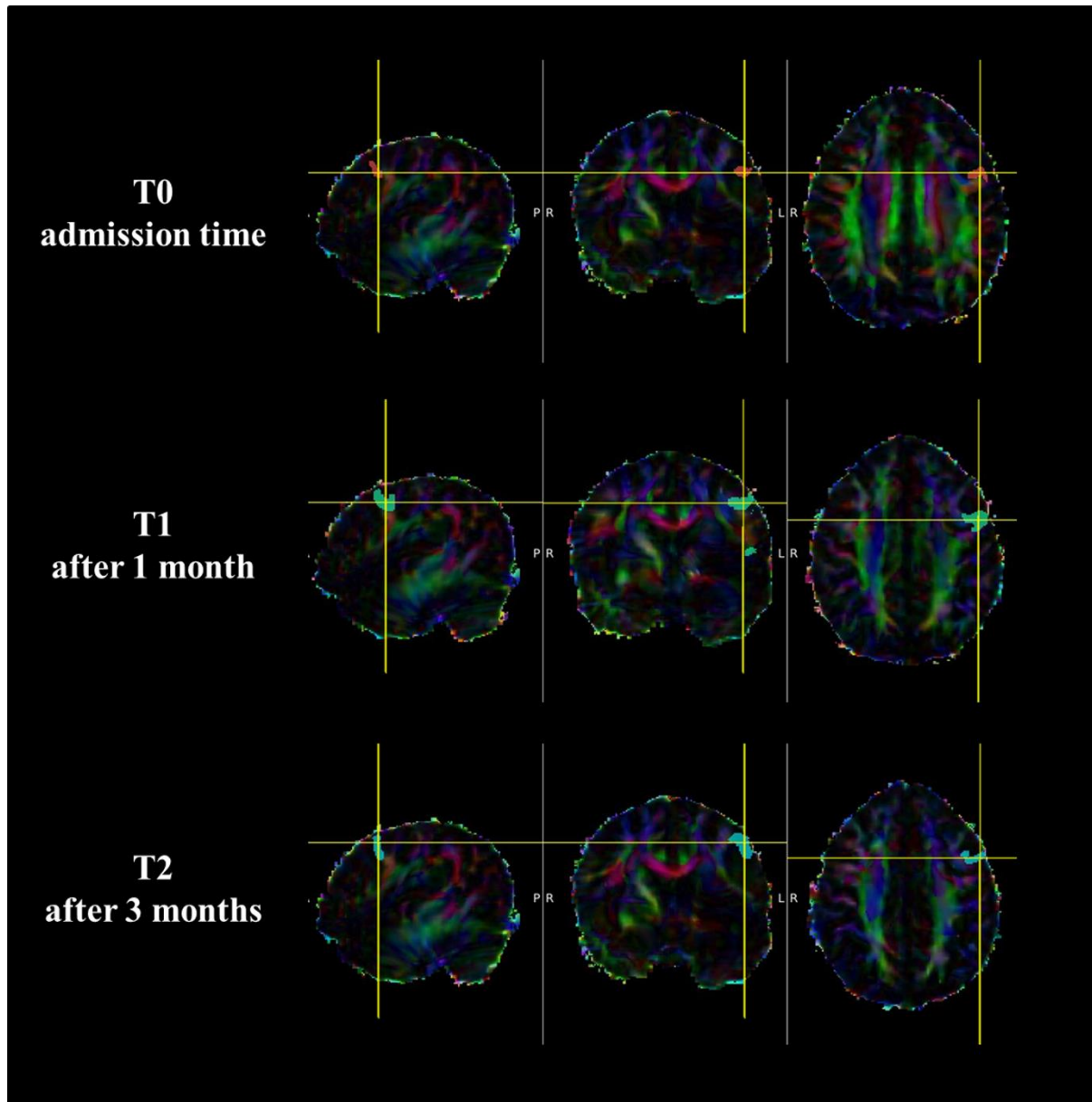
Figure D *Integration of diffusion tensor imaging (DTI) and functional magnetic resonance imaging (fMRI) at single level in the considered stroke patient. The volumes of connections were evaluated at T0, T1 and T2 – Scaccianoce et al., 2016*
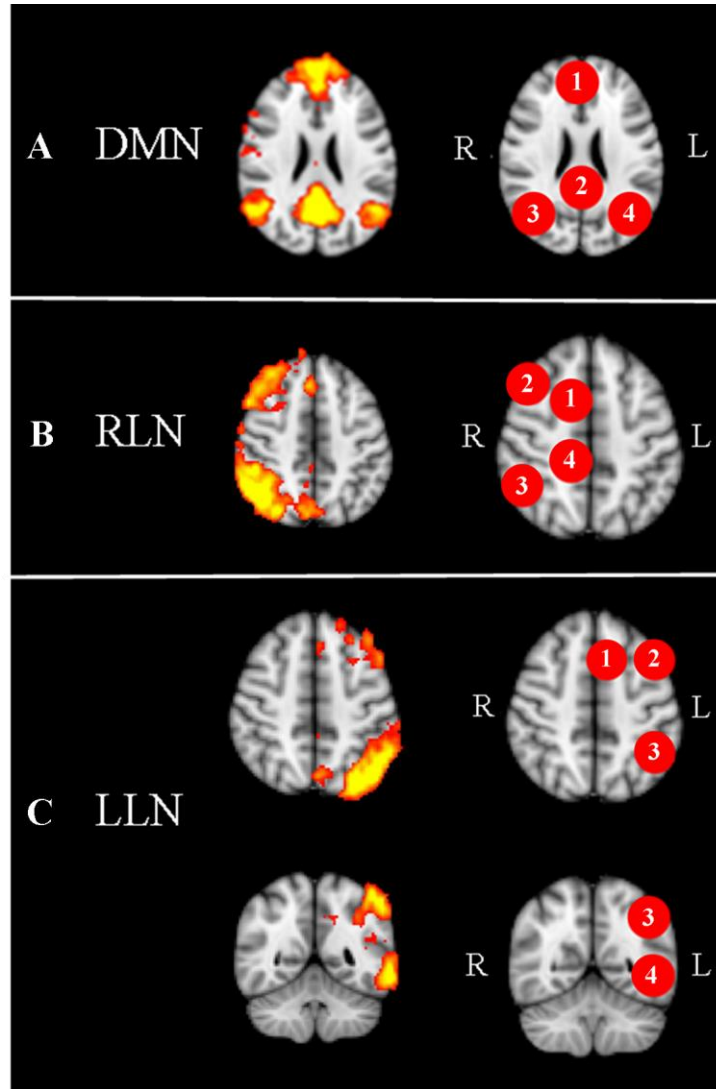
Figure E *Clustering of the default mode network (DMN, panel A), right lateral network (RLN, panel B) and left lateral network (LLN, panel C) according to the anatomical separation criterion.*

Quality control in High Angular Resolution Diffusion Imaging (HARDI)

Considering the results of study (iii), in Figure F, an example of artifacts is shown in sagittal and axial view along with their corrections in the same view for comparison purpose.

Regarding the results of study (iv), outliers were found in the aAF and the pAF of those subjects whose dataset had been classified as corrupted by the visual inspection. As expected, no artifacts were detected in the control tract (i.e., the IFOF). Importantly, outliers were well identified by means of the residual vs. the SH6 and the DT models.
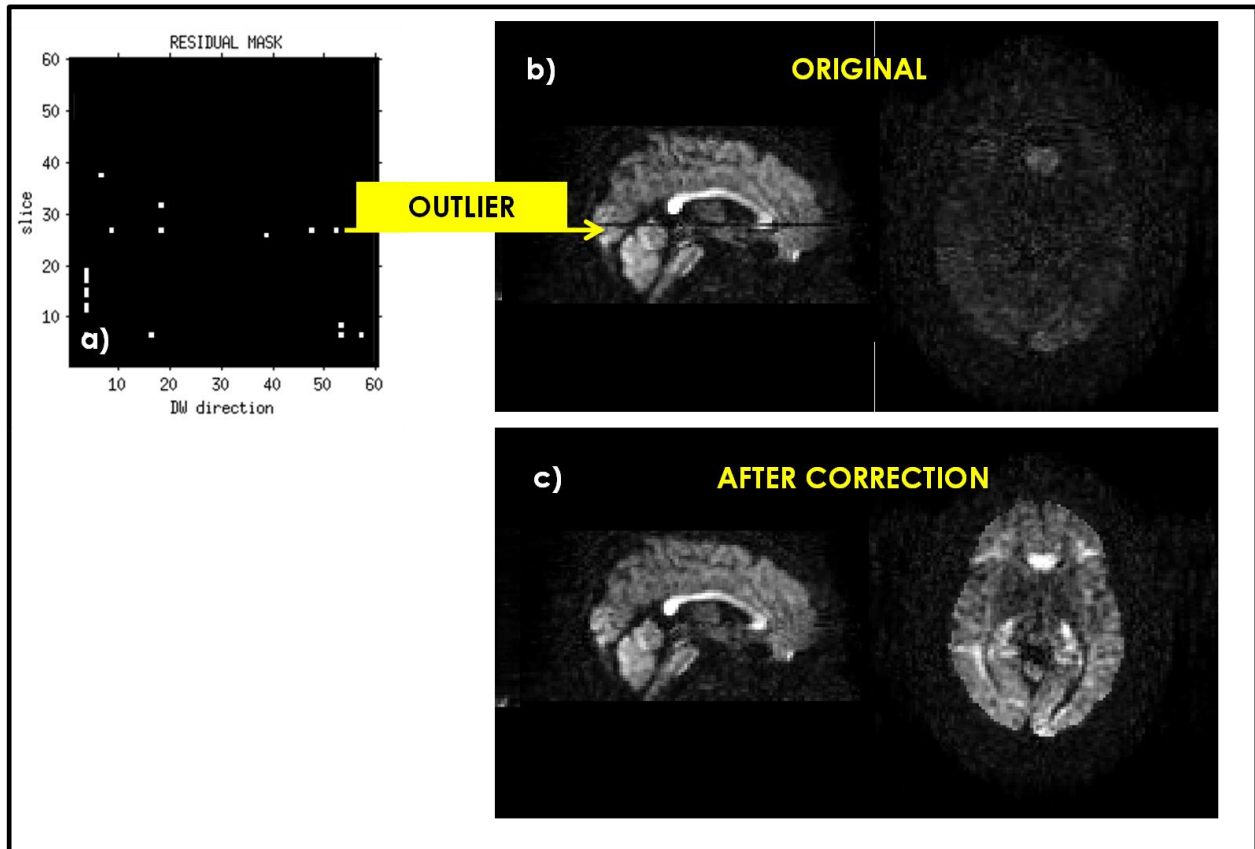
Figure F *Panel a) illustrates the outlier mask in which one of the outlier value is identified and its location displayed in sagittal and axial views before (panel b) and after (panel c) correction*

Discussion and Conclusion

In this thesis we investigated some aspects related to the study of brain connectivity as whole, both relevant to the physiological connection represented by tracts/fascicles/bundles considered in the structural

connectivity and by the functional responses and activity correlations. In this study, clearly emerged that the progress on both sides is a core element in permitting to advance towards further integration methods, overcoming the "shadow line" which still separates the insight into the white matter and the gray matter connections. The high challenge deals also with anatomo-functional integration aspects which largely rely on mesoscale details of the brain circuits at the edge of current instrumentation and analysis methods.

We proposed two methods that allowed respectively the localization and the quantification of the connections between WM and GM and the correlation between structural and functional metrics. Both approaches worked at network level addressing technical issues mainly related to the limitation of the neuroimaging tool used for these analysis (e.g., the impossibility to approach gray matter when using deterministic tractographic algorithm, the asymmetry issue raised when performing probabilistic tractography, *etc).* As a result of this integration analysis at network level, we should stress that our studies confirmed the idea that any functional coordination should be mediated by connecting fibers only in case of highly specialized networks (i.e., the language circuit and the two lateral RSNs). The DMN, indeed, showed no correlation between SC and FC values, suggesting the existence of associative and indirect paths, such as polysynaptic structures, which connect gray matter regions but are not detectable with our tractography. This finding led us to also work on improving tractographic techniques and ameliorate the quality of the diffusion data. For this reason, we further address the problem of artifacts in DW images. We first worked at single level proposing a new method for artifact identification and removal, then at group level developing a new pipeline for the quality control of tractography-derived measures. Both these approaches aim at providing better and better diffusion data to be integrated with the functional ones.

It is also noteworthy that the application of the structural and functional data in clinical environment was demonstrated to be a very interesting instrument to assess circuitry modifications and adaptation, allowing for monitoring the changes due to both pathology and therapeutic interventions (Irimia et al., 2014). This may eventually aid in the development of patient-specific tailored rehabilitation approaches.

To conclude our work suggests that many other studies will be needed on the topic of the integration of structural and functional data; nevertheless, we strongly believe that this kind of integration is the most fascinating and challenging route to pursue in neuroscience to gain more comprehension of the brain in its overall highly complex behavior.

1. Introduction

The interest in neuroimaging performed by magnetic resonance imaging (MRI) has constantly increased in the last decades as a powerful and non- invasive mean to investigate human brain connectivity in terms of both structure and function, with the objective to explore physiological cognitive process and pathophysiological mechanisms.

The capabilities of MRI to provide with different contrasts, micro-structural features, and functional activation were recognized since long time and in the last decade permitted to develop methods addressing the overall brain organization and function (van der Kolk et al., 2013), the understanding of which is a major challenge open to future research with striking translational implications in neurological clinics. Studies in this field (also involving huge projects both in Europe and in the United States of America) are often indicated under the label of "brain connectome" (Sporns et al., 2005; Maier-Hein et al., 2017; Craddock et al., 2013; Pestilli et al., 2014; Smith et al., 2013; Glasser et al., 2013; Smith et al., 2015), to emphasize the core position of understanding connection patterns and integrated functions, beyond the specialization of brain cortical areas.

Originally, two different and parallel neuroimaging research streams were developed: the structural connectivity (SC), represented by bundles of fibers (alias tracts or fasciculi), and functional connectivity (FC) expressed by the coordinated activity of specialized cortical areas. Specifically, SC is evaluated by tractographic dissection of the white matter (WM) based on diffusion weighted imaging (DWI), while FC is assessed by correlation analysis on cortical activity elicited either asking subjects to perform a task (fMRI) or in resting state condition (rsfMRI).

More recently, a challenging research field in neuroscience is exploring the whole human brain organization considering the relationship between SC and FC. Although great interest has been posed in the integration of SC and FC information, this topic still presents several methodological challenges related on one hand to

the compatibility of WM and GM investigation, especially at their boundary and on the other hand to tractography reconstruction, often affected by artifacts.

In this scenario, this doctoral project aims at developing novel neuroimaging techniques to combine structural and functional data, and improving the quality of SC data by mean of the identification and removal of artifacts in the DW images. In details, this thesis will focus on:

i.   Integration of deterministic tractography and task-driven functional magnetic resonance imaging and its application into a clinical neurorehabilitation context;

ii.   Integration of probabilistic tractography and resting-state functional magnetic resonance imaging;

iii. Artifact identification and removal in High Angular Resolution Diffusion Imaging data;

iv.   Artifact identification in tractographic reconstruction for automatic quality controls in group analyses

All the described methods, will be supported by an extensive literature review of the existing techniques for studying SC and FC, providing with the most crucial steps of the pipelines followed to evaluate the brain connectivity from row MRI images.

Importantly, our methods were developed with the final aim to be translated in the clinical practice by the validation of workflows to be applied to images acquired with clinical scanner, thus introducing the multimodal imaging methods of "connectomics" in the clinical routine.

1.1. Functional brain connectivity

Functional brain connectivity refers to the co-activation of gray matter (GM) areas reflected by a statistical dependency among remote neurophysiological events (Friston, 2011). This information is obtained by the functional magnetic resonance imaging (fMRI) (Kwong et al., 1992; Ogawa et al., 1990), a technique based on the measure of the blood oxygen level dependent (BOLD) signal or contrast (Amaro and Barker 2006),

that provides an indirect estimate of the neural activity. Specifically, when a specific brain district is activated, it presents an increase in oxygenated hemoglobin and a decrease in de-oxygenated one. The latter has paramagnetic properties that contribute to an increase in the local microscopic magnetic field inhomogeneity which lengthen the T2* relaxation time and delays signal fading (Logothesis et al., 2001). Therefore, neural activation is indirectly translated into an increment of BOLD signal above baseline by 3-5%. The small entity of BOLD contrast, lower in size to noise, requires specific statistics to map activated areas. As better detailed in the next paragraphs, correlation with externally measurable tasks (or imposed stimuli) is referred to as task-driven fMRI and addresses the response of specialized GM areas. Conversely, the search for co-activations is mainly performed in resting-state condition (i.e., with no stimuli or tasks), thus observing the ongoing brain activity through the BOLD signal and collecting resting state fMRI (rsfMRI) data, from which statistical dependencies or correlation between areas (even distant ones) can be extracted.

1.1.1. Task-driven functional magnetic resonance imaging

Task-driven fMRI aims at investigating the neural underpinnings and brain activity elicited by a task accomplished by the subject many times during the fMRI scan, to capture the related brain activation differences compared to the rest condition (i.e., the baseline) (Vidaurre et al., 2017).

To test a biological hypothesis, an fMRI experiment must be designed within the constraints of the temporal characteristics of the BOLD fMRI signal and of the various confounding effects to which fMRI signal is susceptible). The three elements necessary to comprehensively describe a fMRI task-driven experiments are: experimental design, data acquisition, and data analysis (Goebel 2007; Buxton 2009; Huettel 2012; Poldrack 2012; Friston et al., 2007).

The task-driven experiment can be designed as block-design or event-related design. In block-design, epochs (or blocks) of stimulation/activity are alternated to rest epochs, thus implying boxcar input functions. In event-related design, activation is concentrated at time points (events) either marked by some randomized

stimulus or by some subject's response; so, the input function is a series of pulses marking the events. The block-design is commonly used in clinical experiments where the subject is required to perform a task (e.g., finger tapping or word repetition) continuously for about 30 seconds alternatively to a rest period of approximately 30 seconds. Activated cortex is identified by block-to block periodic BOLD signal changes that are correlated with the task paradigm. Advantages of block-design includes its simplicity and power for detection of an activation response. In particular, block paradigms summate the hemodynamic response over multiple neural events within each block, yielding relatively high BOLD contrast-to-noise ratios (Buchbinder 2016). The event-related design consists in providing the subject with activation and control stimuli in a randomized order. Due to the delay in the hemodynamic response, events need to be sufficiently separated in time (i.e., using a long inter-trial interval) (Buchbinder 2016), which may reduce the statistical power of the trial. However, it can be demonstrated that a correct randomization of intervals permits a correct data analysis even in presence of overlapped hemodynamic responses relevant to events fallen by chance in close time positions (Buchbinder 2016). Advantages of this strategy are avoidance of cognitive adaptation that may occur during extended blocks, more flexible analysis strategies, and greater power to measure the hemodynamic response (Buchbinder 2016).

The continuous improvements in fMRI data acquisition are out of the scope of this work. Briefly, they include an increase in magnetic field strength (e.g, evolving from 1.5T to 3T in clinical applications, up to 7T in the most recent neuroimaging research), head coils, and acquisition sequences for higher time resolution and noise compensation (Feinberg et al., 2010; Poser et al., 2010; Lee et al., 2010; Liu et al., 2018). Here, it is worth recalling the basic elements of fMRI scans. The most common MRI sequence used for capturing cortical activation is the echo planar imaging (EPI) that allows a rapid acquisition of multiple brain slices, thus yielding a time sample over the (almost) entire brain volume within 2-3 seconds, namely at a sufficiently high temporal resolution, given the slow hemodynamic response (duration of about 12 seconds) (Goebel 2007). Due to the need of fast scans and to the poor SNR, spatial resolution is limited (Liu et al., 2018); a typical voxel size is 3mm^3 that is afterwards registered on a more detailed anatomical image,

commonly a T_1-weighted image with a voxel size of $1mm^3$. Collected data are finally analyzed after some preprocessing steps to correct artifacts and geometrical distortion, considering the slice-dependent time shifts relative to the task paradigm (Buxton 2010) and removing high spatial frequency noise and low temporal frequency drifts. The statistical analysis, commonly the general linear model (GLM), is then applied to assess the likelihood of the activation of each voxel (Huettel 2012) whose result is a parametric map in which each voxel is assigned its activation significance in the usual terms of low probability of the null hypothesis (type I inferential error) (Buchbinder 2016). Importantly, the large number of voxels tested in parallel imposes to always consider correction for multiple comparisons.
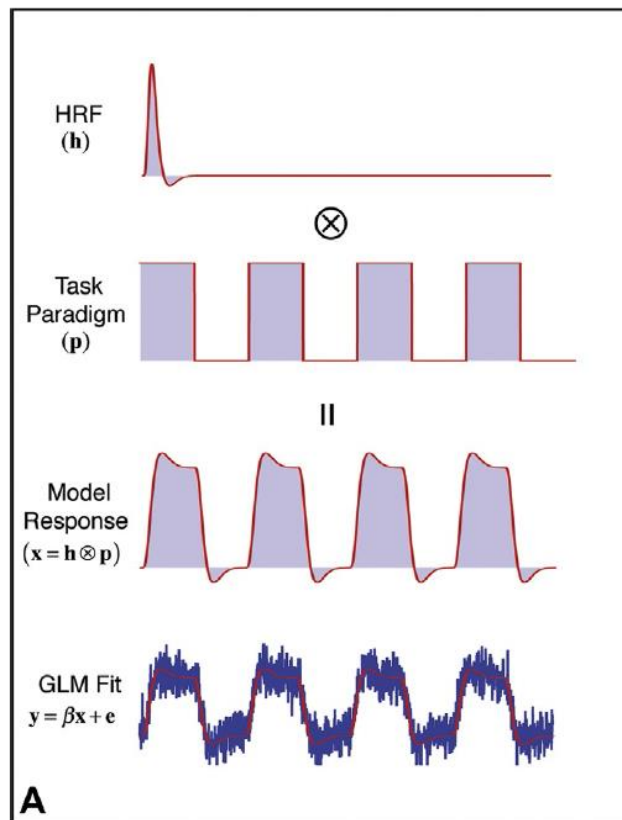
Figure 1.1 *Simulated data for modelling the blood oxygen level-dependent (BOLD) response (x) computed by convolution of the hemodynamic response function (HRF) (h) with the task paradigm function (p). Being y the measured signal, the GLM computes the value of β that yields the best approximation of the data vector y by the model in the sense of minimizing the magnitude of the error e (the least-squares error) – Buckbinder et al., 2016*

1.1.2. Resting-state functional magnetic resonance imaging

Resting-state functional magnetic resonance imaging (rsfMRI) was started by the seminal work of Biswal and colleagues (1995), where a correlation between the motor area time courses and areas considered at rest was observed. This phenomenon suggested that also in the absence of external stimuli, the brain reveals a latent activity that can be ascribed to the neuronal baseline functioning of the different cortical areas. More interestingly, it was noticed that in this silent condition, the brain is organized in well-defined networks composed by sets of cortical areas which show correlated BOLD signal fluctuation at low frequencies (i.e., around 0.01-0.1 Hz) (Beckmann et al., 2005). These networks are currently and worldwide recognized as Resting State Networks (RSNs) that functionally reflect distinctive brain circuitries (Beckmann, et al. 2005; Damoiseaux, et al. 2006; De Luca, et al. 2006; Smith et al. 2009; Veer et al. 2010) (Figure 1.1).

RSNs can be roughly divided into task-positive network and task-negative networks which are anti-correlated to the former ones (Fox et al., 2005). The task-positive networks consist of regions routinely activated during goal-directed task They include dorsal-lateral and ventral prefrontal regions, insula, and SMA, activated by a variety of demanding cognitive tasks (Cabeza et al., 2000). The task-negative networks consist of regions commonly exhibiting activity drops during task performance (McKierman et al., 2003) and include a set of regions often referred to as a "default system" to connote greater activity at rest than during the performance of various goal-directed tasks (Gusnard et al., 2001).

The analysis of the resting patterns can be performed in two different ways: either using seed-voxel approaches, namely regressing the resting data against a single voxel time course (Fox et al., 2005), or adopting the independent component analysis (ICA), a technique which decomposes a two-dimensional (time $\times$ voxel) data matrix into a set of time courses and associated spatial maps, that together describe the hidden signal (McKeown et al 1998).
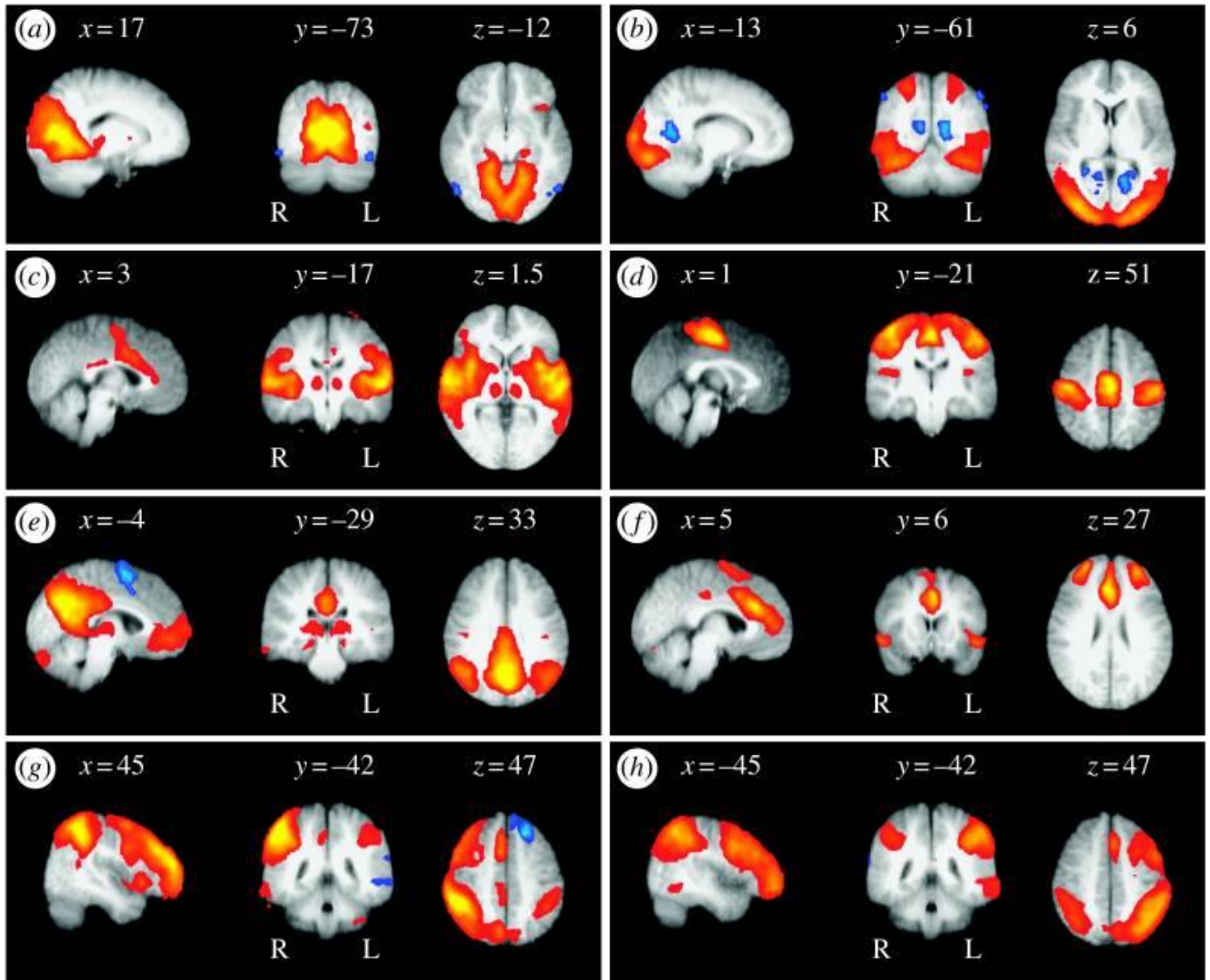
Figure 1.2 *Example of resting state networks (RSNs) – Beckmann et al., 2005*

1.2. Structural brain connectivity

Structural brain connectivity refers to the network of white matter axonal fiber bundles that compose the

physical pathways, which link different gray matter regions. Diffusion-weighted imaging (DWI), is the

magnetic resonance technique that allow to extrapolate *in-vivo* micro-structural information of the brain

white matter, following the diffusion of the water molecules (Le Bihan et al., 1986; Basser and Pierpaoli,

1996; Basser and Özarslan, 2014). The physics of Brownian motion implies that molecules diffusing in a medium with diffusion coefficient D, after a time t are dispersed in the three dimensional directions with distribution ~ G(0, 6tD) (i.e., Gaussian with variance 6tD). In biological tissues, compared to solutions, the movements of the particles are hindered by macromolecules and cellular organelles and also restricted by the confinement created by membranes. If hindering is the prevalent mechanism appearing at the macroscopic voxel scale, the Gaussian distribution with variance proportional to the diffusion time holds, though with a decreased apparent diffusion coefficient (ADC, Basser et al., 1994). This statistical model is commonly considered in biological tissues, at least as a common approximation overlooking restrictions imposed by biological barriers (e.g., cell membranes) which would alter the distribution shape (Basser et al., 1995). Model refinements address both the non-isotropic features of tissues, namely those of fiber bundles, and deviation from Gaussianity due to restrictions (Zhang et al., 2012, Edwards et al., 2017). This thesis work will deal mainly with the former aspect, comparing the basic model of diffusion tensor imaging with the more complex one of spherical harmonics and spherical deconvolution.

The way to detect the directions of diffusion movements is by using sharp bipolar gradient pulses, to encode the diffusion effect in the specific gradient direction. Briefly, according to Stejskal–Tanner equations, the Brownian mixing of spins (de-phased by the fist pulse and re-focused by the second) is sensed as diffusion weighted signal attenuation by $A = S/S_0 = \exp(b \cdot D)$, where the b-value [s/mm^2] characterizes the diffusion gradient pulse and determines the attenuation of the DWI image S compared to the reference image S_0 (alias b=0 image, which is mainly T_2 weighted due to the long echo time T_E required by the insertion of the diffusion gradient). The basic implementation of the bipolar diffusion gradient implies two opposite pulses of short duration δ (order of msec), amplitude G, and time separation (i.e., diffusion time) τ. This yields $b = \gamma^2 G^2 \delta^2 (\tau - \frac{1}{3}\delta)$ (Beaulieu, 2002), where γ is the gyromagnetic ratio of protons. It is worth remarking that in this context, D represents the ADC relevant to the specific direction marked by the gradient pulse. As shown in the next paragraphs, anisotropic DWI data relevant to many directions with different ADC values require

appropriate interpretation models, which in turn will give the basic local features used to reconstruct neural tracts and evaluate their features.

1.2.1. Diffusion Tensor Imaging

In the cerebral WM, fibers are mainly myelinated axons organized in bundles. In this specific case, the principal diffusion direction is along the main axis of the fibers where the velocity of the molecules is from three to six times higher than in the orthogonal direction. To describe this feature of a prevalent direction, a more accurate mathematical description of the diffusion phenomenon was developed by extending the Gaussian diffusion model to the 3D anisotropic case. The scalar ADC parameter was substituted by the diffusion tensor **D** (see Eq.1) introduced by Basser et al. (1995), thus originating the Diffusion Tensor Imaging (DTI) technique.

$$D= \begin{pmatrix} Dxx & Dxy & Dxz \\ Dyx & Dyy & Dyx \\ Dzx & Dzy & Dzz \end{pmatrix} \quad (1)$$

Diffusion tensor **D** is a symmetric matrix, with six degrees of freedom, and takes into account the diffusion changes in the 3-dimensional space, often visualized as the diffusion ellipsoid. The direction of its principal axes corresponds to the direction of the eigenvectors associated to the diffusion tensor matrix while the length of the main axes of the ellipsoid is proportional to the corresponding eigenvalues. The terms in the principal diagonal represent molecular mobility along axis x, y, and z of the reference frame [x, y, z] of the MRI scanner gradients and the non-diagonal ones reflect correlation between these orthogonal directions. The principal eigenvector (e_1) (corresponding to the highest eigenvalue (λ_1)) in each voxel (Jackowski et al., 2005) represents the principal diffusion direction and corresponds therefore to the prevalent fiber direction within the resolved voxel. The most used parameters that can be computed from the diffusion tensor are the main diffusivity (MD) and the fractional anisotropy (FA). The former is simply the trace of **D** (equal to the average of the eigenvalues) and represents a mean ADC over all directions. The latter indicates the anisotropy level (0 for isotropic, 1 for fully directional) by highlighting the eigenvalue differences. Since **D**

is a symmetric matrix, six acquisition directions (plus reference S_0) could be theoretically sufficient to compute the 6 tensor parameters in each voxel of the image. However, the need to improve SNR suggests fitting the DTI model over more directions (maximally scattered over the sphere) and currently 30 directions is a common standard in clinical DTI (with at least one b=0 image every 10 DW images – Decoteaux, 2015).

Although its wide-spread use in both base and clinical research, it is largely acknowledged that DTI presents strong limitations mainly derived from the assumption of the Gaussianity of the model that allows to depict one fiber configuration in each voxel ignoring the most complex configuration like the crossing and kissing fibers (Landman et al., 2010; Tournier et al., 2011). Considering that the common size of a voxel for DWI acquisition is 2mm isotropic, it was estimated that between 66% and 90% of white matter voxels presenting an FA values greater than 0.1 contain more than one fiber direction (Lenglet et al., 2009). To disentangle this complexity, the need of having more diffusion weighted directions for non-Gaussian diffusion models arose, thus leading to the development of high angular resolution diffusion imaging (HARDI) techniques (Tuch 2002; Jones et al., 2013).

1.2.1. High Angular Resolution Diffusion Imaging and new models beyond DTI

HARDI techniques are currently the state of the art of DWI acquisition directed to more reliable and rich tractographic reconstructions (i.e., more direction, more data, more virtual fibers). To be defined as a HARDI acquisition, the number of diffusion direction cannot be lower than 45 (and up to 200) and the *b-value* used should be higher than 1000 s/mm^2 (and up to 4500 s/mm^2). Their introduction as typical acquisition schemes in brain structural studies promoted the development of new sophisticated analysis techniques both model-free and model-based (Decoteaux et al., 2015). Nevertheless, HARDI is generically related to the 3D advanced diffusion imaging (Tuch, 2002) that can be performed by techniques that sample the q-space (i.e., the space of empirical diffusion distribution) with different schemes (e.g., Cartesian, spherical both single- and multi-shell, radial, *etc.*) such as diffusion spectrum imaging (DSI) (Callaghan et al., 1988), Spherical Deconvolution (SD) (Tournier et al., 2004), q-ball imaging (Tuch et al., 2002) and the

Ball-and-Sticks model (Hosey et al., 2005; Behrens et al., 2007), just naming but a few. In this work, SD and spherical harmonics (SH) functions will be considered so a more detailed description of these techniques will be provided. In this perspective, the concepts of *diffusion propagator* and orientation distribution function (ODF) will be briefly recalled in the next paragraphs.

The diffusion signal S(**q,t**) is often replaced by its attenuation E(**q,t**) derived by the diffusion signal normalized by the diffusion signal measured without any sensitization (i.e., with b=0 s/mm^2) (Decoteaux, 2015). Mathematically the relation is expressed as E(**q,t**)= S(**q,t**)/S(0). It was demonstrated (Callaghan et al., 1988) that this attenuated signal is function of the space probability distribution that describes the diffusion process of the water molecule, and this probability is called *diffusion propagator* p(**r**,t) (2).

$$E(\mathbf{q,t}) = \int_{R_3} p(\mathbf{r}, t) \exp(-2\pi i q T r) dr \qquad (2)$$

One of the most important characteristic of the diffusion propagator is the orientation distribution function (ODF) ψ (Cory, 1990) defined as the radial integral of the *diffusion propagator* in spherical coordinates (3).

$$\psi\ (\vartheta,\varphi) = \int_0^\infty p(\mathbf{r}, \vartheta, \varphi) r^2 dr \qquad (3)$$

Therefore, ODF function contains all the angular information of the *diffusion propagator* and is represented as a spherical function on the unit sphere by means of the glyphs, namely a mesh in which every single vertex is proportional to the value of the ODF on the sphere (Decoteaux, 2015).

At this stage, the problem of diffusion is how to reconstruct the ODF based on discrete spherical HARDI samples to produce angular functions whose maxima are aligned to the underlying fiber structure. However, the ODF is intrinsically a "blurry" phenomenon since it indicates the probability to have a diffusion along a certain direction. For this reason, several methods were proposed to improve the resolution of the ODF reconstruction (Jones et al., 2013, Tournier et al., 2004 and 2007), among which the Spherical deconvolution (SD) technique is a major one.

The main assumption of the SD model is that the ODF is a blurred object derived from the convolution between the real object and something that acts as a filter. Therefore, the deconvolution process is accomplished to have back the original object. Technically speaking, the measured diffusion signal **S** is the convolution of a single fiber response function **R** with the real fiber orientation distribution **F**, that is our unknow function (Tournier et al., 2004). Alternatively, this relation can be seen in the spherical harmonics space as a multiplication of **R** and **F**.

Spherical harmonics (SH) are frequency-space basis functions defined as the set of infinite harmonics, ideal to describe a complex function with spherical symmetry, as well as Fourier series can depict complex signal in standard space. Diffusion weighted measurements are collected along different encoding directions end the more are the directions the more they cover the surface of a sphere (Frank 2002). For this reason, spherical harmonics basis of order l and phase m (Tournier et al., 2007; Descoteaux et al., 2009; Decoteaux et al., 2010) are mathematical tool well-suited for describing directional changes over the many HARDI directions, specifically in regions with complex WM architecture (Hess et al., 2006). To fill the conceptual gap between the natural system for imaging (i.e., the Cartesian one) and the spherical framework, the rotation in three dimensions of the diffusion coordinates are to be considered. Indeed, HARDI measurements, intrinsically have a spherical symmetry since they are composed by a series of 3D rotations (Frank 2002), therefore SH bases allow to reconstruct the angular component of the diffusion signals.

For the nature of the diffusion signal, SH basis are real and symmetric so **S** is usually estimated by a truncated SH series of order l_{max} and a number of coefficients R such that R= $(l_{max}+1)(l_{max}+2)/2$. Odd orders of the SH describe asymmetric components, representing then image artifacts (Frank 2002).
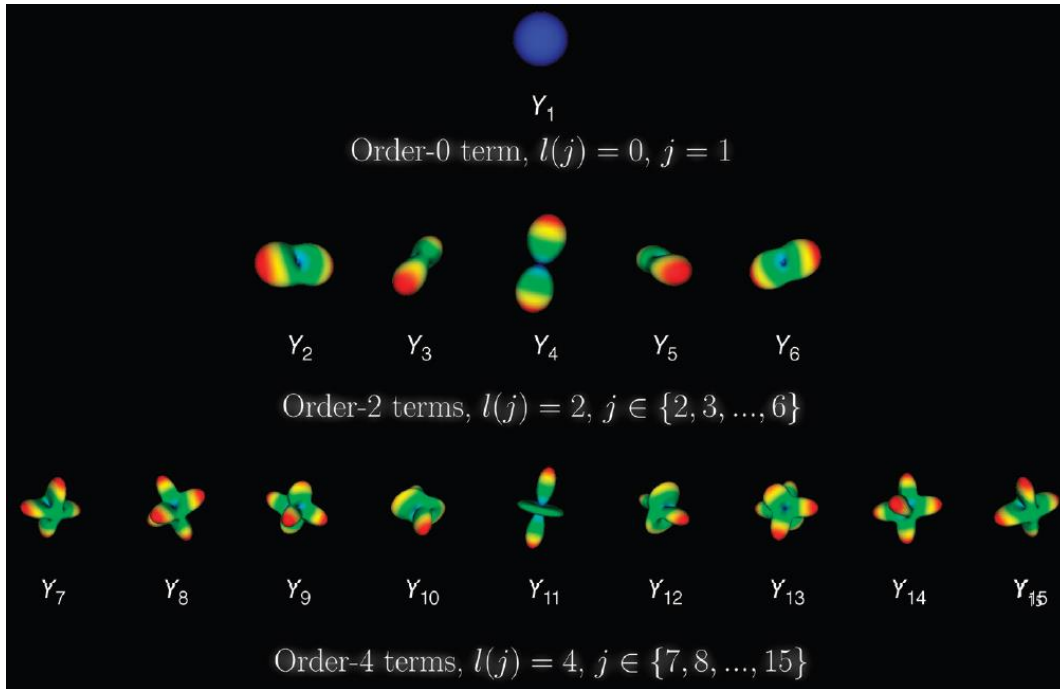
Figure 1.3 *Representation of first 15 elements of the spherical harmonic (SH) basis – Adaptation from Decoteaux et al., 2015*

The order *l* of the SHs gives the smoothness of the function, namely the higher is the order the sharper is the function, resulting in an improved angular resolution (zero-order, indeed, represents isotropic diffusion in absence of noise). However, using high *l* values can lead to instability (Tournier et al., 2004; Alexander et al., 2005) and produce negative fiber ODF values and false spurious peaks. To address this issue, constraints regularizations were introduced to insure stability and positivity (Decoteaux et al., 2007 and 2009; Dell'Acqua et al., 2010; Anderson, 2005; Tournier et al., 2007; Alexander et al., 2005; Ramirez-Manzanares et al., 2007) leading to the well-known constrained spherical deconvolution (CSD).

1.2.2. Deterministic and Probabilistic Tractography

Regardless the model used to characterize the diffusion signal, the most useful application of the DWI is in the fiber tractography.

It's important to specify that fibers reconstructed through tractography techniques do not have to be considered real white matter tracts, but just a reflection of the axonal architecture. That is why the estimated curves displayed curves are commonly named 'virtual fibers' ore "streamlines". This aspect has to be taken into account when tractography data are discussed.

After the diffusion tensor computation, the principal direction of diffusion is computed for every voxel. Then, preserving the continuity in the reconstructed fibers at the voxel boundary is necessary to visualize the fibers like continuous lines. Several algorithms have been proposed by researchers during the last decade but each of them belongs to one of the two categories in which these algorithms have been classified: deterministic and probabilistic algorithms (Jones, 2008).

Deterministic algorithms are a subset of line-propagation algorithms, in which the reconstruction of a streamline starts from a chosen seed point, often the center of an image voxel, and continues voxel-by-voxel following a direction parallel with the principal eigenvector (Basser et al., 2000). Termination criteria of the line-propagation algorithms have been introduced. The most common thresholds used are a minimum FA value (Jones, 2008), under which the anisotropy level becomes too low, and the maximum angle that the fiber can bend from one step to the next (Beherns et al., 2003; Parker et al., 2003). Although no general consensus is found in the literature, common threshold values are FA > 0.2 and bending angle < 30°.

Although, the main concept is that deterministic tractography produces maximum likelihood pathways through the DW dataset (Anwander et al., 2006), the limitations in this kind of approach are the impossibility to reconstruct more than one trajectory per seed point, the univocal direction imposed inside each voxel, and the inability to evaluate the relative reliability of each trajectory. Probabilistic algorithms have been proposed to solve the limitation of the deterministic ones. In fact, a multitude of possible trajectories starting from each seed point are calculated and a probability value is assigned to each direction according to diffusion data along their whole pathway. Although many probabilistic algorithms exist, the result is always a probabilistic map (one map for each seed point), which contains the information about the probability to

connect any point in the brain, starting from the seed. In this case the termination criteria regard only the curvature angle (Jones, 2008), because probabilistic algorithms are not dependent on having a defined principal eigenvector and then they do not require a FA threshold.

1.3. Open challenges and author's contribution

This doctoral thesis is inserted in the context of the investigation of the brain connectivity by means of advanced MRI techniques, namely the functional MRI to study functional activation of gray matter areas under different psycho-physical condition, and the diffusion weighted MRI to highlight the white matter connections which underlying specific brain circuitries. Specifically, the studies described in the next chapters aim at integrating these two imaging modalities to investigate the brain considered as a whole. There is no consensus or standard guidelines about how to combine structural and functional data, therefore this project has the purpose of addressing open methodological challenges and technical issues related to diffusion weighted imaging.

First, we investigated the physical connection between WM bundles and GM areas and quantified the extent of this connection. Previous works demonstrated the correlation of the gray/white matter junction thickness to detect specific pathologies like the focal cortical dysplasia (Blackmon et al., 2011; Xiaoxia Qu et al., 2014). However, no studies used the information of WM/GM connection as a marker of brain plasticity when investigating follow-up in patients under neurorehabilitation therapy. Moreover, our studies contributed to shed lights onto specific brain circuitry in both active and resting brain status, confirming the existence of strong links within major functional networks.

Nevertheless, dealing with functional and structural connectivity data, we identified the latter as the weaker and the more limited in terms of accuracy of results and definition of quality as well as workflow standards. For this reason, the second part of this doctoral project aims at identifying artifacts in DW images in HARDI datasets. Specifically, we first developed a method for automatic detection of corrupted datasets and their

correction; then we proposed a fast and effective quality control on tractographic datasets, well suitable when performing group analysis, regardless the model used for describing the diffusion signal.

It is noteworthy that all the developed methods were built with clinical datasets encouraging the translation of these research into medical routine for improving diagnosis precision and follow-up accuracy in rehabilitation context.

All the studies described in this doctoral thesis were published and/or presented at International MRI conferences.

1.3.1. Author's scientific publications

Papers

- Combined DTI–fMRI Analysis for a Quantitative Assessment of Connections Between WM Bundles and Their Peripheral Cortical Fields in Verbal Fluency - **E. Scaccianoce**, M.M. Lagana, PhD, F. Baglio, MD, M.G Preti PhD, N.P. Bergsland, P. Cecconi,MD, M. Clerici, MD, G. Baselli, G. Papadimitriou, N. Makris, MD – Brain Topography(2016)

- Mapping temporo-parietal and temporo-occipital cortico-cortical connections of the human middle longitudinal fascicle in subject-specific, probabilistic, and stereotaxic Talairach spaces" - N. Makris, A. Zhu, G. M. Papadimitriou, P. Mouradian, I. Ng, Y. Kao, **E. Scaccianoce**, G. Baselli, F. Baglio, M. E. Shenton, Y. Rathi, B. Dickerson, E. Yeterian, M. Kubicki – Brain Imaging and and Behaviour(2016)

- Assessment of Internal Jugular Vein Size in Healthy Subjects with Magnetic Resonance and Semiautomatic Processing - M.M. Lagana, L. Pelizzari, **E. Scaccianoce,** O. Dipasquale, C. Ricci, F.Baglio, P.Cecconi, G. Baselli – Behavioural Neurology(2016)

- Investigating functional and structural connectivity relationships within data-driven parcellated resting state networks – L. Pelizzari, **E. Scaccianoce** , M.M. Laganà, N.P. Bergsland, O. Dipasquale, I. Costantini, P. Cecconi, M. Clerici, F. Baglio, G. Baselli – *in preparation*

- Mapping residual along tract: a technical note on a fast and effective quality control for tract specific measurements - **E. Scaccianoce**, G. Baselli, M.M. Laganà, F. Dell'Acqua – *in preparation*

CONFERENCE PROCEEDINGS

- "A Fast and Effective Strategy for Artifact Identification and Signal Restoring with HARDI data" at International Society of Magnetic Resonance in Medicine, Singapore, May 2016

- Artifact Identification and Signal Restoring in HARDI data by using spherical harmonic model" at Organization for Human Brain Mapping, Geneva, June 2016

- A semi-automatic method for anatomical measures of the internal jugular veins" at International Society for Neurovascular Diseases, New York City, May 2016

- A diffusion tensor imaging study of autoimmune limbic encephalitis" at XLVI Congresso nazionale della Società Italiana di Neurologia, Genova, October 2015

- Correlation of Brain Structural and Functional Connectivity Indexes" at 37th Annual Conference of the IEEE Engineering in Medicine and Biology Society, Milan, August 2015

- Mapping residuals along tracts: an effective quality control approach for tract specific measurements" at International Society of Magnetic Resonance in Medicine, Toronto, May 2015

- Do the structural connections reflect the functional connectivity within specific resting state networks?" at Risonanza Magnetica In Medicina 2015: Dalla Ricerca Tecnologica Avanzata Alla Pratica Clinica, Verona, April 2015

- A novel approach of fMRI-guided tractography" at International School Of Clinical Neuroanatomy, THE PARIETAL LOBE, Catania, May 2014

- Functional and structural connectivity changes in a case study of cervical dystonia treated with botulinum toxin and motor re-learning techniques" at 3rd International Workshop on Synaptic Plasticity: from bench to bedside, Milazzo, June 2014

- Optimization of inverse fMRI-guided tractography technique: application to language circuit in typical condition" at GNB2014, Pavia, June 2014

2. Integration of deterministic tractography and task-driven functional magnetic resonance imaging

The main results presented in this chapter were published in Scaccianoce et al., (2016) "A method for quantitative assessment of connections and their peripheral cortical fields using combined DTI tractography and fMRI in verbal fluency".

One of the most challenging objectives in recent neuroscience is defining the white matter connections, which involving the micro-scale of fiber span through the whole brain, and their organization in circuits within specific functional networks of specialized cortical areas (Makris et al., 2009). The elucidation of the specific circuitries underlying brain activations is considered a fundamental step for both understanding a given behavior or physiological state (Greicius et al. 2009; Raichle et al. 2001) and recognizing potential pathological biomarkers (Mayberg et al. 2005). Assessing brain damages at the network level, indeed, offers the possibility to investigate anomalous interaction between regions that alone show normal activation (Grefkes and Fink, 2011; Rehme and Grefke, 2013).

In the present studies, magnetic resonance imaging (MRI) technique is used to perform a multimodal analysis of the brain at structural (i.e. WM fibers) and functional (i.e. GM areas) network levels. Specifically, diffusion tensor imaging (DTI) and functional magnetic resonance imaging (fMRI) were selected since their combination was demonstrated to be suitable for the integrated exploration of neural circuitries (Honey et al. 2009; Aslan et al. 2011; Turken et al. 2008; van Eimeren et al. 2008; Glenn et al. 2007; Morgan et al. 2009; Vernooij et al. 2007; Propper et al. 2010).

The most recent literature reported different approaches aim at combining structural-functional information. The first strategy consists in correlating microstructural integrity indicators assessed through diffusion measurements (e.g., fractional anisotropy), and blood oxygenation level dependent (BOLD) signal evaluated by functional activity (Morgan et al. 2009; Forstmann et al. 2008; Zhang et al. 2010; Shlosser et al. 2007). Although this method provides with information on network complexity at high level, it does not

highlight direct white matter (WM)-gray matter (GM) connections in a topographical context. The second approach, instead, aims at integrating in the same framework DTI and fMRI data by performing tractography using GM functional activations as seed regions, leading to a technique named fMRI-guided (fMRI-driven) tractography, whose applications include virtual surgical planning (Kleiser et al. 2010), neurodegenerative diseases (Preti et al. 2014; Bonzano et al. 2009), and investigations in healthy subjects (Staempfli et al. 2007; Greicius et al. 2009). Differently from fMRI-guided tractography method, Hua and colleagues (2009) proposed to consider the projections of well-known bundles, investigating which cortical areas were directly linked with the considered bundles. With this method, though, no inference could be drawn regarding structural-functional relationships. Following this idea, we proposed a novel combined DTI-fMRI analysis of the language network by assessing topographically and quantitatively the connections between the left arcuate fascicle (AF) and the left cingulum bundle (CB) with their peripheral cortical field recruited during a verbal fluency task. This method was developed on healthy subjects and tested in a neurorehabilitation context to demonstrate the importance of assessing brain circuitry changes longitudinally.

2.1.1. Materials and methods

Subject population

Twenty-five healthy subjects (HSs) were enrolled at Don Gnocchi Foundation (Milan, Italy). A clinical interview determined that all subjects had no impairment in daily living functional activities and no major psychiatric illnesses, with attention to exclude subjects with a history of depression.

MRI acquisition protocol

Brain magnetic resonance imaging (MRI) scans were acquired using a 1.5 Tesla scanner (Siemens Magnetom Avanto, Erlangen, Germany) with the following sequences: axial dual-echo turbo spin echo (TR/TE1/TE2 = 2650/28/113 ms, , flip angle = 150°, 50 interleaved 2.5-mm-thick slices, matrix size = 512×512, FOV = 250×250 mm2); coronal FLAIR (TR/TI/TE=9000/2500/121 ms, flip angle=150°, 24 4-mmthick slices, matrix size=240x210, FOV=256×205mm2). In the same session the following axial MRI

sequences were also acquired. 1) 3-dimesional T1-weighted magnetization prepared rapid gradient echo (MPRAGE) (TR/TE/TI = 1900/3.37/1.1 ms, flip angle = 15°, 176 contiguous slices, matrix size= 192×256, FOV = 192×256 mm2) as anatomical reference. 2) Diffusion weighted (DW) pulsed-gradient spin-echo echo planar imaging (EPI) (TR = 7000 ms, TE = 94 ms, 50 2.5-mm-thick slices, matrix size = 128×96, FOV = 320×240 mm2), with diffusion gradients (b-value= 900 s/mm2) applied in 12 non-collinear directions and one image without diffusion weighting (i.e., b-value=0). Two runs were acquired. The DW sequence parameters were selected to optimize signal to noise ratio (Laganà et al., 2010), compatible with time-limited clinical protocols. 3) Single-shot gradient echo EPI sequence (38 interleaved 3 mm-thick slices, TR/TE = 3000/50 ms, matrix size = 64×64, FOV = 250×250 mm2) using blood oxygenation level dependent (BOLD) contrast for functional imaging, during a paced-overt verbal fluency task. The stimuli were presented with an MR-compatible visual system (VisuaStim Digital system from Resonance Technology Inc.), including E-Prime software (E-Prime 2.0 Psychology Software tool, http://www.pstnet.com) to ensure the exact timing of prompts during MR acquisitions. Each session included 6 experimental blocks in which the subject was required to list six different objects belonging to a specific category (e.g., flowers). Each experimental block was alternated with 6 control blocks (30 seconds each, for a total duration of 6 minutes). Subjects were instructed to say the word "nothing" if they were unable to generate an exemplar when they saw an exclamation mark. Asking subjects to produce the word "nothing" (rather than simply remain silent) served to better match the articulatory components of the task and the control conditions. During the control blocks, instead, subjects read the word "nothing" presented on the screen every 2.5 seconds (Basho et al., 2007). Finally, the relationship between the fMRI activation and the in-scanner performance on the task was evaluated through the percentage of the correctly uttered words.

DTI data analysis

Pre-processing of DW images included the correction for distortions induced by eddy currents and head motion by means of FSL package (http://www.fmrib.ox.ac.uk/fsl/), having the b=0 image of the first run as

the reference image and rotating the B-matrix according to the local spatial orientation correction (Leemans and Jones, 2009). The diffusion tensor (DT) was then estimated for each voxel, tensor decomposition was performed and fractional anisotropy (FA) was computed. Each subject images were normalized by non-linear warping to the Montreal Neurological Institute (MNI) FA template, based on their FA image. The same warp was locally applied to the tensor of each voxel. Deterministic tractography was performed with the following parameters: brute-force approach (Conturo et al. 1999), interpolated streamline algorithm, FA < 0.20 and angle between two subsequent directions $> 35°$ as stopping criteria (Preti et al. 2014). Left AF and left CB were reconstructed with TrackVis v.0.5.1 (www.trackvis.org) as the main bundles involved in the considered verbal fluency task (Baglio et al. 2014; Preti et al. 2014; Makris et al. 1997; Makris et al. 2002; Catani et al. 2002; Catani and de Schotten 2008; Propper et al. 2010; Morgan et al. 2009). The above-mentioned tracts were dissected from specific regions of interest (ROIs) as described in Catani and de Shotten (2008). Specifically, a single ROI composed by approximately five slices in axial view was used for AF tractography. A large half-moon shaped region was defined on the most dorsal part of the AF. The lowest region was defined around the posterior temporal stem. The lateral border of the ROI passed through the bottom part of the frontal, parietal and temporal sulci. The precentral sulcus demarcated the anterior border of the ROI (Fig. 2.1, panel a). For the CB dissection, instead, a single ROI on approximately 30 axial slices was chosen. A single cigar-shaped region was defined on the top three slices. When the CB separates into two branches, an anterior and posterior region was defined on each slice from the parahippocampal gyrus to terminate in the anterior part of the medial temporal lobe (Catani and de Shotten, 2008) (Fig. 2.1, panel b).
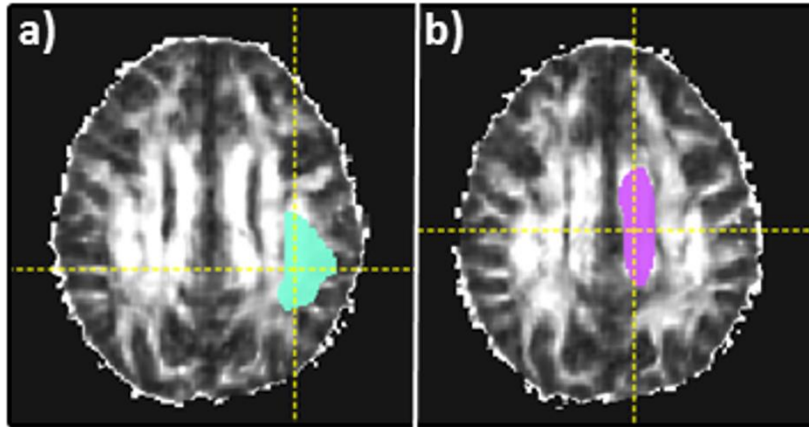
Figure 2.1 *Region of interest (ROI) used for reconstructingarcuate fascicle (AF) (a) and cingulum bundle (CB) (b) – Scaccianoce et al., 2016*

fMRI data analysis

Pre-processing of fMRI images was performed by FSL FEAT v5.98 (Smith et al. 2004) including the following steps: motion correction, non-brain tissue removal, spatial smoothing with a Gaussian kernel of 5 mm full width at half maximum (FWHM) and a high pass filter cutoff of 60 s. The active cortical areas elicited by the categorical-fluency (versus control condition) were identified at single level by statistical analysis (first level, general linear model) (GLM; Friston et al. 1994), introducing movement parameters as covariates. A contrast of parameter estimates (COPE) image was obtained for each subject and then non-linearly registered to the MNI space, using the transformations by estimating: 1) the transformation of the EPI to the high-resolution structural T1-MPRAGE using linear registration (FLIRT – Jenkinson and Smith 2001; Jenkinson et al. 2002) with the brain-boundary registration cost function (BBR - Greve and Fishl 2009); 2) the non-linear warping of the T1-MPRAGE to MNI standard space with FNIRT (Smith et al. 2004). The resulted normalized COPE images of each subject were used for group analyses (second level, one sample t-test) to estimate the main effect of the task. A threshold of t=1.73, corresponding to a P<0.05 significance level (according to N-1=20 degrees of freedom) was applied to the t map resulting from the second level analysis and each estimated cluster was determined by Z>2.3, corresponding to a corrected

cluster significance threshold of P=0.05 (Worsley et al. 2001). Finally, the relationship between the sensitivity to fMRI clusters and the in-scanner performance on the task was evaluated through the percentage of the correctly uttered words and resulted very close to 100% (i.e., 98,81±2.32%).

DTI and fMRI data integration: single subject and group level

Since the bundles reconstructed with this tractographic algorithm normally are stopped before approaching gray matter, due to the FA decrease in the cortex proximity (Basser et al. 2000; Conturo et al. 1999), both the AF and the CB of each subject were extended into gray matter for 10 mm to reach the most proximal cortical regions. Both extremities of every streamline were extended by using an in-house Matlab script (Matlab R2010a, MathWorks, http://www.mathworks.it/products/matlab) following the direction of the vector connecting the coordinates of the two last voxels. Finally, each extended tract was masked with a GM atlas (Hui et al., 2005) to select only those parts reaching the cortex. The necessary processing steps on diffusion data to obtain fiber extension are summarized in figure 2.2, left side, panel a.

Regarding the functional data, from the center of gravity (COG) of each cluster obtained by group-fMRI analysis, 11-mm-radius spheres were drawn to restrict the analysis to the specific cortical areas identified by the cluster peaks and also to take into account the inter-subject variability (Drobyshevsky et al. 2006). The necessary processing steps on functional data to obtain cortical activations centered in the COG are summarized in figure 2.2, left side, panel b.

DTI-fMRI integration was then performed both at single and group level in standard space.

At single level, the AF and CB projections of each subject were intersected with group fMRI activation spheres; the topographic location (i.e., which Brodmann areas were involved) and the extension, in terms of mm^3, were evaluated. The median value and confidence interval at 95% ($CI_{95\%}$) of the connection volumes between the projections of AF and CB at single level and spheres from fMRI activation were finally computed.

At group level, the group projections of AF and CB were obtained by averaging the single subject projections among all the HSs. These averaged volumes were then thresholded at 0.6 (Mori et al., 2009; Aslan et al. 2009), a useful step to limit the random error due to noise and partial volume effects (Hua et al. 2009). The group projections were intersected with the group fMRI activations (Fig. 2.3); then, the volumes of connection were mapped and measured, and the relative weight of each BA was also calculated and expressed both as absolute values and relative percentages (i.e., how much the specific Brodmann area overlapped with the connection). The Dice coefficient and the coefficient of variability were computed to test the physiological inter-individual variability of GM-projected bundles, considering the tract projections of every single subject compared to the group projections for both AF and CB. Finally, the Dice coefficient was also calculated for the volumes generated by the overlap between the DTI projections and the group fMRI activations.
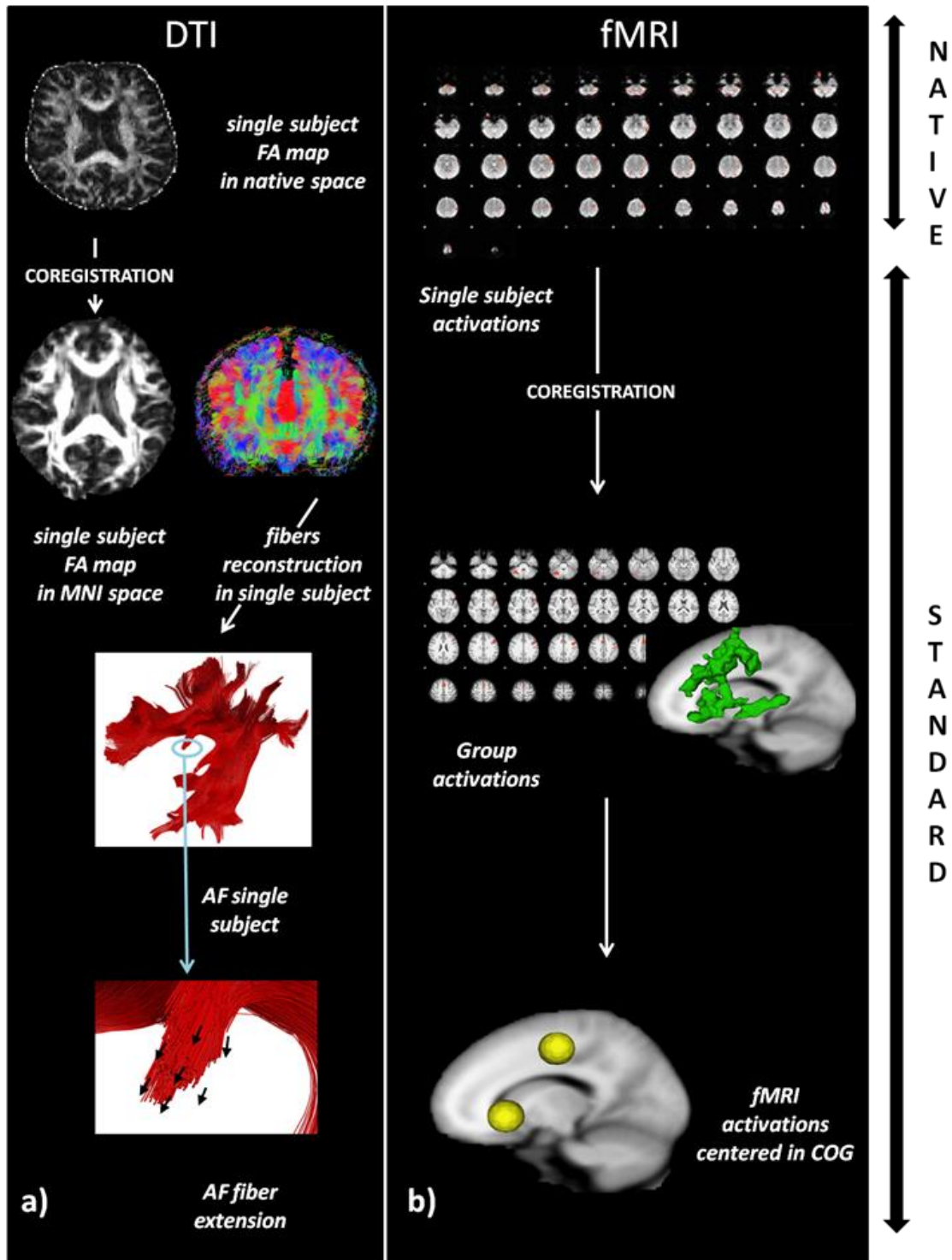
Figure 2.2 *Pipeline of DW images (panel a) and fMRI images (panel b) to perform the structural-functional data integration– Scaccianoce et al., 2016*
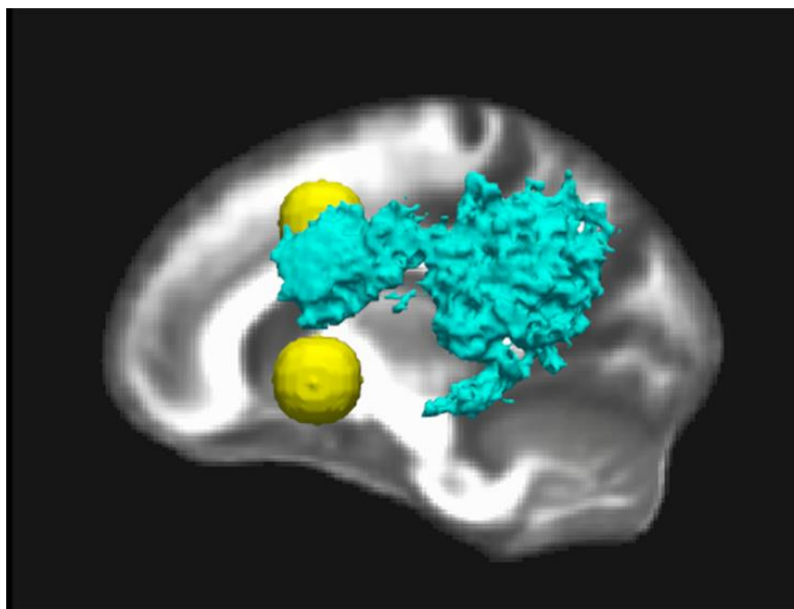
Figure 2.3 *Integration of diffusion tensor imaging (DTI) and functional magnetic resonance imaging (fMRI): AF group projections (light blue), functional activations starting from the center of gravity (COG) of the signal peak (yellow) - left view – Scaccianoce et al., 2016*

2.1.2. Results

As a result of the clinical interviews, none of the 25 subjects showed neurological problems. T1- and T2-weighted images didn't depict any anatomical abnormalities. fMRI sequences, instead, presented movement artifact in 4 out of 25 subject datasets that were finally excluded.

DTI and fMRI data analysis

For diffusion data, fiber reconstruction of left AF and CB were successfully performed for all 21 subjects. Tract FA and MD values (not shown) resulted homogeneous within the 21-subject group, revealing a normal anatomy (Catani and de Shotten, 2008).

Regarding the functional activations, four statistically significant activation clusters (Z>2.3) were obtained (Tab. 2.1).

Cluster index	Voxels	Z-max x (mm)	Z-max y (mm)	Z-max z (mm)	Z max	COG x (mm)	COG y (mm)	COG z (mm)	Z COG	Cortical areas
1	14617	-50	-13	43	4.17	-43.88	4.75	39.1	2.28	Precentral gyrus
2	9698	31	-60	-31	4.28	33.8	-64.7	-27	2.62	Cerebellum
3	8980	-54	17	-3	4.22	-55.9	4.76	0.808	-*	Sup. Temp. gyrus
4	8682	-2	14	50	5.2	-1.34	13	50.7	4.93	Sup. Front. gyrus

Table 2.1 *Standard space coordinates of COG and respective Z-intensity value of four activation clusters (clusters 1, 3 and 4 are located in the left hemisphere, cluster 2 is located in the right hemisphere) – Scaccianoce et al., 2016*

*This Z-intensity value could not be assessed because the respective COG was not included in an activation cluster

Consistently with previous findings (Baglio et al. 2014; Preti et al. 2014), the HSs exhibited a typical activation pattern of paced overt verbal fluency task: activated areas related to the category-driven word generation (e..g., left inferior and middle frontal cortex) and areas associated with the paced response and overt articulation (e.g., cingulate cortex, right superior parietal cortex, insular cortex, thalamus, basal ganglia), with some contralateral activation in the cerebellum.

DTI and fMRI data integration: single subject and group level

Considering the extended tracts, the cortical areas involved at both single and group level of AF projections were the primary somatosensory cortex (BAs 3/1/2), premotor cortex (BA 6), prefrontal dorsolateral cortex (BA 9), occipital areas (BAs 19/18/17), parieto-temporal cortex (BAs 21/37, 40 - Wernike's areas) and the inferior frontal gyrus (BAs 44/45 - Broca's area).

The single and group CB projections, instead reached the primary somatosensory cortex (BAs 3/1/2), premotor (BA 6), prefrontal dorsolateral cortex (BAs 8 and 9), occipital areas (BAs 19/18/17), prefrontal cortex (BA 10), parietal cortex (BAs 5 and 7), anterior and posterior cingulated cortex (BAs 24/32, 29, 30 and 31), and the orbitofrontal area (BA 11). The analysis of the physiological interindividual variability of GM-projected bundles showed a mean Dice coefficient of 0.637 (σ=0.134) for AF projections and 0.730 (σ=0.105) for CB projections while the coefficient of variability was equal to 0.210 for AF and 0.144 for CB.

The fMRI activation areas, were identified in left inferior and middle frontal cortex, cingulate cortex, right superior parietal cortex, insular cortex, thalamus and basal ganglia, in accordance with previous works (Baglio et al. 2014; Preti et al. 2014).

Concerning the intersection between either the AF or the CB streamlines extended to the cortex and the active fMRI areas, we focused on the 4 regions that are typically considered part of the language network, namely BA 6 (dorsal premotor cortex), BA 8 (prefrontal dorsolateral cortex), BA 24/32 (anterior cingulate cortex), BA 44/45 (Broca's area) (Lubrano et al., 2014; Valk 2011; Golistanerad et al., 2015; Friederici 2017). Table 2.2 presents the statistics of intersection volumes [mm^3] and emphasizes the interindividual variability by reporting the confidence interval (CI$_{95\%}$). Similarly, Table 2.3 displays the volumes of intersection between the group fMRI activation spheres and the group tract projections, also considering the percentages represent how much the specific Brodmann area overlap with the intersection.

Noticeably, most of the connections related to CB falls into the BA 24/32, in both single and group analysis, while the connection related to the AF show a different percentage distribution at single level, compared to the group one, even though the volume in mm^3 of the dorsal premotor cortex (BA 6) has similar extension both at single and group level**.**

The volumes of the connections between group fMRI activation spheres and the AF group projections were located in Broca's area (left inferior frontal gyrus, BAs 44/45) and in the premotor cortex (middle frontal

gyrus, BA 6) (Tab. 2.3). The volumes of the connections between the CB group projections and dilated fMRI activation resulted in the anterior cingulate cortex (BAs 24/32) (Tab. 2.3).

BAs	Intersection single-subject AF-fMRI mm^3 [CI$_{95\%}$]	Intersection single-subject AF-fMRI %[CI$_{95\%}$]	Intersection single-subject CB-fMRI mm^3 [CI$_{95\%}$]	Intersection single-subject CB-fMRI %[CI$_{95\%}$]
6	541 [388-768]	49 [46-61]	45 [6-272]	7[1-17]
8	0[0-0]	0[0-0]	22 [0-85]	2[0-7]
24/32	0[0-0]	0[0-0]	299 [148-505]	45[30-55]
44/45	59 0[0-219]	8.1[0-14]	0[0-0]	0[0-0]

Table 2.2 Median value and confidence interval (CI$_{95\%}$) of the volumes of intersection between extended AF and CB single subject projections and dilated fMRI activations – Scaccianoce et al., 2016

BAs	Intersection group AF-fMRI mm^3 [%]	Intersection group CB-fMRI mm^3 [%]
6	555 (10)	116 (2.1)
8	1 (0.1)	26 (11.1)
24/32	-	569 (47)
44/45	127 (17.7)	-

Table 2.3 Volumes of intersection between extended AF and CB single subjects projections and dilated fMRI activation (the percentages represent how much the specific Brodmann area overlap with the intersection) – Scaccianoce et al., 2016

Finally, to further investigate interindividual variability, Table 2.4 presents the mean of the Dice coefficients between the volumes generated by the union of the DTI projections to the cortex of all subjects and the group fMRI activated areas considering each pair of either bundle and one of the 4 Brodmann areas. Remarkably, in the pairs where significant connections were found, the group areas of influence of the bundle and the activated area display high overlaps with Dice indexes ranging from 0.83 to 0.97. This confirms, at least at a group statistical level, a substantial agreement for all the recognized overlaps, namely: AF with BA 6 and BA 44/45; CB with BA 6, BA 8, and BA 24/32.

Bundle	BA6	BA8	BA24/32	BA44/45
AF	0.97	-	-	0.83
CB	0.95	0.89	0.95	-

Table 2.4 *Averaged Dice coefficient evaluated for the volumes generated by the overlap between the DTI projections and the group fMRI activations– Scaccianoce et al., 2016*

2.1.3. Discussion

In this work, we introduced a novel approach to study in quantitative manner the topography of a specific brain circuitry by coupling the WM bundle cortical projections and the activated GM areas. In order to combine structural and functional information, we chose the language network for its specific anatomical definition (Mori et al, 2002; Makris et al., 2005) and because the verbal fluency has been extensively studied both structurally and functionally (Basho et al. 2007, Preti et al. 2014; Giménez et al.2006; McDonald et al. 2008; Levin, 2003; Paulesu et al. 1997), therefore serving as test-bed to assess the validity of our method.

Our study, included diffusion and functional datasets of 21 healthy elderly subjects (68.5±5.8 years) to investigate the relationship between cortical regions elicited by a verbal fluency task and cortico-cortical fiber tracts associated with this function (i.e. AF and CB). Our results confirmed the association between these bundles, recognized to be involved in language processing (Makris et al. 2002; Catani and de Schotten 2008; Propper et al. 2010; Morgan et al. 2009) and the GM areas elicited by a verbal fluency task (Baglio et al 2014; Basho et al.2007; Giménez et al., 2006; Paulesu et al. 1997; Binder et al. 1997). The topographical correspondence between the AF and CB projections and the fMRI activations corroborated previous studies which have attributed an important role in language processing to the above-mentioned WM tracts (McDonald et al. 2008; Makris et al. 1997; Makris et al. 2002; Catani et al. 2002).

In this work, two novel aspects were introduced compared to previous approaches, which have combined DTI and fMRI data (Kleiser et al. 2010; Hua et al., 2009, Preti et al., 2014). The first one concerns the specific localization of white and gray matter components of a specific network, i.e. the language circuit. The second one regards the quantitative assessment of the WM-GM interconnections. In this fashion, we proposed a translation from a qualitative evaluation to a quantitative one when studying the structural-functional connectivity. Further, an interesting implication of this study is the possibility to translate our research into the clinical practice, since the proposed analysis pipeline is applicable on images acquired using clinical scanners, which in most cases are still 1.5T as the one used in our pilot study, and basic connectivity analysis protocols and tools; i.e. task driven fMRI, for functional responses and DTI for structural connectivity.

To conclude, this analysis represents an innovative way for and integrated study of brain circuitries as it takes into account volumetric measures of the connections between a given fiber bundle and its peripheral cortical field. Therefore, the proposed technique improves our analytic capabilities in structural and functional connectivity investigations using multimodal neuroimaging in clinical routine.

2.1.4. Application to stroke patient: a longitudinal case study

We also tested the proposed DTI-fMRI integration method in a 65-year-old man who sustained an ischemic stroke (3 months prior) in the left middle cerebral artery territory. The patient was referred to Neuro Rehabilitation Unit of Don Carlo Gnocchi Foundation to undergo a neurorehabilitation treatment. At the admission in the center (T0), the patient presented a self-selected gait velocity of 0.52 m/sec, used a cane when walking and there were no significant cognitive deficits, only a mild impairment in verbal expression. The rehabilitation goals were to increase walking speed and endurance, to improve speech abilities and to promote his overall quality of life and well-being. Post-stroke management for this individual involved both conventional speech activities and a task oriented biofeedback approach (for details on protocol see Jonsdottir et al., 2010). The patient was treated for one month and at the hospital discharge (T1) self-selected gait velocity of the patient had increased by 16% to 0.61 m/sec and speech production had improved. To test the speech abilities structural MRI data were also acquired at the admission time, after 1 month at hospital and finally at 3-month follow-up (T2). Data was collected using the protocol described in the section 'MRI acquisition protocol' and analyzed as described in the paragraph 'DTI data analysis', while DTI and fMRI integration was performed at the single subject level, focusing on the arcuate fasciculus (AF), and was prospectively evaluated at T0 (admission), T1 (discharge after 1 months rehabilitation), and T2 (followup, after further three months).

As a result, at T1 we observed an increased WM-GM connection in BA 6, compared to T0, which improvement persisted at T2. Furthermore, at both T1 and T2 we registered a connection located in BA 44/45 that was not revealed at T0. All the results are summarized in Table 2.5 and Figure 2.4.

The need of understanding cognitive deficits at brain network level rather than studying cortical activities or structural anatomy separately, is currently an issue that cannot be neglected when treating focal pathologies such as stroke. Previous studies (Grefkes et al., 2011; Rehme et al., 2013) have demonstrated that the structural connectivity sometimes reflects an anomalous interaction between two regions in patients with residual functional impairments in spite of normal functional activations. In stroke patients, indeed, the

presence of WM structural damages (Ciccarelli et al. 2008; Newton et al. 2006) makes the characterization of functional recruitment very challenging. Further, the importance of evaluating the damage at network level leads to the possibility of investigating whether collateral pathways are enrolled to accomplish functions commonly assigned to specific and well-known networks, such as the language circuit. In neurodegenerative pathologies such as Alzheimer's disease (AD), instead, our method may be useful to evaluate the damage progression. A combined investigation of WM and GM may indeed provide further insight into the study of residual and/or collateral connections which allow the remapping of a specific functionality (Wittenberg 2010; Reuter-Lorenz and Park, 2014).

Further analysis on this topic may include the possibility to mask the WM tracts with the patient own parcellated brain instead of using a standard GM atlas. Comparing the results obtained by masking the tracts with the GM atlases with the ones revealed by masking with the subject's parcellation may provide more precise information about the language network of the specific patient.

Finally, these findings suggest that our method could well be useful as a quantitative instrument to assess circuitry modifications and adaptation, allowing for the monitoring the changes due to both pathology and those induced by therapeutic interventions (Irimia et al., 2014). This may eventually aid in the development of patient-specific tailored rehabilitation approaches.

	Connection group AF-fMRI mm^3	Connection group AF-fMRI mm^3	Connection group AF-fMRI mm^3
BAs	T0	T1	T2
6	236	677	617
8	-	-	-
24/32	-	-	-
44/45	-	22	9

Table 2.5 *Volumes of connection between extended AF projections and dilated fMRI activation of the considered stroke patient – Scaccianoce et al., 2016*
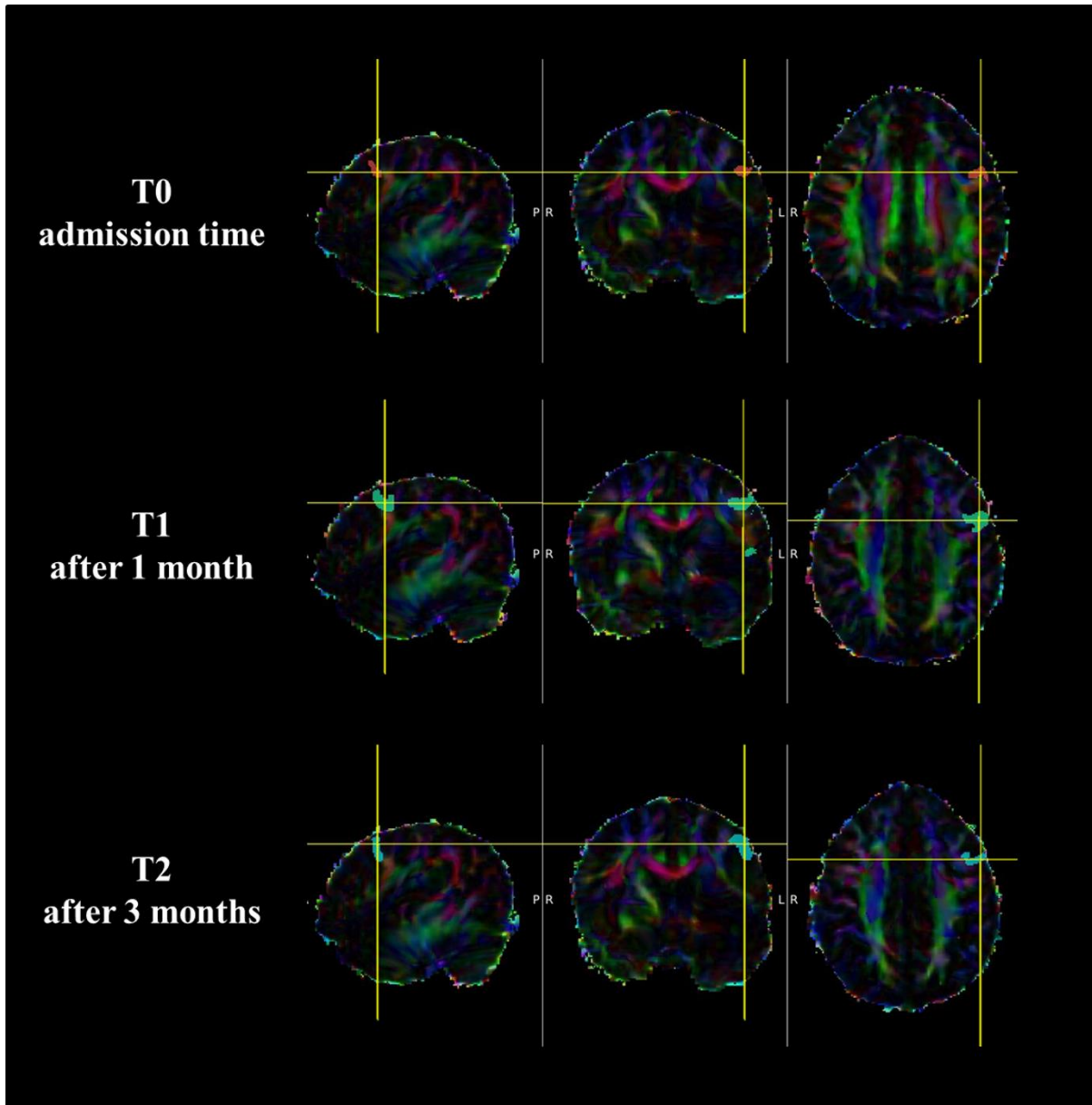
Figure. 2.4 *Integration of diffusion tensor imaging (DTI) and functional magnetic resonance imaging (fMRI) at single level in the considered stroke patient. The volumes of connections were evaluated at T0, T1 and T2 – Scaccianoce et al., 2016*

3. Integration of probabilistic tractography and resting-state functional magnetic resonance imaging

In this chapter, a summary of the following works is presented: i) "Investigating functional and structural connectivity relationships within data-driven parcellated resting state networks" – Pelizzari, Scaccianoce et al., 2017; "Correlation of Brain Structural and Functional Connectivity Indexes" presented at at 37th Annual Conference of the IEEE Engineering in Medicine and Biology Society (2015); ii) "Do the structural connections reflect the functional connectivity within specific resting state networks?" at Risonanza Magnetica In Medicina 2015: Dalla Ricerca Tecnologica Avanzata Alla Pratica Clinica (2015).

In the study presented in Chapter 2, deterministic tractography was used to derive diffusion metrics and therefore perform the integration of structural data with the functional ones. However, deterministic algorithms are mainly governed by two parameters: the bending angle and the fractional anisotropy (FA) that determine the stopping of the fiber reconstruction when reaching above threshold values if fiber direction is highly uncertain, as it happens in deep gray matter, in proximity of the cortex and in presence of complex fiber configuration (Stieltjes et al., 2001; Behrens et al., 2003; Behrens et al., 2007; Hagmann et al., 2007, 2008; Honey et al., 2009; Yo et al., 2009). To solve this issue, probabilistic algorithms have been developed to get the streamlines continued even in those areas presenting high uncertainty, with the additional advantage to be more robust against noise than the deterministic ones (Behrens et al., 2003) and to allow fiber reconstruction (at least probabilistically) between a starting ad an ending ROI. In this context, structural connectivity uncertainty is represented by probability density functions (PDFs) of diffusion model parameters, whose definition in a Bayesian framework is performed by the posterior distribution on the parameters given the data (1):

$$P(\omega|Y,M) = \frac{P(\omega|Y,M)P(\omega|M)}{P(\omega|M)} \qquad (1)$$

being ω the set of chosen parameters, Y the measured data and M the model.

The issue with this representation is that the denominator of the equation (1) is an integral often not analytically solvable. Moreover, the addressed joint posterior distribution between unknown and observed data, usually includes a single parameter or a subset of parameters (Behrens et al., 2003). One possibility to simplify the problem is using the Markov Chain Monte Carlo (MCMC) sampling scheme that, in relatively short computational times, draws samples in areas with high probability (Gilks et al., 1996; Gamerman, 1997). Specifically, the basis for this approach is to construct a Markov chain which has, as its invariant distribution, the (posterior) distribution of interest. Importantly, the probabilistic tractography can take full advantage of the HARDI scan schemes since the MCMC approach can exploit a richer signal by random extractions without the need of an explicit model.

In the present work, we exploit this computational approach performing probabilistic tractography by means of BEDPOSTX i.e., Bayesian Estimation of Diffusion Parameters Obtained using Sampling Techniques (Beherens et al., 2003), where our set of parameters ω is represented by the different directions that a fiber can follow voxel after voxel. The probabilistic approach was adopted since we were interested in correlating the functional connectivity (FC) between two ROIs with the structural connectivity (SC). Hence, the latter was best aimed at by a probabilistic and robust approach also permitting to connect a start point (or seed) ROI with an end point ROI. This definition, however, implied a slight asymmetry in results depending on which of the two ROIs is given the role of seed or of end-point. As better explained in the methods, this problem was overcome by combining the SC evaluated in both directions.

Coming to the addressed ROIs, we applied this algorithm to evaluate SC in parallel to correlation algorithms for FC among ROIs obtained by splitting specific resting state networks (RSNs) into spatially segregated clusters (Costantini et al., 2016). The clustering approach was first introduced by our group in the context of FC alone thus addressing correlations internal to the of RSNs to better understand the anatomo-functional structure of these circuits. Indeed, RSNs can be blindly separated by independent component analysis (ICA) thanks to the high degree of temporal dynamics coherence among their voxels and to the maximization of

spatial independence. This process is highly informative and reproducible relevant to the separation of the RSNs which were recognized by the literature (De Martino et al. 2007; Perlbarg et al. 2007; Tohka, Foerde et al. 2008; Kundu et al. 2012; Storti et al. 2013; Salimi-Khorshidi et al. 2014). However, it gives no information about the interactions inside each RSN. A separation into clusters and the derivation of the cluster ensemble signal through the first (i.e. the temporal one) step of the dual regression relevant to each subject for each extracted cluster is hypothesized to shed new light about the functional activity and possible damages of the RSNs.

Subsequently, it was recognized that the separation of clusters within the RSNs was suited to evaluate both FC by the correlation of ROI signals and also the SC by the probabilistic tractography. Therefore, the analysis was conducted at both structural and functional level to correlate the network SC information with its internal FC. In this pilot study, we selected the Default Mode Network (DMN) and the Left and Right Lateral Network (LLN and RLN) because these networks are considered robust demonstration of functional connectivity: specifically, the DMN is highly connected at rest and remains always active as background when performing tasks (Greicius et al. 2003); the two lateralized fronto-parietal networks, instead, overlap to brain areas that underlie specific cognitive paradigms such as memory, language and perception (Pievani et al., 2014).

3.1.1. Materials and methods

Subject population

In this analysis, nineteen healthy subjects (HSs) were enrolled in the Don Gnocchi Foundation (Milan, Italy), after Ethics Committee approval.

The study population included right-handed subjects who had no neurological disorders and gave their informed consent according to the principles of Helsinki Declaration.

MRI acquisition protocol

Brain magnetic resonance imaging (MRI) was performed using a 1.5 Tesla scanner (Siemens Magnetom Avanto, Erlangen, Germany). For anatomical reference, a 3D T1-weighted Magnetization Prepared Rapid Acquisition Gradient Echo (MPRAGE) image was acquired for each subject using the follow parameters: repetition time [TR]=1900 ms, echo time [TE]=3.37 ms, inversion time [TI]=1100 ms, flip angle=15◦, voxel size=1×1×1mm^3, matrix size = 192×256, number of axial slices=176. The structural images were recorded using a pulsed-gradient spin-echo planar imaging (EPI) (TR = 6700 ms, TE = 99 ms, voxel size = 1.9×1.9×2.5 mm^3, matrix size = 128×128, number of axial slices = 40) with two runs of diffusion gradients (b-value= 900 s/mm2) applied in 30 diffusion non-collinear directions and one unweighted image (i.e., b-value=0). In the same session subjects were asked to relax, keep closed eyes and not sleeping to acquire an 8-minutes rsfMRI by an EPI sequence with the following parameters: TR = 2500 ms, TE = 30ms, flip angle = 70°, voxel size = 3.1×3.1×2.5 mm^3, matrix size = 64×64, number of axial slices = 39,190 volumes.

rsfMRI data analysis and FC indexes calculation

The processing of the MPRAGE images included the removal of the skull and all the other non-brain tissues and therefore a visual inspection of each slice to verify that no brain portions were automatically excluded. The pre-processing of the rsfMRI consisted of: motion correction (Motion Correction FMRIB's Linear Image Registration Tool [MCFLIRT]–Jenkinson et al., 2002), spatial smoothing (FWHM=5 mm) and high-pass temporal filtering (cut off frequency=0.01 Hz). Single subject independent component analysis (ICA) was performed by MELODIC (Multivariate Exploratory Linear Optimized Decomposition into Independent Components, Filippini et al., 2009; Beckmann et al., 2004) while de-noising from motion artifacts and noisy components was obtained by FIX (Salimi-Khorshidi et al., 2014, Griffanti et al., 2014). Then, for each 4D single subject dataset, a two-step of registration was accomplished: a linear registration on the subject's MPRAGE using FLIRT (FMRIB's Linear Image Registration Tool [FLIRT]–Jenkinson and Smith, 2001; Jenkinson et al., 2002) followed by a non-linear registration on the MNI152 standard space done by FNIRT

(FMRIB's Non Linear Image Registration Tool [FNIRT]– Jenkinson et al., 2012). Finally, a resampling to $2\times2\times2$ mm^3 resolution of the registered images was executed.

RSNs were identified by spatial group ICA (MELODIC, Beckmann et al., 2005) with dimensionality set to 30 (Soddu et al., 2016, Elman et al., 2014, Meyer et al., 2013). Among them, the DMN, the LLN and the RLN were visually selected according to the RSN templates provided by Smith and colleagues (2009). The three chosen RSNs were divided into atomically separated clusters of voxels (Costantini et al., 2016) that were used as regions of interest (ROIs) both for functional and structural connectivity analyses.

Using the dual regression approach (Beckmann et al., 2009; Filippini et al., 2009) subject-specific spatial maps and time series associated to each ROI belonging to DMN, LLN and RLN were extracted. All components classified as non-noise (i.e. part of a RSN) were kept for being used as covariates in subsequent analysis. Subsequently, FC was assessed by two indexes between time series of each pair of ROIs belonging to the DMN, RLN and LLN: the full linear correlation (FC$_{full}$) and the partial linear correlation (FC$_{par}$) expressed both by Z-scores. Specifically, FC$_{full}$ was estimated by Pearson's correlation coefficient to estimate the global functional relationship between each pair of ROIs; FC$_{par}$, instead, was evaluated to quantify the direct functional relationship between two ROIs not mediated through the other areas, namely considering two ROIs A and B, the FC$_{par}$ was computed by correlating the time series associated to A and B, regressing out the time series associated to all the other ROIs.

Finally, first subject-specific FC$_{full}$ and FC$_{par}$ matrices were constructed for the DMN, the RLN and the LLN; then, group FC$_{full}$ matrix and group FC$_{par}$ matrix were built for each RSN evaluating the median FC values across the 19 subjects for each pair of ROIs.

DWI data analysis and SC index calculation

For all subjects, DW images were corrected for eddy current-induced distortions and head motion using the FSL package (http://www.fmrib.ox.ac.uk/fsl/), with the b=0 image of the first run as the reference image and the B-matrix rotated accordingly (Leemans and Jones, 2009). The distribution of the diffusion directions

(i.e. θ,Φ angles in spherical polar coordinates) including two principal directions to model crossing fibers, was obtained by a Bayesian estimation (Bayesian Estimation of Diffusion Parameters Obtained using Sampling Techniques [BEDPOSTX]–Behrens et al, 2003). Probabilistic tractography (Probabilistic Tracking with crossing fibres [PROBTRACX] –Behrens et al, 2007) was performed *between the* pairs of extracted ROIs in the DMN, LLN and RLN considered as seed and target regions. The following parameters were set: number of samples within each voxel=5000, curvature threshold=0.2, step length=0.5 mm, maximum number of steps allowed=2000. To correct the asymmetry of the method (Cao et al., 2013), namely the different result obtained if setting either ROI A or B as seed and target region, the following approach was used: probabilistic tracts were created setting A as seed and B as target and *viceversa*. These tracts were then registered to MNI standard space ($2 \times 2 \times 2$ mm^3 resolution) with the two-step registration process described above (i.e., linear first and non-linear in the end). Then, the two registered tracts were normalized to the respective maximum intensity and multiplied to obtain the joint probability map of the tract, namely a "product tract". In order to avoid false positive results, a threshold at 15% of the maximum connectivity value is usually applied (Khalsa et al., 2014), so a threshold of 2,25 % (i.e., 0.15×0.15) was applied to our "product tract". The number of voxels above threshold of the product tract was defined as the SC index for each pair of ROIs (Khalsa et al.,2014). Single subject SC matrix was constructed for each RSN, considering the SC indices obtained by all the pairs of ROIs; then, group SC matrix was computed as the median values across subjects for each RSN. Further, at group level, a group probabilistic atlas of the tracts was generated and labelled with the JHU-ICBM white-matter atlas by averaging the individual thresholded product tracts across subjects, after their binarization. Then, the probabilistic atlases were thresholded at 0.2 (i.e. only the voxels of the atlas in which at least the 20% of the subjects presented the tract were considered) and mapped with the JHU-ICBM white-matter atlas to identify well-known anatomical bundles.

FC and SC correlations

For each pair of ROIs in all the considered RSNs, the relationships between FC_{full} and SC and between FC_{par} and SC were evaluated using Spearman's correlations, due to the non-Gaussianity of the considered data samples.

The pipeline that led to this analysis is summarized in figure 3.1.
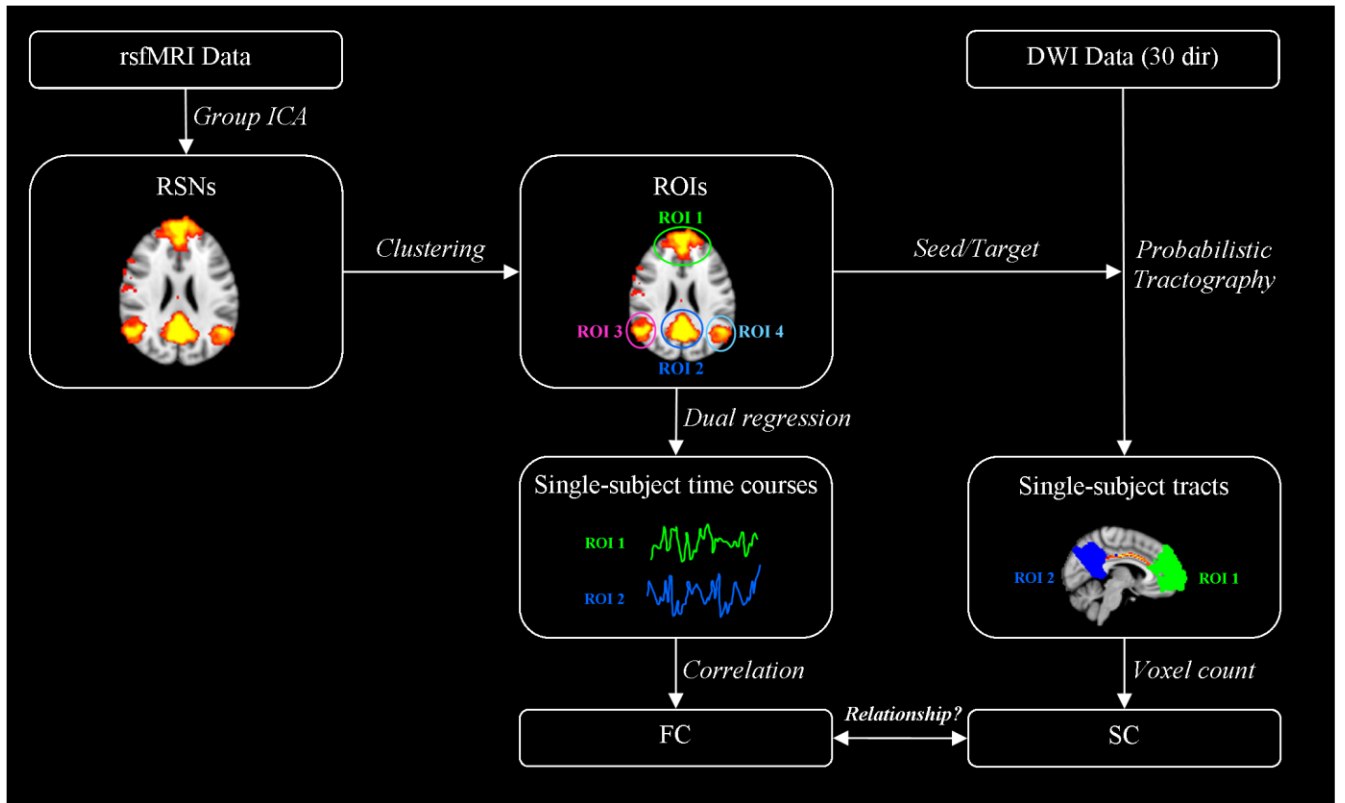
Figure 3.1 Method pipeline. Independent component analysis (ICA) to extrapolate resting state networks (RSNs). RSNs were split into their constitutive regions of interest (ROIs) and used to extract time series to evaluate functional connectivity (FC) indexes, defined as the full (FC_{full}) and partial (FC_{par}) correlation coefficients between them. The same ROIs were used as seed and target regions to perform probabilistic tractography. The number of voxels of the processed probabilistic tract volume was defined as structural connectivity (SC) index. The purpose of this method was to explore the relationship existing between FC and SC within the RSNs

3.1.2. Results

FC indexes

The splitting of DMN into anatomically separated clusters of voxels resulted in the medial prefrontal cortex (DMN_1), posterior cingulate cortex (DMN_2), right inferior parietal cortex (DMN_3) and left inferior parietal cortex (DMN_4) (Figure 3.2, panel A).

The split of the RLN resulted in the right superior frontal gyrus (RLN_1), right frontal cortex (RLN_2), right parietal cortex together with right temporal cortex (RLN_3) and right cingulate gyrus (RLN_4) (Figure 3.2, panel B). The LLN was divided in the left superior frontal gyrus (LLN_1), left frontal cortex (LLN_2), left parietal cortex together with left cingulate gyrus (LLN_3) and left temporal cortex (LLN_4) (Figure 3.2, panel C).
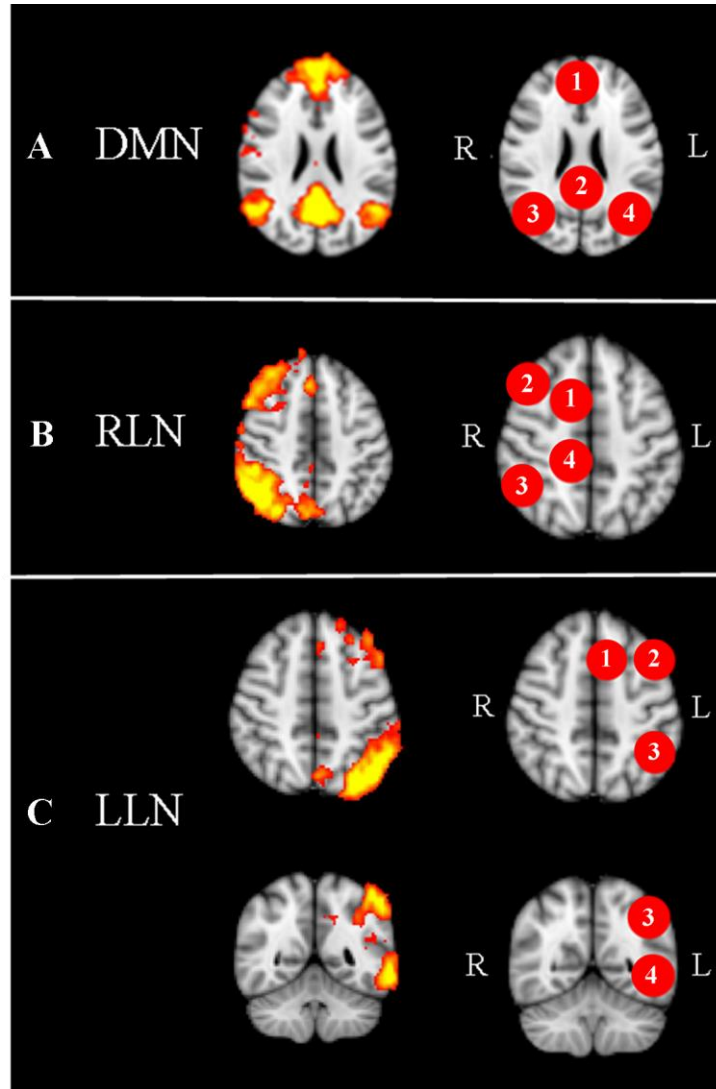
Figure 3.2 *Clustering of the default mode network (DMN, panel A), right lateral network (RLN, panel B) and left lateral network (LLN, panel C) according to the anatomical separation criterion*

Considering the full correlation at group level, FC_{full}, the DMN ROIs showed FC_{full} values (Z-scores) higher than 6 (Figure 3.3, panel A) with the highest value between the DMN_1 and the DMN_2. Within the RLN, and the LLN, instead, the highest FC_{full} index was found between the RLN_2 and the RLN_3 (Figure 3.3, panel B) and, similarly, between the LLN_2 and the LLN_3 (Figure 3.3, panel C).
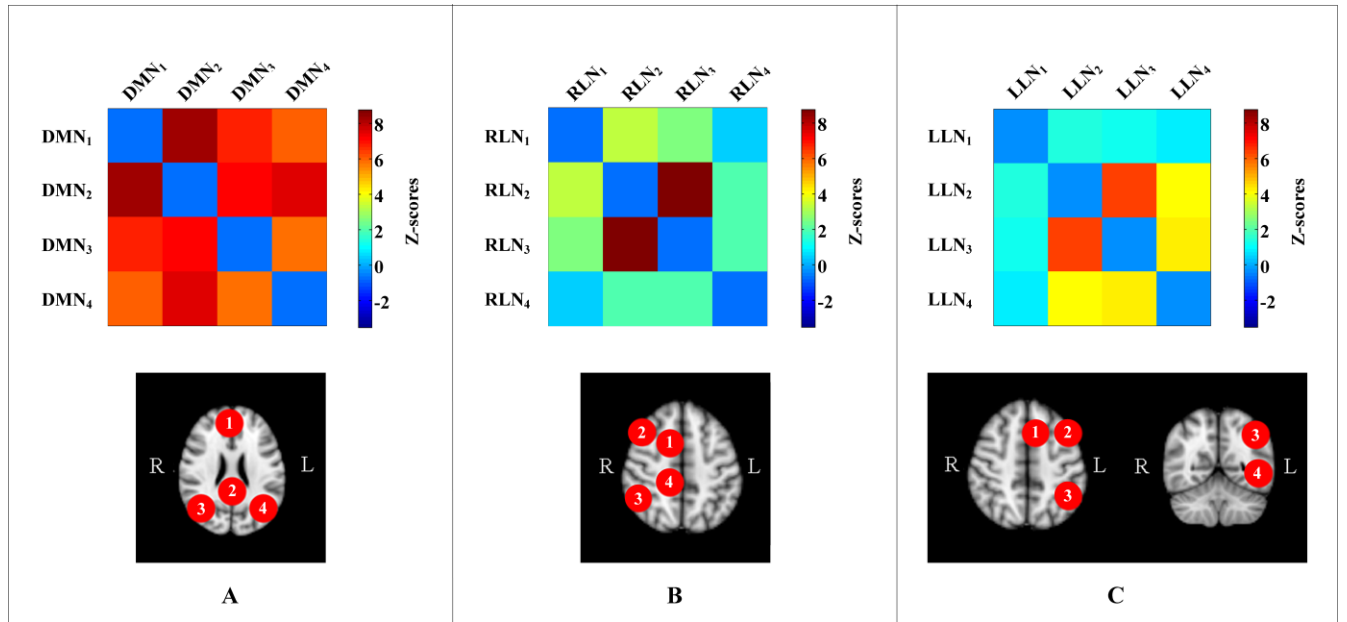
Figure 3.3 *Functional connectivity matrices. Group median full functional connectivity (FC_full) matrices expressed as Pearson correlation coefficient transformed into z-score, evaluated within the default mode network (DMN, panel A), right lateral network (RLN, panel B) and left lateral network (LLN, panel C)*

Considering group partial coreelation, FC_{par}, the highest value within the DMN was obtained between the DMN_2 and the DMN_4 (Figure 3.4, panel A). FC_{par} estimate within the two frontoparietal RSNs showed the link between the frontal ROIs (RLN_2 and LLN_2 respectively) with the parietal ones (RLN_3 and LLN_3 respectively) as the strongest one (Figure 3.4, panels B and C).

FC_{par} index values resulted lower than FC_{full} ones for all the pairs of ROIs.
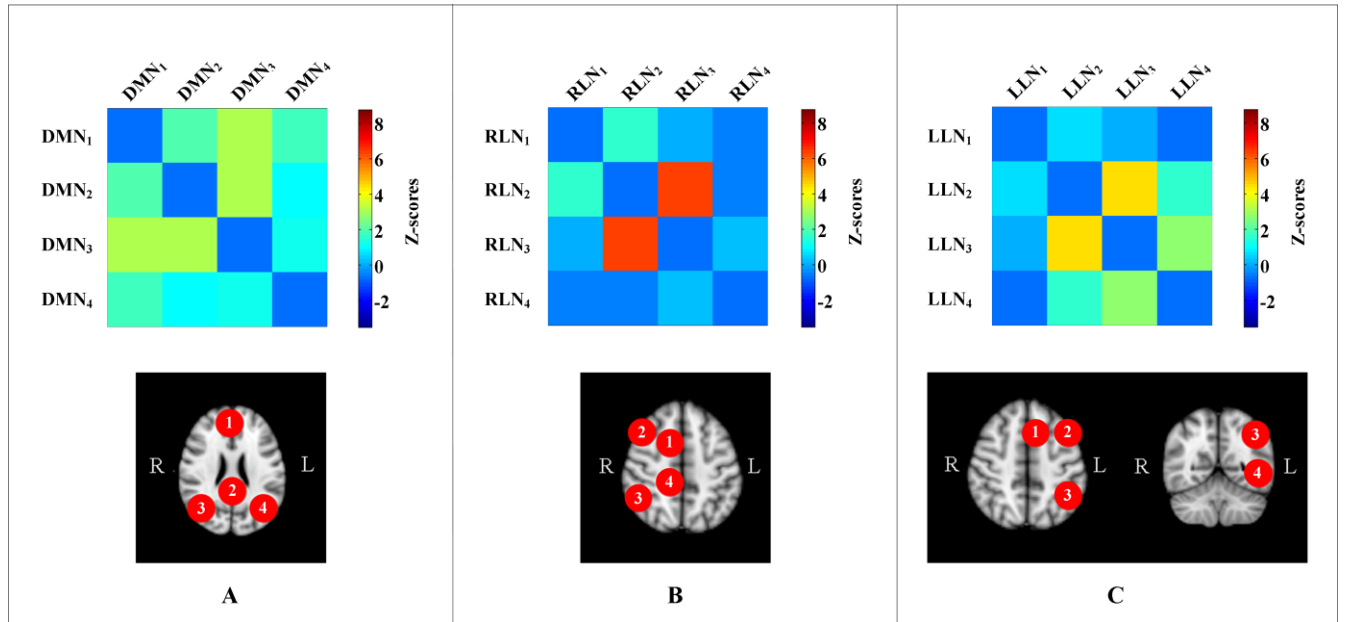
Figure 3.4 *Functional connectivity matrices. Group median partial functional connectivity (FC$_{par}$) matrices expressed as the linear partial correlation coefficient transformed into z-score, evaluated within the default mode network (DMN, panel A), right lateral network (RLN, panel B) and left lateral network (LLN, panel C)*

SC Index

Structural links between the considered RSNs were found between all the ROIs except for the connection between left superior frontal gyrus (LLN$_1$) and the left temporal cortex (LLN$_4$), which was not showed in 5 subjects, and the connection between the left inferior parietal cortex (DMN$_4$) and the right inferior parietal cortex (DMN$_3$), not found another subject.

At the group level, the highest SC value was found in the DMN between medial prefrontal cortex (DMN$_1$) and left inferior parietal cortex (DMN$_4$) (Figure 3.5, panel A) with a thresholded volume of the probabilistic tract equal to 524 voxels. In the RLN, the highest SC were observed between the right frontal cortex (RLN$_2$) and right parietal-temporal cortex (RLN$_3$) (i.e., 496), and between the right frontal cortex (RLN$_2$) and the right cingulate gyrus (RLN$_4$) (i.e., 425 voxels) (Figure 3.5, panel B). In LLN, the highest SC index (i.e., 491 voxels) was found between the left frontal cortex (LLN$_2$) and the left parietal cortex (LLN$_3$) (Figure 3.5, panel C). The SC indices were lower than 350 voxels for all the remaining pairs of ROIs.
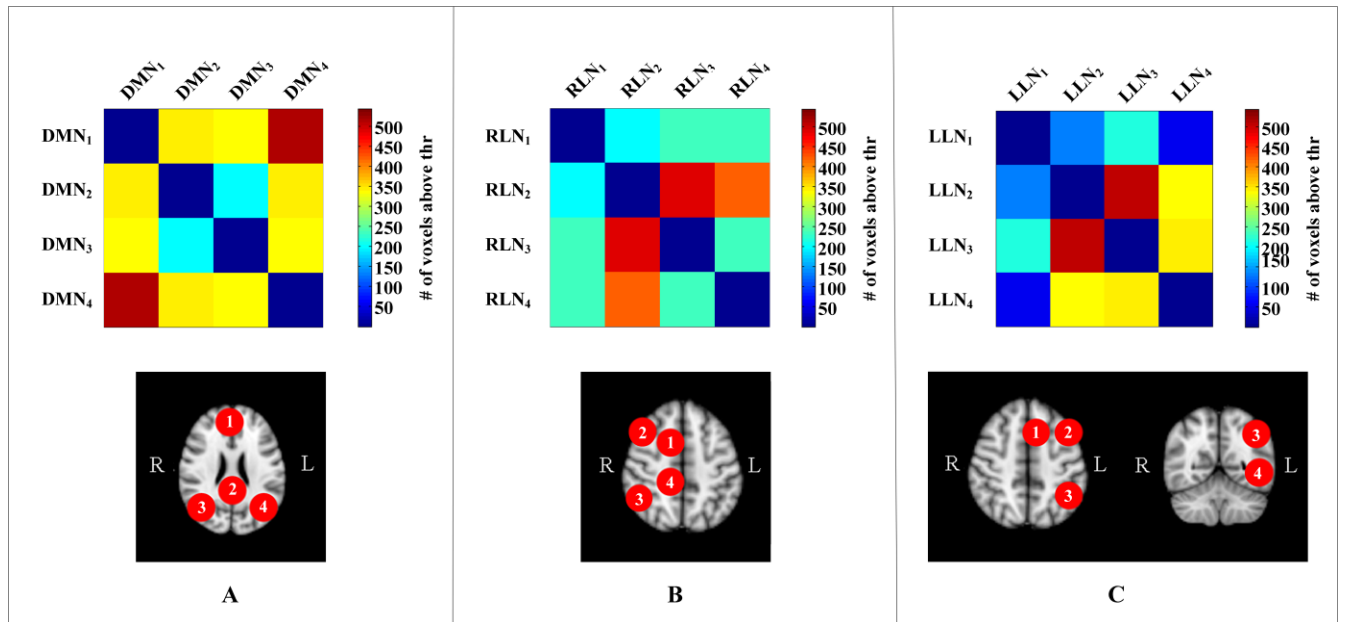
Figure 3.5 *Structural connectivity matrices. Group median structural connectivity (SC) matrices expressed as number of voxels above threshold, evaluated within the default mode network (DMN, panel A), right lateral network (RLN, panel B) and left lateral network (LLN, panel C)*

The mapping of the probabilistic tracts onto the JHU-ICBM white matter atlas (Table 3.1), both interhemispheric association and projection bundles were observed to connect the ROIs belonging to the DMN, the RLN and the LLN. Moreover, a mixture of well-known fiber bundles was found in correspondence of the probabilistic reconstructed tracts. Specifically, the left and the right cingulum were found to be the most relevant fascicles that connected DMN_1 and DMN_2. The Splenium of the corpus callosum and superior longitudinal fasciculus (SLF) were involved instead in DMN_3 and DMN_4 structural link. The ipsilateral SLF and inferior fronto-occipital fasciculus (IFOF) were found to be the bundles that mostly connected DMN_1 with DMN_3 and DMN_1 with DMN_4. RLN_2 and RLN_3 were found to be connected by almost only (93%) the right SLF. Similarly, the left SLF and IFOF linked the LLN_2 and LLN_3. Moreover, the left SLF was observed to be the most relevant fascicle involved in LLN_2-LLN_4 and LLN_3-LLN_4 connections.

Pairs of ROIs	Bundles belonging to the group atlas tract [% of V]													V [# of voxels]
	ATR		CIN		CC			IFOF		ILF		SLF		
	l	r	l	r	g	b	s	l	r	l	r	l	r	
DMN$_1$ ↔ DMN$_2$	-	-	54	36	<10	-	<5	-	-	-	-	-	-	576
DMN$_1$ ↔ DMN$_3$	-	-	-	-	-	-	-	-	19	-	<5	-	69	309
DMN$_1$ ↔ DMN$_4$	11	-	-	-	<5	-	-	37	-	15	-	26	-	827
DMN$_2$ ↔ DMN$_3$	-	-	-	-	-	-	<5	-	11	-	<10	-	65	303
DMN$_2$ ↔ DMN$_4$	<10	-	<5	-	-	-	37	<5	-	17	-	18	-	690
DMN$_3$ ↔ DMN$_4$	<10	<5	-	-	-	<5	42	-	<5	<5	<5	14	14	696
RLN$_1$ ↔ RLN$_2$	-	13	-	19	<5	<5	-	-	-	-	-	-	-	292
RLN$_1$ ↔ RLN$_3$	-	<10	-	44	-	-	-	-	-	-	-	-	24	374
RLN$_1$ ↔ RLN$_4$	-	-	-	89	<5	-	-	-	-	-	-	-	-	421
RLN$_2$ ↔ RLN$_3$	-	-	-	-	-	-	-	-	<10	-	-	-	93	784
RLN$_2$ ↔ RLN$_4$	-	19	-	13	-	-	16	-	48	-	-	-	<5	728
RLN$_3$ ↔ RLN$_4$	-	<5	<10	37	-	-	40	-	-	-	-	-	-	425
LLN$_1$ ↔ LLN$_2$	13	-	-	-	-	-	-	-	-	-	-	24	-	172
LLN$_1$ ↔ LLN$_3$	-	-	69	-	-	-	-	-	-	-	-	<10	-	398
LLN$_1$ ↔ LLN$_4$	<5	-	-	-	-	-	-	-	-	-		60	-	60
LLN$_2$ ↔ LLN$_3$	<5	-	-	-	-	-	-	23	-	-	-	72	-	662
LLN$_2$ ↔ LLN$_4$	-	-	-	-	-	-	-	-	-	-	-	98	-	527
LLN$_3$ ↔ LLN$_4$	-	-	-	-	-	-	-	-	-	<5	-	94	-	675

Table 3.1 *For each pair of regions of interest (ROIs) of the default mode network (DMN), right lateral network (RLN) and left lateral network (LLN) a group probabilistic atlas was constructed as the group average probabilistic tract. Then, the white matter bundles constituting each atlas tract were mapped using the JHU-ICBM white-matter atlas. The fascicles associated to the group probabilistic atlas tracts obtained between all the pair of ROIs and the percentage of the volume of the involved bundles with respect to the group atlas tract volume (V, expressed as number of voxels) are reported*

ATR = anterior thalamic radiation; CC = corpus callosum (g = genu, b = body, s = splenium); IFOF = inferior frontal-occipital fasciculus; ILF = inferior longitudinal fasciculus; SLF = superior longitudinal fasciculus; l= left; r= right.

FC and SC correlations

Focusing on FC$_{full}$-SC correlation results, a non-significant correlation was found within the DMN (r=0.01, p=0.916). On the other hand, a positive significant FC$_{full}$-SC correlation was observed within the RLN (r=0.214, p=0.022) and the LLN (r=0.489, p<0.0001).

The FC$_{par}$-SC correlation analysis led to similar values of FC$_{full}$-SC ones in the RLN (r=0.228, p=0.015) and in the LLN (r=0.466, p<0.0001). Within the DMN, even if still not-significant, the FC$_{par}$-SC correlation was found to be higher than the FC$_{full}$-SC one (r=-0.015, p=0.878).

3.1.3. Discussion

The present work shows a detailed analysis of brain connectivity, by considering both FC and SC within three specific RSNs which are commonly investigated in rsfMRI group studies (van den Heuvel et al., 2009; Damoiseaux et al., 2006; Beckmann et al., 2005), namely the DMN, the RLN and the LLN. For different reasons, these networks are considered robust demonstration of functional connectivity: specifically, the DMN is highly connected at rest and remains always active as background when performing tasks (Greicius et al. 2003). The two lateralized fronto-parietal networks, instead, overlap to brain areas involved in specific cognitive paradigms such as memory, language and perception (Pievani et al., 2014).

From a methodological perspective, the novelty of this work includes two aspects: firstly, the approach used for overcoming the issue of the asymmetry when computing probabilistic tracts differently according to the seed point considered. Secondly the idea of correlating the two functional metrics with the structural one. Furthermore, the problem of a parcellation of the RSNs extracted by low-dimensional spatial ICA has been addressed by several authors; e.g., by incrementing the number of extracted independent components in high-dimensional ICA (Abou-Elseoud et al. 2010 and 2011; Tohka et al. 2008; Cole et al. 2010).

In this study, RSNs were extracted by the standard low-dimensional ICA and then split into ROIs by exploiting their anatomical segregation (Costantini et al., 2016), with the advantage to obtain a parcellation of the RSNs with a direct readability in terms of functionally specialized and anatomically segregated areas,

diversely from the blind parcellation furnished by high-dimensional ICA (Dipasquale et al., 2015). For the clustering of the RSNs a data-driven approach was used, and this was demonstrated by the asymmetry showed in the two lateral networks. In fact, within the LLN the temporal cortex was separated from the parietal one (LLN_4 and LLN_3 respectively) while for the RLN both these areas were included in the RLN_3 ROI. This result may reflect the well-known differences between left and right hemisphere functioning and roles: right fronto-parietal regions underlie visuospatial orienting attention (Rushworth et al., 2007; Shulman et al., 2010; Rossi et al., 2014), while left fronto-parietal areas are dominant in language comprehension and involuntary orienting, namely attention in relation to limb movements (Rushworth et al., 2007; Rossi et al., 2014; Zhou et al.,2014). This difference was also shown in the FC patterns and SC group matrices.

For each pair of ROIs, the FC_{par} values resulted lower than the FC_{full} ones since, by the partial correlation between two generic ROIs A and B furnished by multivariate analysis, we regressed out the contribution of the all remaining ROIs from the computation of the functional relationship between them. Therefore, FC_{par} better fits a parallelism with the SC index, which account for direct anatomical A to B connections. Differently from FC_{full}, the highest FC_{par} value within the DMN was observed between DMN_2 and DMN_4, rather than between DMN_1 and DMN_2. This result highlights that the functional communication between DMN_1 and DMN_2 is likely mediated by other structures, further supporting the hypothesis of the highly integrative nature of the DMN. On the other hand, for both the frontoparietal networks, the highest FC_{full} and FC_{par} values were observed between the frontal ROIs and the parietal ones (RLN_2-RLN_3 and LLN_2-LLN_3 respectively), underlying the strong direct functional connection between these areas.

Concerning structural connections, the probabilistic tractography detected remarkable bundles between all the pairs of the considered RSN ROIs. Left and right cingulum were found to be the most important pathways linking the medial prefrontal cortex (DMN_1) and the posterior cingulate cortex (DMN_2), while in both the fronto-parietal networks the important role of the SLF in connecting the frontal and parietal cortex was observed. These findings agree with a previous study that investigated structural connectivity within

the RSNs with DTI (Van den Heuvel et al., 2009) and support the suitability of probabilistic tractography to investigate the structural connections within the RSNs. The group SC analyses led to high index values either when a predominant fasciculus connected the considered ROIs (e.g. DMN_1-DMN_2 connected by left and right cingulum, RLN_2-RLN_3 connected by right SLF) or when a wide ensemble of tracts was involved (e.g. RLN_2-RLN_4 connection). Low SC values, instead, may be ascribed to the small ROI dimensions. It is intuitive to infer that, since fiber tracking imposes the seed and target regions as waypoints, if a ROI is small, the reconstructed probabilistic tract will be thin, even if the associated bundle is anatomically thick. This would explain why RLN_1 and LLN_1 did not seem strongly linked to the other ROIs belonging to the same RSN, even if remarkable fascicles were involved (Table 1). Notably, clearly different SC values were observed between the contralateral pairs DMN_1-DMN_3 and DMN_1-DMN_4, (higher for DMN_1-DMN4), in accordance with the left-right asymmetry of the SLF volume (Wang et al., 2016).

Despite the intuitive notion that any functional coordination should be mediated by connecting fibers, the correlation analysis underlined that high FC_{full} between different gray matter regions does not necessarily imply high SC (Honey et al. 2009; van den Heuvel 2009), since pathways out of the focus of our SC analyses may be involved. Specifically, our findings confirmed the highly integrative nature of the DMN due to high FC_{full} and SC values, but, contrary to what could be intuitively expected, no significant correlation was found between FC_{full} and SC within it. This result could be justified by the existence of associative and indirect paths, such as polysynaptic structures, which connect gray matter regions but are not detectable with tractography, thus, contributing to FC_{full} but not to SC values (Honey et al. 2009). Indeed, considering the FC_{par}-SC rho and p values within the DMN and comparing them with the respective FC_{full}-SC correlation results, we observed that even if a non-significant correlation was found in both cases, the correlation values improved when FC_{par} was considered. This may be in keeping with the hypothesis that the ROIs of the DMN do not communicate only directly between each other but that the communication between them is also mediated by different regions (Bucker et al., 2008). This suggests that the DMN is a highly integrative RSN, interfering with whole brain activity. The remarkable bundles involved in the connections of the DMN ROI

pairs underlined in fact that this functionally robust RSN is also highly structurally connected. Therefore, the absence of a significant correlation between the FC and the SC indices cannot be considered alone a condition that determine the absence of a relationship between the functional and structural connections.

On the other hand, a positive significant correlation between FC_{full} and SC and between FC_{par} and SC was obtained within the two fronto-parietal RSNs. The lower dispersion of the data within the RLN with respect to LLN may be justified by the tiny size of two out of four identified ROIs that influence the probabilistic tractography output. In contrast to the LLN that was split in three large clusters of voxels of comparable size (LLN_2, LLN_3, LLN_4) and in just one smaller one (LLN_1), the RLN was divided into two large (RLN_2 and RLN_3) and two small clusters (RLN_1 and RLN_4). This resulted in only one pair of ROIs that was characterized by both a high FC and a high SC (RLN_2-RLN_3) and in a remaining group of ROI pairs that showed lower FC and SC values. The robust positive significant correlations between FC_{full} and SC and between FC_{par} and SC observed within the LLN suggest that LLN is a highly function-specific network and, hence, direct structural links between its ROIs may reflect the functional communication between them. Since the relationship existing between function and structure is not always straightforward, the FC_{full}-SC and FC_{par}-SC correlation investigation can provide further information about the RSNs.

We would like to point out that this work shows an example of coexistence of segregation and integration process within the human brain (Deco et al., 2015). The extracted RSNs, indeed, are per se a demonstration of segregation in terms of differentiation within RSN specific spatial patterns of different time dynamics. On the other hand, considering the structural connections and the functional correlations highlighted within each RSN, are related to the integration of separated areas. Moreover, considering the partial correlation among the nodes of each RSN implies investigating the segregation of two single nodes regardless the contribution of the others; on the other hand, looking at the full correlation among the nodes of each RSN leads to consider the integration between different cortical areas that need to interact for accomplishing a specific task. With our work of integration between structural and functional measurements we aimed at

understanding how much the white matter structures can reflect the functional interactions. However, this was limited by two main factors: firstly, the dynamic nature of the functional activity obviously clash the static nature of the structural analysis, leading to difficulties in understanding the real support of structure to function; secondly, the open challenge of isolating the external (or internal) stimuli to understand the real cause of the activation of specific brain regions supported by specific white matter architecture. Nevertheless, the proposed method presented some limitations mostly related to the diffusion data analysis.

First, probabilistic tractography requires a seed and a target region definition. Considering two ROIs (ROI A and ROI B), the reconstructed probabilistic tract obtained imposing A as seed and B as target slightly differs from the probabilistic tract obtained setting B as seed and A as target. However, there is no physiological reason to privilege one way with respect to the other one and hence, in order to overcome this mismatch, in this exploratory study the probabilistic tracts were generated in both directions and processed in order to obtain a single SC value for each pair of ROIs.

Then, quantifying the strength of a WM link is not trivial. Defining the probabilistic score as SC index is tempting but the probability of connection does not exactly represent the strength of connection (Jbabdi et al., 2011). On the other hand, the number of voxels above threshold that we adopted in this study represents the probabilistic tract volume expressed in voxels. Although it does not always mirror the strength of the connection due to its dependence on the distance, it is linked to the probabilistic tract thickness (Khalsa et al., 2014). Furthermore, by considering the thresholded probabilistic tract, false positives are excluded, or at least reduced, before the SC computation.

Finally, we have to consider that the study was performed with data obtained from a 1.5T scanner while recent researches predominantly use 3T scanners due to the higher signal to noise ratio. However, given that1.5T scanners are still widely used in clinical settings and that the final aim of clinical research is translation into clinical practice, it is important to test methods for investigating functional and structural connectivity also with these data.

Our combined analysis demonstrated the need of studying the brain as a complex but unique entity exploiting both functional and structural information not only for better understanding the healthy brain but also to shed light on pathological conditions. Specifically, in the clinical context of neurological rehabilitation, in which progresses rely on neuronal plasticity, FC and SC combined analysis may be useful for the patient follow up, in order to assess the efficacy of the treatment whose aim is preventing the worsening of symptoms, allowing to preserve the patient abilities (Cramer et al., 2011; Scaccianoce et al., 2016). Indeed, monitoring the clinical condition with quantitative approaches can have substantial translational impact, especially when used in conjunction with measures of neuropsychological function (Irimia et al., 2014).

In conclusion, although the absence of FC-SC correlation should not be necessarily interpreted as a lack of relationship between functional synergies and structural connections, its evaluation can provide additional information about the RSN connectivity. Furthermore, the evaluation of both FC_{full}-SC and FC_{par}-SC correlations allows to highlight the degree to which indirect pathways may influence the RSN connectivity. Potentially, the proposed method could be extended also to other RSNs, according to the clinical question we are interested in. The high complexity of human brain requires, indeed, an approach as wide as possible in its functioning investigations, since considering only an aspect would be restrictive.

4. Artifact identification and removal to improve tractography reconstruction

In this chapter the following works are summarized: "A Fast and Effective Strategy for Artifact Identification and Signal Restoring with HARDI data" presented at the International Society of Magnetic Resonance in Medicine, Singapore, Scaccianoce et al., 2016; "Mapping residual along tract: a technical note on a fast and effective quality control for tract specific measurements" – Scaccianoce et al., 2018; "Mapping residuals along tracts: an effective quality control approach for tract specific measurements" presented at International Society of Magnetic Resonance in Medicine, Toronto, Scaccianoce et al., 2015.

4.1. The issue of artifacts and their identification based on signal outlier detection approach Quality control pipeline to identify corrupted fiber bundles

This thesis already stressed the fast grow of tractography based on diffusion-weighted imaging (DWI) form the first seminal works (Le Bihan et al., 1986; Turner et al., 1990; Basser et al., 1994; Catani et al., 2002), next extending to the clinical environment to assess the integrity of the cerebral bundles by means of diffusion-derived indexes, contributing to the diagnosis of several neurological pathologies which involve WM architecture in a non-invasive way (MCGrath et al., 2013; Catani et al., 2008; Doricchi et al., 2008).

For this reason, the amount of DWI data acquired for both research and clinical purpose is constantly growing, making more and more difficult (if not impossible) a visual inspection of all the produced DWI datasets. Furthermore, the sake for higher quality tractography reconstructions and the need to disambiguate fiber direction where non-univocal (the well-known "fiber-crossing" problem) has pushed towards acquisition of more and more directions, under the general paradigm of high angular resolution diffusion imaging (HARDI) (Tuch et al., 2002). Consequently, artifact detection on all DWI images relevant to the many HARDI directions is often a challenge, even for the more expert researchers or physicians. Such artifacts are caused most times by head movements recorded during the scan session (Alhamud et al., 2015;

Zwiers, 2010; Pannek et al., 2012). Moreover, the DWI sensitivity to microscopic changes makes the diffusion images particularly sensitive also to tiny movements, related both to scanner issues (e..g., instrumental vibration, Gallichan et al., 2010) and physiological movements (e.g., cardiac pulsation and breathing, Nunes et al., 2005, Chung et al., 2010; Chang et al., 2005). Procedures for artifact detection and correction during DWI pre-processing (e.g. eddy current corrections, Andersson and Sotiropoulos, 2015) already exist, but sometimes they are not sufficient to identify and remove all of them. Consequently, within diffusion images often survive artifacts displayed as localized signal dropouts (Benner et al., 2011; Andresson and Sotiropoulos, 2014), especially in those brain regions affected by cardiac pulsation, such as the cerebellum as well as genu and splenium of the corpus callosum (Walker et al, 2011). This leads to biased estimations of the diffusion parameters, which obviously negatively affects the relevant measurements (Pannek et al., 2011; Walker et al., 2011) and ultimately limits the diagnostic value of tractography. Hence, accurate artifact detection techniques are needed even after the pre-processing stage to detect those artifacts that standard procedures fail to identify.

One of these techniques was proposed in 2005 by Chang and colleagues, who developed a voxel-wise method for a robust estimation of the diffusion tensor, trying to eliminate the physiological noise that always affects the DWI scans. The main idea is identifying the potential outliers by reiterating the weighted least-squares (LS) regression while excluding them, thus converging to an outlier-free fitting. The LS regression model, indeed, considers only a very specific signal variability that is caused by thermal noise that has Gaussian distribution. Signal variability produced by physiologic noise (e.g., cardiac pulsation), instead, does not follow any parametric distribution. One of the possibility to address this problem is using robust estimators (Mangin et al., 2002), were considered by Chang et al. (2005). Their algorithm is called RESTORE (Robust Estimation of Tensor by Outlier Detection) and its flow diagram is shown in Figure 4.1.
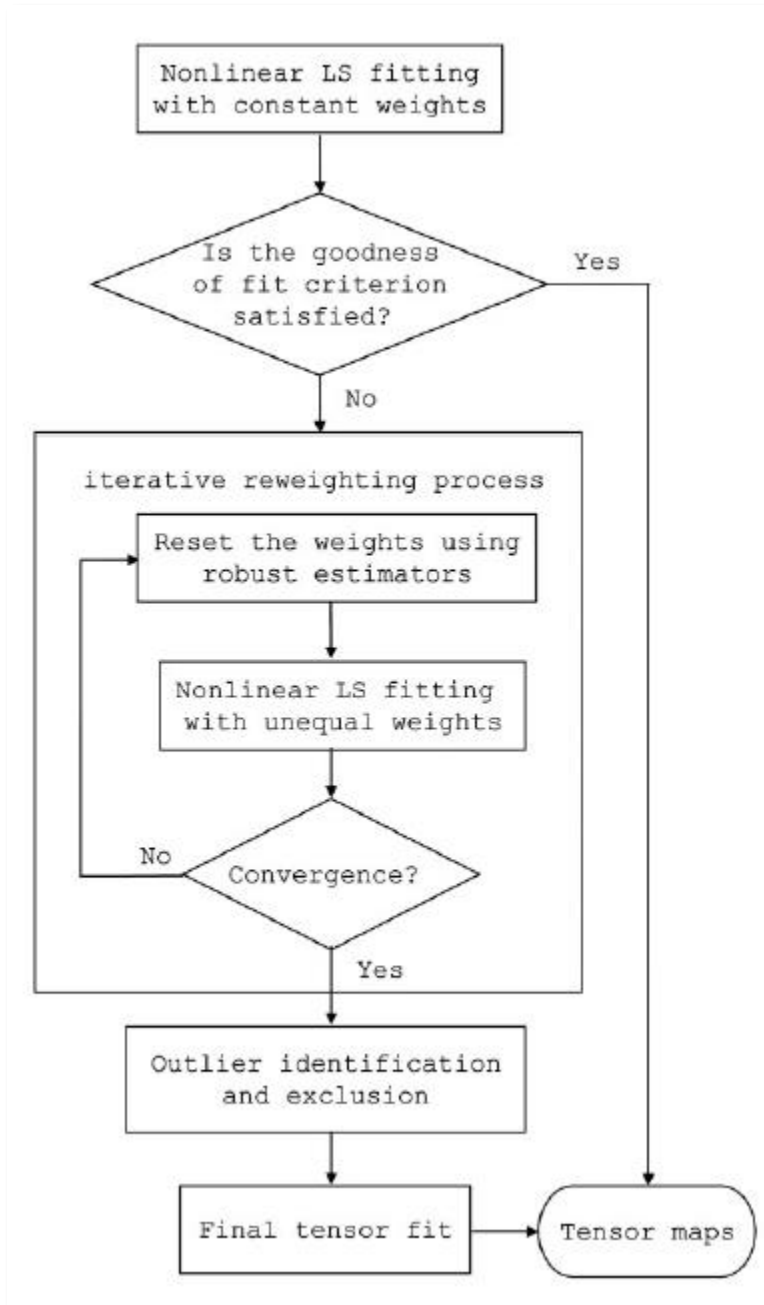
Figure 4.1 *Flow diagram of RESTORE algorithm – Chang et al., 2005*

Although RESTORE was demonstrated to be an effective solution in reducing physiological noise (Chang et al., 2012), it was shown that it leads to incorrect solutions when it excludes too many data points and

leads to the calculation of "ill-defined" B-matrices. To address this issue, Chang and colleagues (2012) improved RESTORE algorithm adding two constraints to avoid the non-convergence of the problem: 1) the exclusion only of negative maximum residuals, since physiological noise leads to signal drops rather than increases; 2) the check at each iteration of the goodness of fit criterion (Figure 4.2). This new method was called *informed* RESTORE and currently is a frequently applied tool to remove physiological artifacts in datasets acquired with low redundancy (less than 30-40 DWI directions) (Chang et al., 2012).
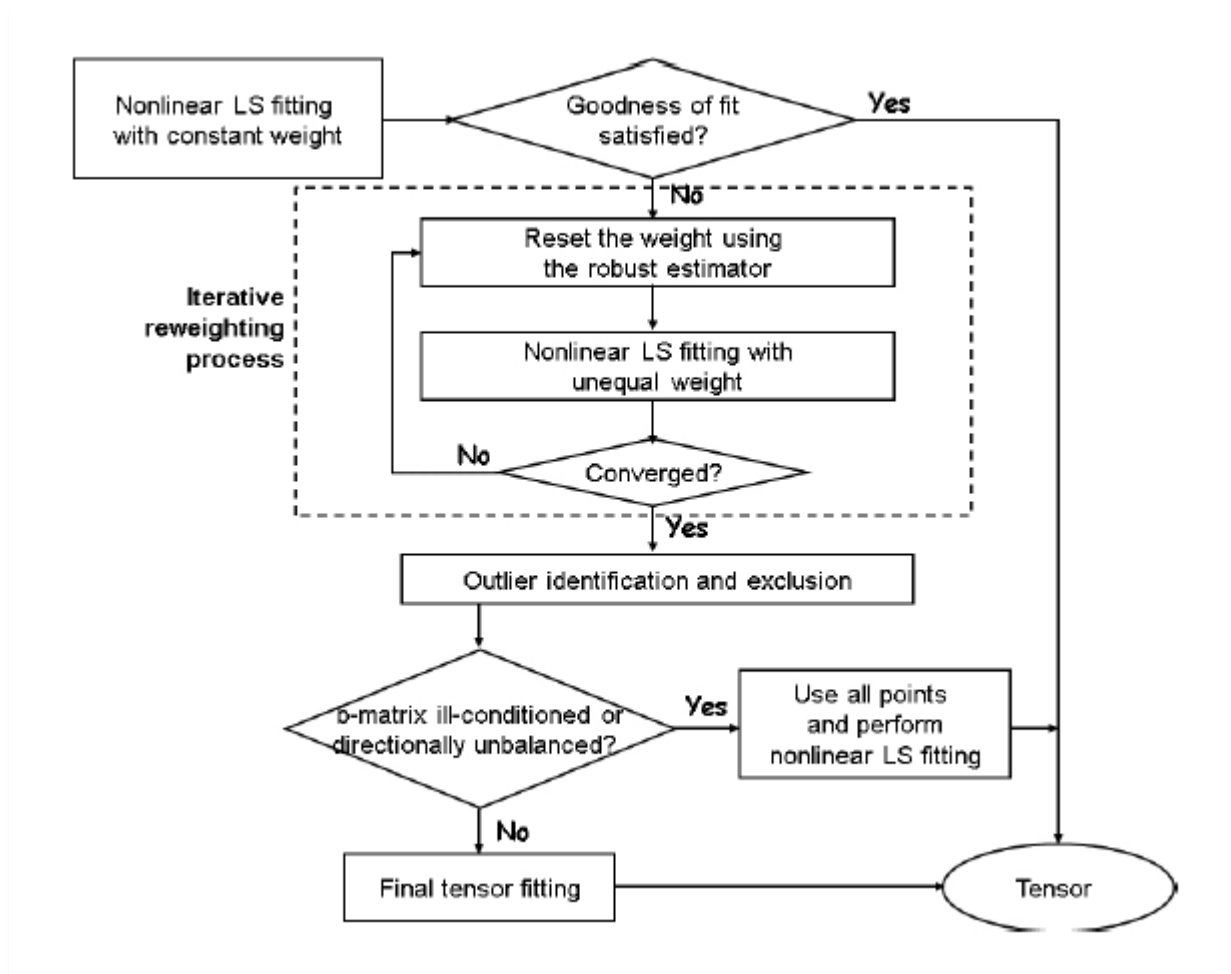
Figure 4.2 *Flow diagram of informed RESTORE algorithm – Chang et al., 2012*

This successful idea was later extended by Pannek and colleagues (2012) and ameliorated to address DW HARDI and high b-values datasets. They developed a new voxel-wise algorithm called HOMOR (Higher Order Model Outlier Rejection) based on the residual of the spherical harmonic (SH) fit at a maximum harmonic degree of 4. The main assumption is that, even in the presence of artifacts, DW signal experiences smooth variation as a function of orientation and does not show angular frequencies that would lead to a SH residual higher than 3 times the signal standard deviation (Pannek et al., 2012). Compared to RESTORE and *informed* RESTORE, this method was demonstrated to be particularly effective in brain areas with crossing, bending and fanning fibers.

More recently, another solution was proposed for diffusion artifacts by Andersson and colleagues (2016) who suggest replacing an affected slice (i.e., slices showing a lower intensity with respect to adjacent ones) by a non-parametric prediction. Specifically, they model diffusion signal distortions by explicitly estimating the eddy currents (ECs), the susceptibility variation map, and head movements. This part of a physical model of the expected values goes beyond the focus of this presentation. Conversely, of interest to us is the approach used in eliminating outliers by model interpolation, as shown in the pseudo-code of Figure 4.3. The algorithm considers data as a Gaussian process (Rasmussen and Williams, 2006), which should be smooth with changes in the diffusion direction and the b-value (in case more than one b-shall was considered). The Gaussian process covariance function can be either defined by marginal likelihood maximization (Rasmussen and Williams, 2006) or by leave-one-out methods (Sundararajan and Sathiya Keerthi, 2001) over a set of observation (i.e., the training data or the trains set). As shown in Figure 4.3, the iterative EC, susceptibility, and movement estimate and correction is refined by constructing a slice-by-slice library of outliers falling outside the current model confidence interval, fixed by the Gaussian process. Model updates are performed leaving out the outliers (i.e., out or range slices, for a given direction and a given b-value); nonetheless, outliers can be readmitted if within range after the model corrections in a subsequent iteration. Being a slice-wise approach, Andersson and colleagues denoted the dropout as a summary statistic upon the entire slice. Notably, this method is implemented in a unique correction process

that takes into consideration both the eddy current-induced (EC) distortions and the movement artifacts, to

avoid that one correction badly influences the other.

```
Initialize:
Make an empty list of outlier slices
Put all original slices into list of used slices
for Every eddy iteration do
    for Every slice in every volume do
        Make prediction based on used slices
        Calculate difference between prediction and original slice
        if Difference indicate an outlier then
            if Slice is already in outlier list then
            |   Replace used slice by prediction
            else
                Make new prediction without current volume
                Replace used slice by new prediction
                Add original slice to outlier list
            end
        else
            if slice is on outlier list then
                Put original slice back into used slices
                Remove slice from outlier list
            end
    end
    Calculate difference between prediction and used slice
    Use difference to update movement and EC parameters
end
```

Figure 4.3 *Pseudo-code for implementing the algorithm for slice-wise outlier detection, data replacement and eddy current-induced distortion correction performed in the same framework– Andersson et al., 2016*

Based on the above-mentioned algorithms, in the next paragraph we propose a novel pipeline for outlier

identification and correction of HARDI datasets where the corrupted data is first identified as outlier and

then regenerated in framework based on signal decomposition using spherical harmonics, whose detailed presentation was provided in the paragraph "High Angular Resolution Diffusion Imaging and new models beyond DTI" of Chapter 1. Right after, we show a fast and effective quality control (QC) of tract specific measurements by mapping residuals along tracts in group DW data analyses.

4.2. Artifact Identification and Signal Restoring in HARDI data

4.2.1. Materials and methods

Subject population

In this analysis, fifteen healthy voluntary subjects (HSs) were enrolled at NATBRAINLAB of King's College London (London, UK).

MRI acquisition protocol and DW analysis

HARDI data were acquired in a single shell using a 3T GE HDx system (General Electric, Milwaukee, WI, USA) with the following parameters: voxel size 2.4x2.4x2.4 mm, slices 60, b-value 3000 s/mm2, 60 diffusion-weighted directions and 7 non-diffusion weighted volumes. DW images of all subjects were corrected for eddy current distortion using the EDDY packet of FSL software (fsl.fmrib.ox.ac.uk/fsl/fslwiki/EDDY). A brain mask was created for each subject to exclude non-brain tissues from the further analysis.

Artifact identification and removal

The steps described in this paragraph were performed using a home-written Matlab code (R2013a, www.mathworks.com).

For each subject, HARDI data were fitted by spherical harmonics of order 8 (SH8) to model complex fiber configuration such as the crossing fibers (Decoteaux et al., 2009). Then the following steps were applied for for creating mean residual map and outlier mask:

1) Residuals were calculated slice-wise (i.e., considering different z values for the same x-y plane) as the absolute value of the difference between the actual HARDI signal and SH8 fitting;

2) the mean value among the residuals was calculated for the considered slice;

3) a residual map was obtained for considering all the computed mean residual values of the slices in each single direction (Figure 4.4, plot on the left side of the panel);

4) a threshold for detecting outliers considering the same slice across the different diffusion directions was computed as: threshold=Q3+1.5*IQR (adapted from Leemans et al., 2008), where Q3 is the 75th percentile and IQR is the interquartile range computed on the residuals;

5) if the mean residual was > then the threshold, the slice in that particular direction was considered outliers (Figure 4.4, plot on the right side of the panel).
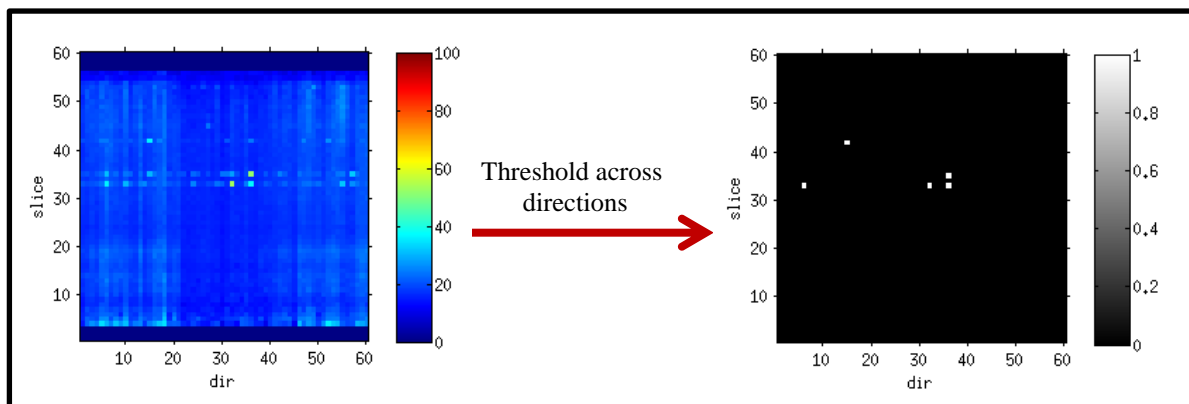
Figure 4.4 *Mean Residual maps (left side) of a single subjet and binary outlier mask (right side) after the application of the threshold. White dots indicate the corrupted slice.*

Finally, corrupted signals were regenerated using new SH coefficients obtained by SH decomposition performed this time without outlier directions. While the identification of outliers was done, as said above, through an 8th order SH fitting, an SH at order 6 was used when regenerating slices of corrupted direction, in order to improve regularization in corrupted regions.

Visual inspection of the datasets was done slice by slice in z-direction by two operators, twice, starting from the top to the bottom of the brain and *viceversa*.

Simulation on an artifact-free dataset was performed to verify the efficacy of the method. Specifically, an uncorrupted slice (i.e., a piece of data at given z position and given diffusion direction) was randomly selected and set to 0 as signal intensity (i.e., deleted). Then the above-mentioned pipeline was applied to the corrupted dataset to regenerate the missing slices. Spherical deconvolution (SD) was run to estimate fiber orientation distribution (FOD) peaks using StarTrack (www.mr-startrack.com) with the following parameters: alpha=1.5, number of iterations=200; damped Richardson Lucy algorithm; absolute threshold=0.04; damping curve profile=8).

4.2.2. Results

As a result, the visual inspection after preprocessing of the diffusion dataset identified 2 subjects with obvious and significant artefacts along different DW directions.

In Figures 4.5 and 4.6, the two examples of artifacts are shown in sagittal and axial view along with their corrections in the same view for comparison purpose. Figure 4.5a illustrates the outlier mask in which one of the outlier value is identified and its location displayed in sagittal and axial views before (Fig. 4.5b) and after (Fig. 4.5c) correction. Similar results are show in figure 4.6 a, b and c.

In Figure 4.7, the deleted slice is shown as original (i.e., "expected correction") and replaced (i.e., "corrected") with our pipeline.

Few seconds were required to correct each subject on normal laptop.

Through FOD estimate we verified that the regenerated slice had the same peak amplitude and fiber orientation as the actual slice (Fig 4.8).
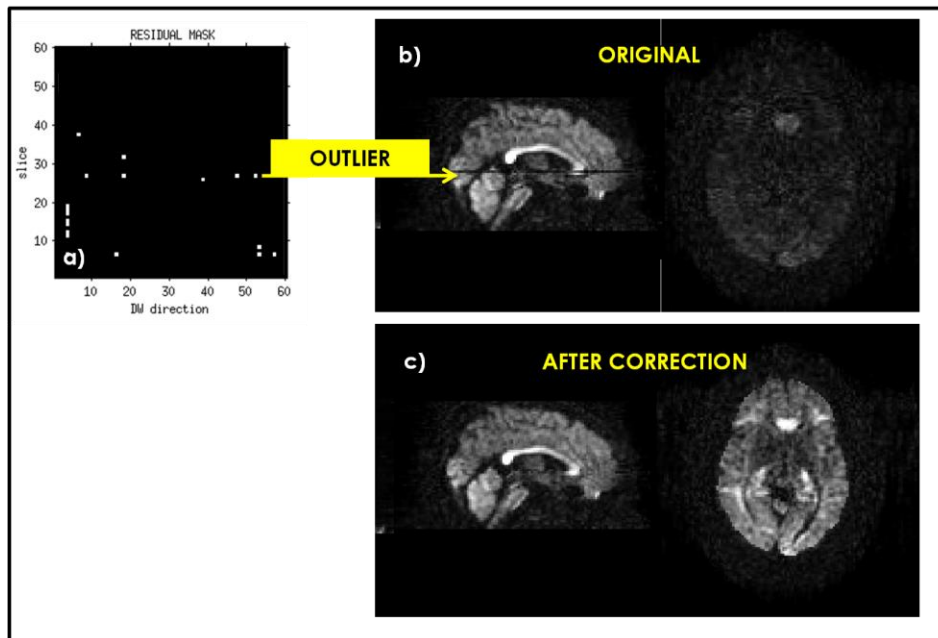
Figure 4.5 *Panel a) illustrates the outlier mask in which one of the outlier value is identified and its location displayed in sagittal and axial views before (panel b) and after (panel c) correction*
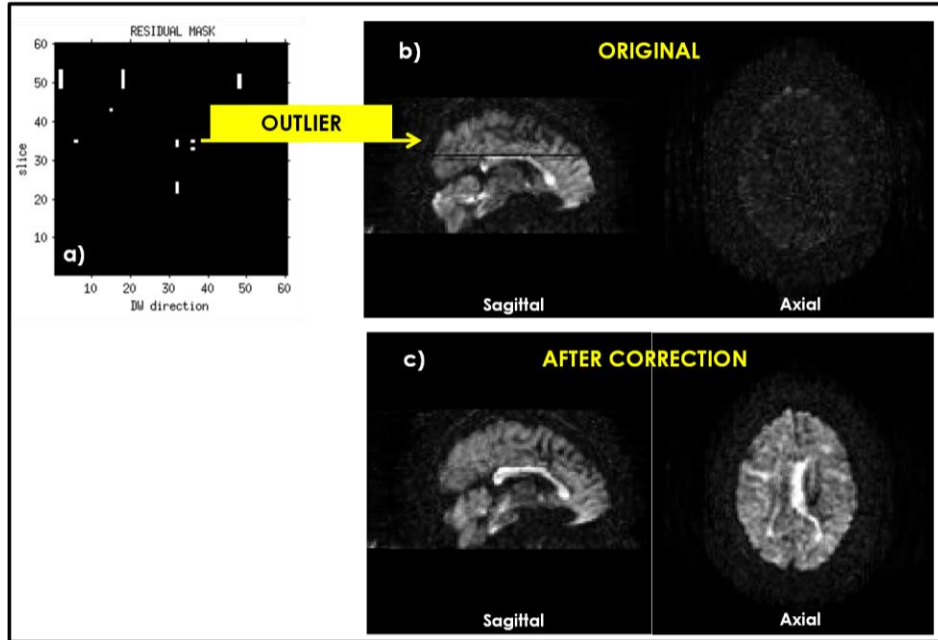
Figure 4.5 *Panel a) illustrates the outlier mask in which one of the outlier value is identified and its location displayed in sagittal and axial views before (panel b) and after (panel c) correction*
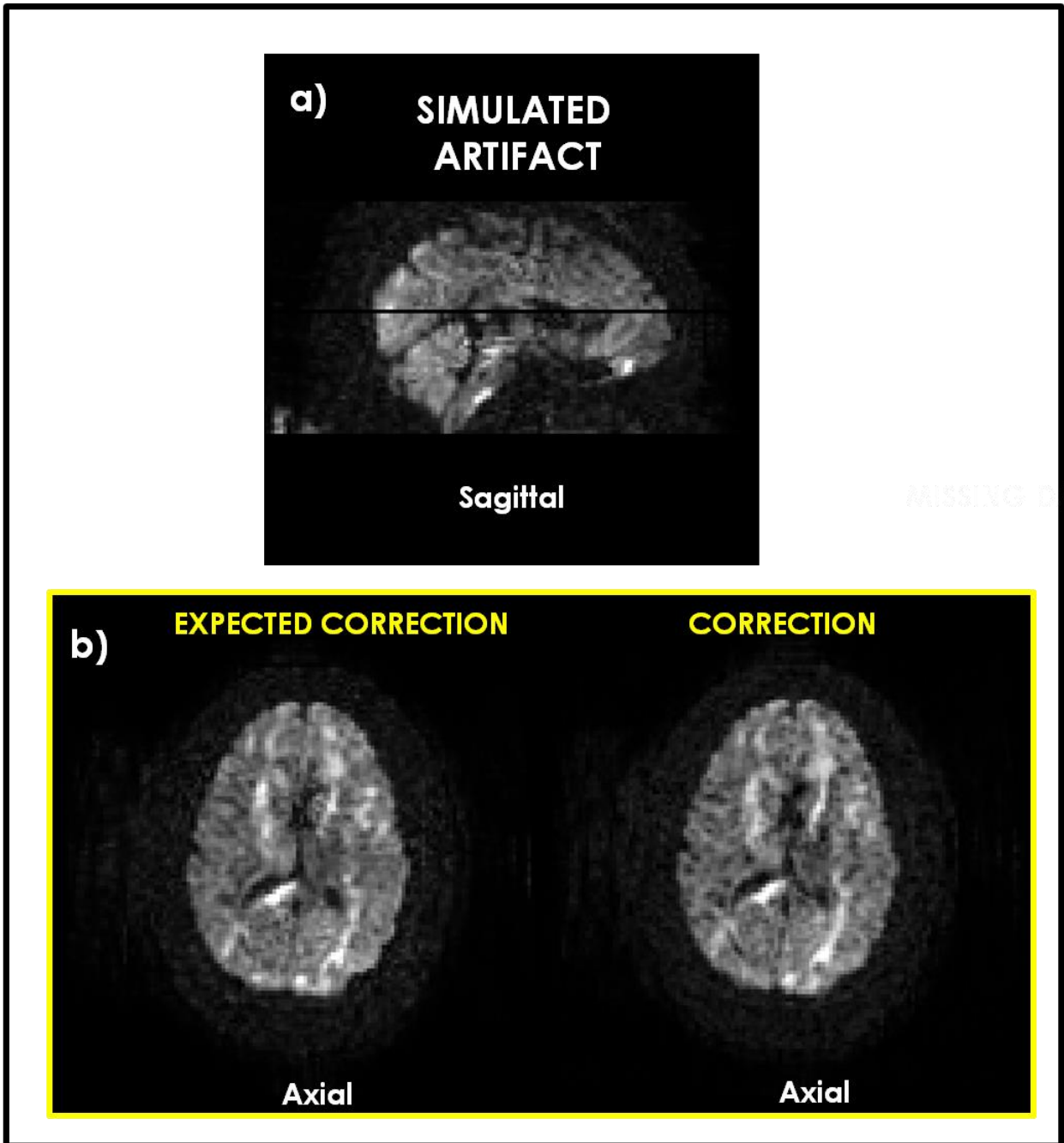
Figure 4.7 *Panel a) shows the corrupted dataset in the sagittal view while panel b) displays the actual (left) and the regenerated (right) data*
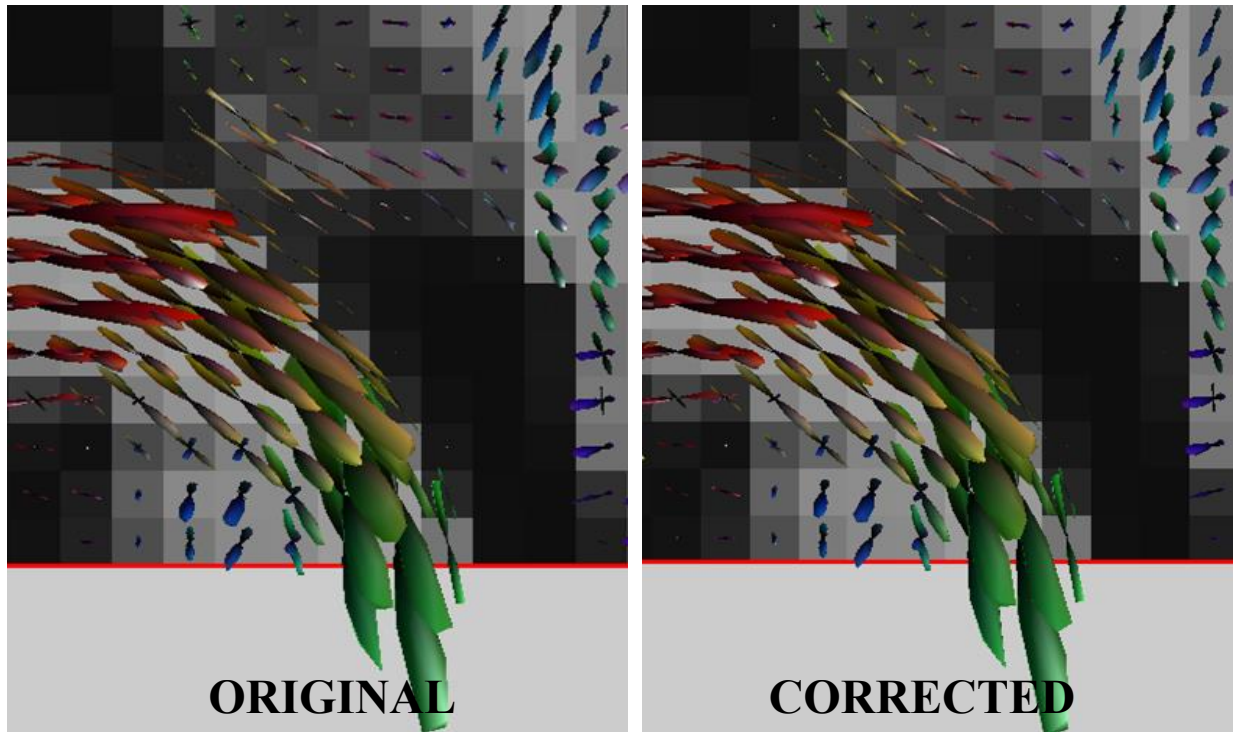
Figure 4.8 *Fiber Orientation Distribution (FOD) of the original slice (left) and after data regeneration (right)*

4.2.1. Discussion

In this work we proposed a slice-wise approach for artifact identification by using the concept of signal outlier detection (Chang et al., 2005; Chang et al., 2012; Pannek et al., 2012; Andresson et al., 2016), and a procedure for regenerate the corrupted slices by fitting the signal by SH model without the artifact slices.

The artifact identification issue in the DW images is becoming a crucial topic because of the huge amount of data acquired for both research and clinical purposes (Catani et al., 2005, 2007; Makris et al., 2005; Cloutman et al., 2012; MCGrath et al., 2013; Catani et al., 2008; Doricchi et al., 2008). In order to conduct reliable tractography studies, the diffusion-derived metrics have to be robust and not affected by artifacts. The final goal, indeed, is not only to provide a reliable depiction of fiber microstructure underlying the diffusion signal but also to evaluate the degree of confidence by an objective quantification of errors. For this reason, advanced techniques, beyond the standard pre-processing procedures for artifact identification,

were developed in the last decade. Chang and colleagues (2005) first suggested to identify corrupted data-points as outliers of residuals between DW signal and the fitted DT model either for exclusion of for a further correction by interpolation. This "cleaning" procedure was then adopted also by Pannek and colleagues in 2012 who replaced the DT model with the SH decomposition one.

Our procedure was demonstrated to be effective in HARDI images where the artifact was caused by a signal drop. However, being the residual defined as absolute value of the difference between the real data and the model, it would be able to identify anomalous signal values either signal drops or signal increases. with both all the slices identified as outliers and in the simulated artifact produced on a dataset of healthy volunteers. HARDI data were selected because are now the gold standard in both clinical and research study due to their possibility to solve complex fiber configurations like crossing and kissing fibers.

The choice of using a slice-wise approach was adopted to reduce some intrinsic problems of the voxel-wise approach such as the balance between sensitivity and specificity due to the low SRN of a single voxel (Andersson et al., 2016), and the choice of the model used for diffusion signal (Chang et al., 2005; Chang et al., 2012; Zwiers, 2010; Collier et al., 2015; Tax et al., 2015). Moreover, it should be considered that the voxels contained in a single slice and in a particular diffusion direction are acquired in a short time lapse under the same excitation pulse, e.g. of an EPI sequence (Andersson et al., 2016), then it is reasonably expected to have uniform data quality within the same slice for a given directions.

Since for the real data there was no "ground truth", the result of the correction process in the corrupted slice (i.e., the regeneration on the entire slice diffusion signal) was visually evaluated. A more precise estimate of the proposed correction procedure was done using the simulated artifact.

Choosing SH6 to fit the signal in the regenerated slice and the SH8 for non-corrupted ones was done to avoid a signal instability that would have originated by overfitting the signal (Decoteaux et al., 2015) (Figure 4.9). More simulations need be done to identify the best fitting without the artifact data (e.g., introducing smoothing parameters as in Hess et al., 2006).
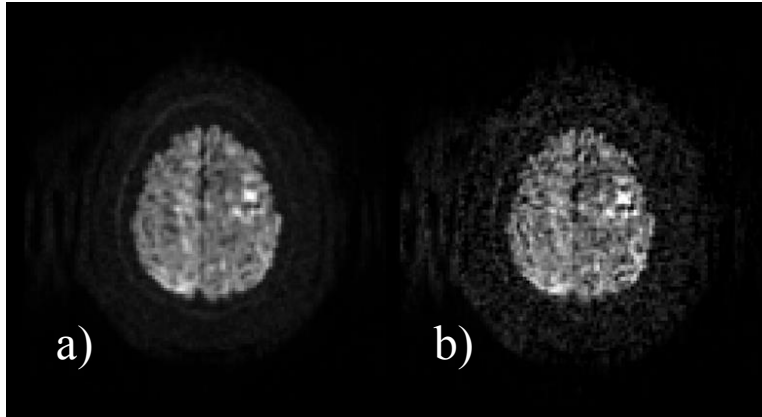
Figure 4.9 Example of overfitting: original slice (a) and regenerated one with SH order 8 (b)

Importantly, this method can be an effective solution to artifact identification and correction at both single and group level since it is possible to identify errors in single subjects and, before correction, compare this results with other subjects acquired in the same session. This would allow to verify if systematic errors occur due to problems with the acquisition sequence and/or parameters.

To conclude, our methods was demonstrated to be a valid solution for automatic artifact identification and correction in HARDI data. Our model-independent approach represents a useful instrument in large studies when visual quality check may be not practical or when data artifacts are not obvious at visual inspection.

4.3. Quality control pipeline to identify corrupted fiber bundles

In this further study we also adopted the concept of diffusion signal residuals on HARDI data and proposed it as a novel metric to be mapped along reconstructed WM bundles, in addition to standard tract specific measurements like fractional anisotropy (FA) and mean diffusivity (MD). Namely, we look for subjects bearing artifacts within group studies, considering the worst cases within a specific tract of the chosen

population. In this way the quality control (QC) can address a specific tract in fiber configuration and detect outliers relevant to tract specific features including the ones addressed by HARDI approaches (e.g., crossing, kissing, benching).

Importantly, the screening approach, based on SHs, can address the QC even of DTI derived tracts, as in the pilot test described in the next paragraph. This could appear as a contradiction, since the tract QC is based on a more complex model (SHs) than that used for the tract reconstruction (i.e., the tensor). Yet, the rationale is that the tract volume and its streamline content, whatever the adopted method to derive it, represents the structure in which we want to test the data quality with a description richness adequate to HARDI scan richness.

Final aim of this method, in fact, is including or not a bundle in a further group analysis. In this fashion, our pipeline might produce various practical outcome; eg.: 1) corrupted datasets which are considered completely unusable might be partially recovered if the tracts chosen for the further analysis pass the QC pipeline; 2) datasets which are initially evaluated as "good" may be discarded when looking at individual tracts if they present tract specific signal outliers. Further, this method allows analyzing datasets with a remarkable number of subjects, avoiding a visual slice-by-slice and direction-by-direction quality check. This approach represents a new way to perform data QC for tract specific measurements and can potentially improve the precision of these measurements in group analysis studies.

4.3.1. Materials and methods

Subject population

A sample of 11 healthy subjects, mean age 32 ± 5 years, was selected from a pre-existing diffusion imaging dataset acquired at NATBRAINLAB of King's College London (London, UK). By a visual inspection of the entire dataset, signal loss artifacts in the superior occipital/parietal regions of the brain were identified in two subjects. Also, these subjects were used as test-bed for the proposed method.

MRI acquisition protocol and DWI analysis

DW images were acquired in a single shell using a 3T GE HDx system (General Electric, Milwaukee, WI, USA) with the following parameters: voxel size 2.4x2.4x2.4 mm, slices 60, b-value 3000 s/mm2, 60 diffusion-weighted directions and 7 non-diffusion weighted volumes.

DW images were firstly corrected for eddy current distortion using the EDDY packet of FSL software (fsl.fmrib.ox.ac.uk/fsl/fslwiki/EDDY). DT model was then applied to process the data using Explore DTI (Leemans et al, 2009).

Since a first visual inspection of our dataset showed that 2 subjects presented signal loss in the superior occipital part of the brain, we chose to manually dissect the right anterior and posterior segment of the arcuate fasciculus (i.e., aAF and pAF) as test tract for our QC algorithm. In addition, the right inferior fronto-occipital fasciculus (IFOF) was selected as control tract. Tractography was performed using Trackvis (trackvis.org). Region of interest (ROIs) were selected with the two-ROIs approach. Specifically, we used spherical ROIs for aAF and pAF, and flat ROIs to dissect the IFOF fibers (Catani and de Schotten 2008). A representative example is shown in Figure Figure 4.10.

Figure 4.10 *From left to right, single subject fiber tractography of anterior segment of the arcuate fasciculus (aAF, sagittal view), posterior segment of the arcuate fasciculus (pAF, coronal view), inferior fronto-occipital fasciculus (IFOF, axial wiew).*

Artifact identification

The visual identification of artifacts by two expert viewers was considered the gold standard to assess the performance of our method.

SH decomposition of order 2, 4 and 6 (hereafter indicated as SH2, SH4, and SH6, respectively) was obtained by a custom written Matlab code.

The residual, defined as difference between the fitted and the measured signals, was computed vs. the DT and the SH4, SH6, and SH8 models. The maximum residual value was selected for each voxel through all the DW directions, to generate maximum residual maps for each subject, as shown in Figure 4.11. Then, fractional anisotropy (FA), mean diffusivity (MD), DT and SH maximum residuals (all orders) were mapped along the chosen tracts. Finally, for each subject, the average values of FA and MD and the maximum residual of DT and SH residuals were identified for each tract.

The threshold for the identification of outliers was calculated across subjects for each metric, namely mean FA, mean MD and maximum DT and SH residual and set at: mean±2*standard_deviation,
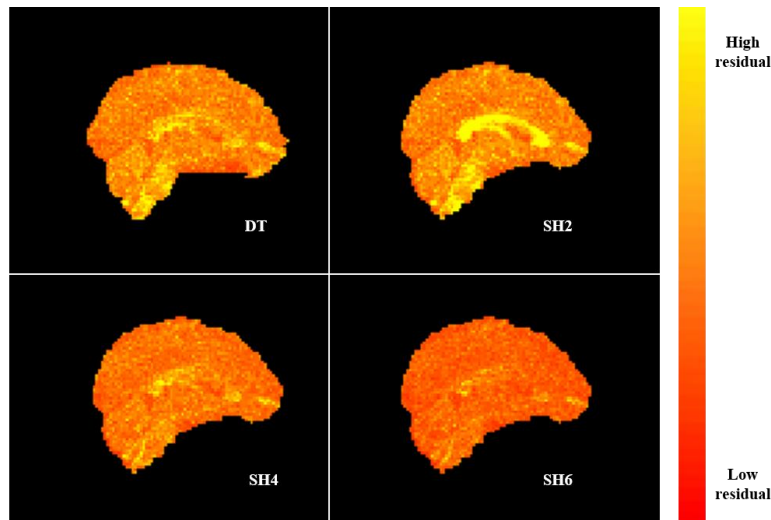
Figure 4.11 *Maximum residual maps of a single subject with no corrupted images obtained as differences between the actual signal and (from top left image) diffusion tensor model (DT), spherical harmonics of order 2, 4 and 6 (SH2, SH4, SH6) model. Lighter color (i.e., yellow) suggests a higher residual value*

4.3.2. Results

Within the considered subject sample, tractography of the right anterior and posterior segment, and right inferior fronto-occipital fasciculus was successfully performed for all subjects, as in the example of Figure 4.10. The computation of standard diffusion metrics FA and MD did not highlight any anomalous value.

For the tracts listed above we looked for those subjects (if any) whose mapped values (i.e., mean FA and MD, and maximum DT and SH residuals) exceeded the threshold as described in the previous section. Table 4.1 shows that outliers were found in the aAF of subject 5 and the pAF of subject 11 whose dataset had been classified as corrupted by the visual gold-standard. As expected, no artifacts were detected in the control tract (i.e., the IFOF).

Sbj	aAF				pAF				IFOF			
	FA	MD	SH6	DT	FA	MD	SH6	DT	FA	MD	SH6	DT
1	0,44	0,00052	64,677	128,765	0,39	0,00055	53,403	91,991	0,47	0,0006	70,2	129,037
2	0,41	0,00053	65,277	124,584	0,4	0,00053	56,036	100,233	0,45	0,00058	57,566	109,317
3	0,46	0,00053	88,915	142,648	0,41	0,00052	76,892	121,005	0,47	0,00056	84,981	147,427
4	0,42	0,00054	95,258	179,329	0,43	0,00054	101,166	204,433	0,49	0,00059	118,29	201,695
5	0,46	0,00052	293,224	420,375	0,43	0,00054	126,158	196,151	0,47	0,00058	148,207	261,093
6	0,45	0,0005	130,79	167,198	0,45	0,00053	88,105	138,916	0,44	0,00056	112,254	180,01
7	0,46	0,00052	83,098	183,048	0,47	0,00055	76,259	155,432	0,48	0,00059	109,263	192,747
8	0,42	0,00053	113,256	186,833	0,42	0,00056	76,119	157,933	0,48	0,00057	100,111	184,345
9	0,5	0,00048	100,601	198,391	0,43	0,0005	92,21	181,38	0,47	0,00054	98,636	216,067
10	0,44	0,00052	81,377	173,607	0,38	0,00052	62,563	94,496	0,46	0,00059	83,281	186,223
11	0,47	0,00051	98,994	160,791	0,38	0,00053	199,041	311,854	0,48	0,00057	167,448	240,397
Threshold	0,50	0,00055	237,744	349,239	0,47	0,00056	174,336	287,926	0,49	0,000611	169,095	276,646

Table 4.1 *Fractional anisotropy (FA), mean diffusivity (MD), residual obtained with spherical harmonics of order 6 (SH6) and diffusion tensor model (DT) for each subject. Last green row contains the threshold value (i.e. mean+2*standard_deviation) for each matric computed across subjects. Yellow cells include above threshold values.*

Importantly, outliers were well identified by means of the residual vs. the SH6 and the DT models. Conversely, SH2 and SH4 (not shown) revealed to be not sensitive to artifacts, most likely due to too a poor

parameterization. Remarkably, MD and FA, the main parameters commonly mapped after DTI, did not display discriminant capability against artifacts.

4.3.1. Discussion

In this work we propose a fast and effective routine for the QC of tract specific measurements by mapping residuals along tracts, which represents a simple and useful tool for artifact detection in group DW data analyses. This method aims at detecting artifacts not corrected by pre-processing procedures. Our results demonstrated that this procedure allows the detection of outliers, wherein the standard metrics such as FA and MD do not.

In this work we inherited the concept of residuals and suggested to apply it for the QC of diffusion dataset when conducting group level analysis in which a visual inspection of all DW volumes would be very time consuming and operator-dependent. Specifically, we propose a routine in which residuals values are mapped along the reconstructed tract and then evaluated along with the standard diffusion-derived metrics such as FA and MD. Moreover, compared to previous literature, we proposed residuals of SH fitting of the appropriate order, aiming at properly describing HARDI data richness, even if the adopted tractography was based on the simpler DTI model. The method was applied on a dataset of 11 healthy subjects, 2 of them presenting artifacts in the superior-occipital region of the brain, which evidence guided us in the selection of the WM bundles to include in this study. Indeed, tractography reconstruction of right anterior and posterior segment of the arcuate fascicle was performed in order to cross the regions involved by the artifacts, while the inferior fronto-occipital fascicle was selected as control tract. As a result, by using the residuals computed considering the signal fitted by SH6 and DT models we were able to automatically recognize the subjects who presented corrupted dataset because identified as outliers among all subjects of our sample. This confirms that residuals based on SH decomposition of higher order can be more sensitive to actual artifacts and less affected by the presence of complex microstructural organization of the tissue (Figure 4.12).
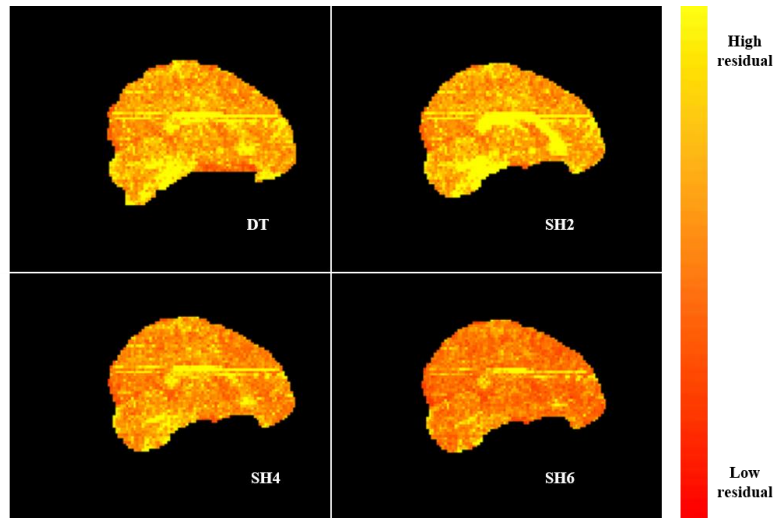
Figure 4.12 Maximum residual maps of a single subject with corrupted images obtained as differences between the actual signal and (from top left image) diffusion tensor model (DT), spherical harmonics of order 2 (SH2) model, spherical harmonics of order 4 (SH4) model, spherical harmonics of order 6 (SH6) model. Lighter color (i.e., yellow) suggests a higher residual value

Standard diffusion-derived measurements (i.e., FA and MD) and residuals obtained by SH2 and SH4 fitting, instead, were not able to detect anomalies in those same subjects. It is noteworthy that outlier regions may appear in different tracts of different subjects, which opens the pathway to more selective QC in the future. In fact, subjects presenting visible artifacts currently suggesting to discard their whole data-set might be partially recovered if the tracts chosen for the further analysis pass the QC pipeline. Conversely, subjects which are initially considered "good quality" samples due to successful tractography and reliable FA and MD values may be discarded when looking at individual tracts if they present signal outliers.

The main features or the presented strategy are: i) it is a cunning automatic solution to avoid operator failures in detecting artifact, since they are not always visible even by expert users: ii) the method is time-saving, especially when analyzing datasets with a remarkable number of subjects to be inspected slice-by-slice in each of the many DW directions; iii) the proposed pipeline guarantees the detection of repeated artifacts due

to scan sequence/acquisition parameters, allowing the possibility to identify machine aberrations; iv) it represent an easily adaptable tool because the residual calculation can be performed regardless the processing used to obtain the tract reconstruction.

4.4. General conclusions on outlier correction and detection in HARDI datasets

Both the presented studies have shown the sensitivity of SH fitting in QC of HARDI data. Considering current direction sampling standards (around 60) and signal quality of 3T scanners, order 8 SH models appeared as most appropriate to punctual detection of out-of-range directional sampling, while order 6 appeared sufficient and more robust to regularization and also sufficient to detect outliers mediated ex-post on the volumes of reconstructed tracts. Conversely, order 4 or less appeared to poor in describing the richness of HARDI datasets, with no significant improvement compared to the simpler tensor model.

The two methods here presented share the same data driven modeling, i.e. SHs, which renders them simpler than true physical models of artifacts sources like EC, susceptibility, and movements. This empirical approach, though limited in artifact description, permits a high flexibility as to the insertion into standard processing pipelines as additional QC and artifact removal/correction step, besides the EC, susceptibility, movement correction steps, which usually are also implemented via empirical (i.e., data-driven) approaches. Namely, if QC and outlier detection is aimed to correction of corrupted data, we adopted a slice-wise approach (i.e., at a given z and a given diffusion direction), in keeping with the previous literature. This is well explained by the short period of a single SE plus EPI sequence in which this piece of data is acquired, which may imply a punctual corruption, due to random events. Conversely, subject QC in group studies, with no restoring attempt, was proposed by the second approach as analyses of SHs mediated over the end-point structures, i.e. tracts.

To conclude, in this chapter, two fast and effective strategies for the QC of HARDI datasets were proposed. These methods, based on the identification of SH residuals mapped along either slices or target tracts,

represents useful instruments for artifact identification when performing analysis on large datasets at group level. In this way, a more reliable diffusion-derived metrics might be extracted, increasing the robustness and the precision of the tractography results either by correcting punctual (i.e., slice) corruption or by excluding outliers relevant to the endpoint structures.

5. Discussion and Conclusion

In the last decades the rapid advancements in neuroimaging techniques developed exploiting the magnetic resonance imaging (MRI) have encouraged he neuroscientists at investigating the human brain in terms of both structure and function, with the objective to explore physiological cognitive process and pathophysiological mechanism.

In fact, the capabilities of MRI to provide non-invasively and *in vivo* with different information at different level of detail (i.e., from the study of synaptic connections to the investigation of whole bundle that connect segregated cortical areas) permitted to develop methods addressing the overall brain network organization associated under the label of "brain connectome" (Sporns et al., 2005; Maier-Hein et al., 2017; Craddock et al., 2013; Pestilli et al., 2014; Smith et al., 2013; Glasser et al., 2013; Smith et al., 2015), to emphasize the core position of understanding connection patterns and integrated functions, beyond the specialization of brain cortical areas.

Among the several neuroimaging techniques available for studying brain functions, task-driven fMRI and resting-state functional magnetic resonance imaging (rsfMRI) have revealed to be extremely useful tool to describe the neuronal activation patterns involving anatomically separated brain regions and reflecting the level of functional communication between them. Regarding brain structures, deterministic and probabilistic tractography have shown to be suitable for extracting white matter pathways that link distant cortical regions.

In this thesis we investigated some aspects related to the study of brain connectivity as whole, both relevant to the physiological connection represented by tracts/fascicles/bundles considered in the structural connectivity and also by the functional responses and activity correlations considered in the functional connectivity. In this study, clearly emerged that the progress on both sides is a core element in permitting to advance to further integration overcoming the "shadow line" which is still separates the insight into the white matter and the gray matter function. The high challenge deals also with anatomo-functional

integration aspects which largely rely on mesoscale details of the brain circuits at the edge of current instrumentation and analysis methods.

We proposed two methods that allowed respectively the localization and the quantification of the connections between WM and GM and the correlation between structural and functional metrics. Both approaches worked at network level addressing technical issues mainly related to the limitation of the neuroimaging tool used for these analysis (e.g., the impossibility to approach gray matter when using deterministic tractographic algorithm, the asymmetry issue raised when performing probabilistic tractography, etc). As a result of this integration analysis at network level, we should stress that our studies confirmed the idea that any functional coordination should be mediated by connecting fibers only in case of highly specialized networks (i.e., the language circuit and the two lateral RSNs). The DMN, indeed, showed no correlation between SC and FC values, suggesting the existence of associative and indirect paths, such as polysynaptic structures, which connect gray matter regions but are not detectable with our tractography. This finding led us to also work on improving tractographic techniques and ameliorate the quality control of diffusion data. For this reason, we further address the problem of artifacts in DW images. We first worked at single level proposing a new method for artifact identification and removal, then at group level developing a new pipeline for the quality control of tractography-derived measures. These approaches permit a high flexibility as to the insertion into standard processing pipelines as additional quality control and artifact removal/correction step, besides the EC, susceptibility, movement correction steps, which usually are also implemented via empirical (i.e., data-driven) approaches. It would be interesting in future works quantifying the extent of each peak of FOD to establish the precision of the reconstruction in order to better and better integrate diffusion data with the functional ones.

It is also noteworthy that the application of the structural and functional data in clinical environment was demonstrated to be a very interesting instrument to assess circuitry modifications and adaptation, allowing for the monitoring the changes due to both pathology and those induced by therapeutic interventions (Irimia

et al., 2014). This may eventually aid in the development of patient-specific tailored rehabilitation approaches. It would be very interesting applying the method described in Chapter 2 to other stroke patients and for longer follow-up periods to enforce the validity of our method. Furthermore evaluation of other brain circuitries in different pathologies can also stress the importance to obtain information from different areas of the brain to understand which method can better shed light onto the specific circuitry.

To conclude our work suggests that many other studies will be needed on the topic of the integration of structural and functional data; nevertheless, we strongly believe that this kind of integration is the most fascinating and challenging route to pursue in neuroscience to gain more comprehension of the brain in its overall highly complex behavior.

6. Bibliography

Abou Elseoud, A., Littow, H., Remes, J., Starck, T., Nikkinen, J., Nissilä, J., … Kiviniemi, V. (2011). Group-ICA Model Order Highlights Patterns of Functional Brain Connectivity. *Frontiers in Systems Neuroscience*, *5*, 37. https://doi.org/10.3389/fnsys.2011.00037

Abou-Elseoud, A., Starck, T., Remes, J., Nikkinen, J., Tervonen, O., & Kiviniemi, V. (2009). The effect of model order selection in group PICA. *Human Brain Mapping*, *31*(8), NA-NA. https://doi.org/10.1002/hbm.20929

Alexander, D. C. (2005). Multiple-fiber reconstruction algorithms for diffusion MRI. In *Annals of the New York Academy of Sciences* (Vol. 1064, pp. 113–133). Blackwell Publishing Ltd. https://doi.org/10.1196/annals.1340.018

Alexander, D. C., Andersson, J. L. R., Assaf, Y., Ball, G., Bartsch, A. J., Basser, P. J., … Wouterlood, F. G. (2014). Contributors. In *Diffusion MRI* (pp. xi–xii). https://doi.org/10.1016/B978-0-12-396460-1.01002-7

Alhamud, A., Tisdall, M. D., Hess, A. T., Hasan, K. M., Meintjes, E. M., & van der Kouwe, A. J. W. (2012). Volumetric navigators for real-time motion correction in diffusion tensor imaging. *Magnetic Resonance in Medicine*, *68*(4), 1097–1108. https://doi.org/10.1002/mrm.23314

Amaro, E., & Barker, G. J. (2006). Study design in fMRI: basic principles. *Brain and Cognition*, *60*(3), 220–232. https://doi.org/10.1016/j.bandc.2005.11.009

Anderson, A. W. (2005). Measurement of fiber orientation distributions using high angular resolution diffusion imaging. *Magnetic Resonance in Medicine*, *54*(5), 1194–1206. https://doi.org/10.1002/mrm.20667

Andersson, J. L. R. (2014). Chapter 4 – Geometric Distortions in Diffusion MRI. In *Diffusion MRI* (pp. 63–85). https://doi.org/10.1016/B978-0-12-396460-1.00004-4

Andersson, J. L. R., Graham, M. S., Zsoldos, E., & Sotiropoulos, S. N. (2016). Incorporating outlier detection and replacement into a non-parametric framework for movement and distortion correction of diffusion MR images. *NeuroImage*, *141*, 556–572. https://doi.org/10.1016/j.neuroimage.2016.06.058

Andersson, J. L. R., & Sotiropoulos, S. N. (2015). Non-parametric representation and prediction of single- and multi-shell diffusion-weighted MRI data using Gaussian processes. *NeuroImage*, *122*, 166–176. https://doi.org/10.1016/j.neuroimage.2015.07.067

Andersson, J., & Sotiropoulos, S. N. (2014). A Gaussian Process based method for detecting and correcting dropout in diffusion imaging. *Proc. Intl. Soc. Mag. Reson. Med. 22 (2014)*, *22*(May 2014), 2567. Retrieved from http://dev.ismrm.org/2014/2567.html

Anwander, A., Tittgemeyer, M., von Cramon, D., Friederici, A., & Knosche, T. (2006). Connectivity-Based Parcellation of Broca's Area. *Cerebral Cortex*, *17*(4), 816–825. https://doi.org/10.1093/cercor/bhk034

Aslan, S., Huang, H., Uh, J., Mishra, V., Xiao, G., van Osch, M. J. P., & Lu, H. (2011). White matter cerebral blood flow is inversely correlated with structural and functional connectivity in the human brain. *NeuroImage*, *56*(3), 1145–1153. https://doi.org/10.1016/j.neuroimage.2011.02.082

Assaf, Y., & Cohen, Y. (2014). Chapter 9 – Inferring Microstructural Information of White Matter from Diffusion MRI. In *Diffusion MRI* (pp. 185–208). https://doi.org/10.1016/B978-0-12-396460-1.00009-3

Baglio, F., Griffanti, L., Saibene, F. L., Ricci, C., Alberoni, M., Critelli, R., … Farina, E. (2015). Multistimulation Group Therapy in Alzheimer's Disease Promotes Changes in Brain Functioning. *Neurorehabilitation and Neural Repair*, *29*(1), 13–24. https://doi.org/10.1177/1545968314532833

Baliyan, V., Das, C. J., Sharma, R., & Gupta, A. K. (2016). Diffusion weighted imaging: Technique and applications. *World Journal of Radiology*, *8*(9), 785. https://doi.org/10.4329/wjr.v8.i9.785

Bartsch, A. J., Biller, A., & Homola, G. A. (2014). Chapter 23 – Presurgical Tractography Applications. In *Diffusion MRI* (pp. 531–567). https://doi.org/10.1016/B978-0-12-396460-1.00023-8

Basho, S., Palmer, E. D., Rubio, M. A., Wulfeck, B., & Müller, R.-A. (2007). Effects of generation mode in fMRI adaptations of semantic fluency: Paced production and overt speech. *Neuropsychologia*, *45*(8), 1697–1706. https://doi.org/10.1016/j.neuropsychologia.2007.01.007

Basser, P. J., Pajevic, S., Pierpaoli, C., Duda, J., & Aldroubi, A. (2000). In vivo fiber tractography using DT-MRI data. *Magnetic Resonance in Medicine*, *44*(4), 625–632. Retrieved from http://www.ncbi.nlm.nih.gov/pubmed/11025519

Basser, P. J., Mattiello, J., & LeBihan, D. (1994). MR diffusion tensor spectroscopy and imaging. *Biophysical Journal*, *66*(1), 259–267. https://doi.org/10.1016/S0006-3495(94)80775-1

Basser, P. J. (1995). Inferring microstructural features and the physiological state of tissues from diffusion- weighted images. *NMR in Biomedicine*, *8*(7), 333–344. https://doi.org/10.1002/nbm.1940080707

Basser, P. J., & Özarslan, E. (2014). Introduction to Diffusion MR. In *Diffusion MRI* (pp. 3–9). Elsevier. https://doi.org/10.1016/B978-0-12-396460-1.00001-9

Basser, P. J., & Özarslan, E. (2014). Chapter 1 – Introduction to Diffusion MR. In *Diffusion MRI* (pp. 3–9). https://doi.org/10.1016/B978-0-12-396460-1.00001-9

Beaulieu, C. (2002). The basis of anisotropic water diffusion in the nervous system - a technical review. *NMR in Biomedicine*, *15*(7–8), 435–455. https://doi.org/10.1002/nbm.782

Beaulieu, C. (2014). Chapter 8 – The Biological Basis of Diffusion Anisotropy. In *Diffusion MRI* (pp. 155–183). https://doi.org/10.1016/B978-0-12-396460-1.00008-1

Beckmann, C. F., DeLuca, M., Devlin, J. T., & Smith, S. M. (2005). Investigations into resting-state connectivity using independent component analysis. *Philosophical Transactions of the Royal Society B: Biological Sciences*, *360*(1457), 1001–1013. https://doi.org/10.1098/rstb.2005.1634

Beckmann, C. F., & Smith, S. M. (2004). Probabilistic Independent Component Analysis for Functional Magnetic Resonance Imaging. *IEEE Transactions on Medical Imaging*, *23*(2), 137–152. https://doi.org/10.1109/TMI.2003.822821

Beckmann, C., Mackay, C., Filippini, N., & Smith, S. (2009). Group comparison of resting-state FMRI data using multi-subject ICA and dual regression. *NeuroImage*, *47*, S148. https://doi.org/10.1016/S1053-8119(09)71511-3

Behrens, T. E. J., Berg, H. J., Jbabdi, S., Rushworth, M. F. S., & Woolrich, M. W. (2007). Probabilistic diffusion tractography with multiple fibre orientations: What can we gain? *NeuroImage*, *34*(1), 144–155. https://doi.org/10.1016/j.neuroimage.2006.09.018

Behrens, T. E. J., Woolrich, M. W., Jenkinson, M., Johansen-Berg, H., Nunes, R. G., Clare, S., … Smith, S. M. (2003). Characterization and Propagation of Uncertainty in Diffusion-Weighted MR Imaging. *Magnetic Resonance in Medicine*, *50*(5), 1077–1088. https://doi.org/10.1002/mrm.10609

Beladi, S., Pathirana, P. N., & Brotchie, P. (2010). Robust ODF smoothing for accurate estimation of fiber orientation. *2010 Annual International Conference of the IEEE Engineering in Medicine and Biology Society, EMBC'10*, 2698–2701. https://doi.org/10.1109/IEMBS.2010.5626551

Benner, T., van der Kouwe, A. J. W., & Sorensen, A. G. (2011). Diffusion imaging with prospective motion correction and reacquisition. *Magnetic Resonance in Medicine*, *66*(1), 154–167. https://doi.org/10.1002/mrm.22837

Binder, J. R., Frost, J. A., Hammeke, T. A., Cox, R. W., Rao, S. M., & Prieto, T. (1997). Human brain language areas identified by functional magnetic resonance imaging. *The Journal of Neuroscience : The Official Journal of the Society for Neuroscience*, *17*(1), 353–362. Retrieved from http://www.ncbi.nlm.nih.gov/pubmed/8987760

Biswal, B., Yetkin, F. Z., Haughton, V. M., & Hyde, J. S. (1995). Functional connectivity in the motor cortex of resting human brain using echo-planar MRI. *Magnetic Resonance in Medicine*, *34*(4), 537–541. Retrieved from http://www.ncbi.nlm.nih.gov/pubmed/8524021

Blackmon, K., Halgren, E., Barr, W. B., Carlson, C., Devinsky, O., DuBois, J., … Thesen, T. (2011). Individual differences in verbal abilities associated with regional blurring of the left gray and white matter boundary. *The Journal of Neuroscience : The Official Journal of the Society for Neuroscience*, *31*(43), 15257–15263. https://doi.org/10.1523/JNEUROSCI.3039-11.2011

Bodini, B., & Ciccarelli, O. (2014). Chapter 11 – Diffusion MRI in Neurological Disorders. In *Diffusion MRI* (pp. 241–255). https://doi.org/10.1016/B978-0-12-396460-1.00011-1

Bonzano, L., Pardini, M., Mancardi, G. L., Pizzorno, M., & Roccatagliata, L. (2009). Structural connectivity influences brain activation during PVSAT in Multiple Sclerosis. *NeuroImage*, *44*(1), 9–15. https://doi.org/10.1016/j.neuroimage.2008.08.015

Buchbinder, B. R. (2016). *Functional magnetic resonance imaging*. *Handbook of clinical neurology* (1st ed., Vol. 135). Elsevier B.V. https://doi.org/10.1016/B978-0-444-53485-9.00004-0

Buckner, R. L., Andrews-Hanna, J. R., & Schacter, D. L. (2008, March). The brain's default network: Anatomy, function, and relevance to disease. *Annals of the New York Academy of Sciences*. https://doi.org/10.1196/annals.1440.011

Buxton, R. B. (2013). The physics of functional magnetic resonance imaging (fMRI). *Reports on Progress in Physics*, *76*(9), 96601. https://doi.org/10.1088/0034-4885/76/9/096601

Buxton, R. B. (2010). Interpreting oxygenation-based neuroimaging signals: the importance and the challenge of understanding brain oxygen metabolism. *Frontiers in Neuroenergetics*, *2*, 8. https://doi.org/10.3389/fnene.2010.00008

Cabeza, R., Dolcos, F., Graham, R., & Nyberg, L. (2002). Similarities and Differences in the Neural Correlates of Episodic Memory Retrieval and Working Memory. *NeuroImage*, *16*(2), 317–330. https://doi.org/10.1006/nimg.2002.1063

Callaghan, P. T., Eccles, C. D., & Xia, Y. (1988). NMR microscopy of dynamic displacements: k-space and q-space imaging. *Journal of Physics E: Scientific Instruments*, *21*(8), 820–822. https://doi.org/10.1088/0022-3735/21/8/017

Cao, Q., Shu, N., An, L., Wang, P., Sun, L., Xia, M.-R., … He, Y. (2013). Probabilistic Diffusion Tractography and Graph Theory Analysis Reveal Abnormal White Matter Structural Connectivity Networks in Drug-Naive Boys with Attention Deficit/Hyperactivity Disorder. *Journal of Neuroscience*, *33*(26), 10676–10687. https://doi.org/10.1523/JNEUROSCI.4793-12.2013

Catani, M., Allin, M. P. G., Husain, M., Pugliese, L., Mesulam, M. M., Murray, R. M., & Jones, D. K. (2007). Symmetries in human brain language pathways correlate with verbal recall. *Proceedings of the National Academy of Sciences of the United States of America*, *104*(43), 17163–17168. https://doi.org/10.1073/pnas.0702116104

Catani, M., & Budisavljević, S. (2014). Chapter 22 – Contribution of Diffusion Tractography to the Anatomy of Language. In *Diffusion MRI* (pp. 511–529). https://doi.org/10.1016/B978-0-12-396460-1.00022-6

Catani, M., Howard, R. J., Pajevic, S., & Jones, D. K. (2002). Virtual in Vivo Interactive Dissection of White Matter Fasciculi in the Human Brain. *NeuroImage*, *17*(1), 77–94. https://doi.org/10.1006/NIMG.2002.1136

Catani, M., Jones, D. K., & ffytche, D. H. (2005). Perisylvian language networks of the human brain. *Annals of Neurology*, *57*(1), 8–16. https://doi.org/10.1002/ana.20319

Catani, M., & Thiebaut de Schotten, M. (2008). A diffusion tensor imaging tractography atlas for virtual in vivo dissections. *Cortex*, *44*(8), 1105–1132. https://doi.org/10.1016/j.cortex.2008.05.004

Chang, L. C., Jones, D. K., & Pierpaoli, C. (2005). RESTORE: Robust estimation of tensors by outlier rejection. *Magnetic Resonance in Medicine*, *53*(5), 1088–1095. https://doi.org/10.1002/mrm.20426

Chang, L. C., Walker, L., & Pierpaoli, C. (2012). Informed RESTORE: A method for robust estimation of diffusion tensor from low redundancy datasets in the presence of physiological noise artifacts. *Magnetic Resonance in Medicine*, *68*(5), 1654–1663. https://doi.org/10.1002/mrm.24173

Christiaens, D., Sunaert, S., Suetens, P., & Maes, F. (2017). Convexity-constrained and nonnegativity-constrained spherical factorization in diffusion-weighted imaging. *NeuroImage*, *146*, 507–517. https://doi.org/10.1016/j.neuroimage.2016.10.040

Chung, S., Courcot, B., Sdika, M., Moffat, K., Rae, C., & Henry, R. G. (2010). Bootstrap quantification of cardiac pulsation artifact in DTI. *NeuroImage*, *49*(1), 631–640. https://doi.org/10.1016/j.neuroimage.2009.06.067

Ciccarelli, O., Catani, M., Johansen-Berg, H., Clark, C., & Thompson, A. (2008). Diffusion-based tractography in neurological disorders: concepts, applications, and future developments. *The Lancet Neurology*, *7*(8), 715–727. https://doi.org/10.1016/S1474-4422(08)70163-7

Cloutman, L. L., & Lambon Ralph, M. A. (2012). Connectivity-based structural and functional parcellation of the human cortex using diffusion imaging and tractography. *Frontiers in Neuroanatomy*, *6*, 34. https://doi.org/10.3389/fnana.2012.00034

Cole, D. M., Smith, S. M., & Beckmann, C. F. (2010). Advances and pitfalls in the analysis and interpretation of resting-state FMRI data. *Frontiers in Systems Neuroscience*, *4*, 8. https://doi.org/10.3389/fnsys.2010.00008

Collier, Q., Veraart, J., Jeurissen, B., den Dekker, A. J., & Sijbers, J. (2015). Iterative reweighted linear least squares for accurate, fast, and robust estimation of diffusion magnetic resonance parameters. *Magnetic Resonance in Medicine*, *73*(6), 2174–2184. https://doi.org/10.1002/mrm.25351

Conturo, T. E., Lori, N. F., Cull, T. S., Akbudak, E., Snyder, A. Z., Shimony, J. S., … Raichle, M. E. (1999). Tracking neuronal fiber pathways in the living human brain. *Proceedings of the National Academy of Sciences of the United States of America*, *96*(18), 10422–10427. Retrieved from http://www.ncbi.nlm.nih.gov/pubmed/10468624

Cory, D. G. (1990). Measurement of translational displacement probabilities by NMR: An indicator of compartmentation. *Magnetic Resonance in Medicine*, *14*(3), 435–444. https://doi.org/10.1002/mrm.1910140303

Costantini, I. D. O. P. L. L. M. B. F. B. G. (2016). Mixed ICA and clustering method introduced to study the life span age and gender changes in the connectivity within the default mode network. *Proceedings International Society of Magnetic Resonace Imaging*. Retrieved from https://www.politesi.polimi.it/handle/10589/97465

Counsell, S. J., Ball, G., Pandit, A., & David Edwards, A. (2014). Chapter 13 – Diffusion Imaging in the Developing Brain. In *Diffusion MRI* (pp. 283–300). https://doi.org/10.1016/B978-0-12-396460-1.00013-5

Craddock, R. C., Jbabdi, S., Yan, C.-G., Vogelstein, J. T., Castellanos, F. X., Di Martino, A., … Milham, M. P. (2013). Imaging human connectomes at the macroscale. *Nature Methods*, *10*(6), 524–539. https://doi.org/10.1038/nmeth.2482

Cramer, S. C., Sur, M., Dobkin, B. H., O'Brien, C., Sanger, T. D., Trojanowski, J. Q., … Vinogradov, S. (2011). Harnessing neuroplasticity for clinical applications. *Brain*, *134*(6), 1591–1609. https://doi.org/10.1093/brain/awr039

Damoiseaux, J. S., Rombouts, S. A. R. B., Barkhof, F., Scheltens, P., Stam, C. J., Smith, S. M., & Beckmann, C. F. (2006). Consistent resting-state networks across healthy subjects. *Proceedings of the National Academy of Sciences*, *103*(37), 13848–13853. https://doi.org/10.1073/pnas.0601417103

Deco, G., Tononi G., Boly M., Kringelbach M. L. (2015). Rethinking segregation and integration: contribution of whole-brain modelling. *Nature Review Neuroscience 16(7)*:430-9. https://doi: 10.1038/nrn3963.

De Luca, M., Beckmann, C. F., De Stefano, N., Matthews, P. M., & Smith, S. M. (2006). fMRI resting state networks define distinct modes of long-distance interactions in the human brain. *NeuroImage*, *29*(4), 1359–1367. https://doi.org/10.1016/J.NEUROIMAGE.2005.08.035

De Martino, F., Gentile, F., Esposito, F., Balsi, M., Di Salle, F., Goebel, R., & Formisano, E. (2007). Classification of fMRI independent components using IC-fingerprints and support vector machine classifiers. *NeuroImage*, *34*(1), 177–194. https://doi.org/10.1016/j.neuroimage.2006.08.041

Dell'Acqua, F., Scifo, P., Rizzo, G., Catani, M., Simmons, A., Scotti, G., & Fazio, F. (2010). A modified damped Richardson–Lucy algorithm to reduce isotropic background effects in spherical deconvolution. *NeuroImage*, *49*(2), 1446–1458. https://doi.org/10.1016/J.NEUROIMAGE.2009.09.033

Dell'Acqua, F., Simmons, A., Williams, S. C. R., & Catani, M. (2013). Can spherical deconvolution provide more information than fiber orientations? Hindrance modulated orientational anisotropy, a true-tract specific index to characterize white matter diffusion. *Human Brain Mapping*, *34*(10), 2464–2483. https://doi.org/10.1002/hbm.22080

Descoteaux, M., Deriche, R., Knosche, T. R., & Anwander, A. (2009). Deterministic and Probabilistic Tractography Based on Complex Fibre Orientation Distributions. *IEEE Transactions on Medical Imaging*, *28*(2), 269–286. https://doi.org/10.1109/TMI.2008.2004424

Descoteaux, M. (2010). High Angular Resolution Diffusion MRI : from Local Estimation to Segmentation and Tractography. *PhD Thesis*, 313. Retrieved from https://tel.archives-ouvertes.fr/tel-00457458/document

Descoteaux, M. (2015). High Angular Resolution Diffusion Imaging (HARDI). In *Wiley Encyclopedia of Electrical and Electronics Engineering* (pp. 1–25). Hoboken, NJ, USA: John Wiley & Sons, Inc. https://doi.org/10.1002/047134608X.W8258

Descoteaux, M., Angelino, E., Fitzgibbons, S., & Deriche, R. (2007). Regularized, fast, and robust analytical Q-ball imaging. *Magnetic Resonance in Medicine*, *58*(3), 497–510. https://doi.org/10.1002/mrm.21277

Dice, L. R. (1945). Measures of the Amount of Ecologic Association Between Species. *Ecology. 26 (3): 297–302.* https://doi.org /10.2307/1932409

Dipasquale, O., Griffanti, L., Clerici, M., Nemni, R., Baselli, G., & Baglio, F. (2015). High-Dimensional ICA Analysis Detects Within-Network Functional Connectivity Damage of Default-Mode and

Sensory-Motor Networks in Alzheimer's Disease. *Frontiers in Human Neuroscience*, *9*, 43. https://doi.org/10.3389/fnhum.2015.00043

Doricchi, F., Thiebaut de Schotten, M., Tomaiuolo, F., & Bartolomeo, P. (2008). White matter (dis)connections and gray matter (dys)functions in visual neglect: Gaining insights into the brain networks of spatial awareness. *Cortex*, *44*(8), 983–995. https://doi.org/10.1016/j.cortex.2008.03.006

Drobyshevsky, A., Baumann, S. B., & Schneider, W. (2006). A rapid fMRI task battery for mapping of visual, motor, cognitive, and emotional function. *NeuroImage*, *31*(2), 732–744. https://doi.org/10.1016/j.neuroimage.2005.12.016

Edgar, J. M., & Griffiths, I. R. (2014). Chapter 7 – White Matter Structure: A Microscopist's View. In *Diffusion MRI* (pp. 127–153). https://doi.org/10.1016/B978-0-12-396460-1.00007-X

Edwards, L. J., Pine, K. J., Ellerbrock, I., Weiskopf, N., & Mohammadi, S. (2017). NODDI-DTI: Estimating neurite orientation and dispersion parameters from a diffusion tensor in healthy white matter. *Frontiers in Neuroscience*, *11*(DEC), 1–15. https://doi.org/10.3389/fnins.2017.00720

Elman, J. A., Madison, C. M., Baker, S. L., Vogel, J. W., Marks, S. M., Crowley, S., … Jagust, W. J. (2016). Effects of Beta-Amyloid on Resting State Functional Connectivity Within and between Networks Reflect Known Patterns of Regional Vulnerability. *Cerebral Cortex*, *26*(2), 695–707. https://doi.org/10.1093/cercor/bhu259

Feinberg, D. A., Moeller, S., Smith, S. M., Auerbach, E., Ramanna, S., Glasser, M. F., … Yacoub, E. (2010). Multiplexed Echo Planar Imaging for Sub-Second Whole Brain FMRI and Fast Diffusion Imaging. *PLoS ONE*, *5*(12), e15710. https://doi.org/10.1371/journal.pone.0015710

Filippini, N., MacIntosh, B. J., Hough, M. G., Goodwin, G. M., Frisoni, G. B., Smith, S. M., … Mackay, C. E. (2009). Distinct patterns of brain activity in young carriers of the APOE- 4 allele. *Proceedings of the National Academy of Sciences*, *106*(17), 7209–7214. https://doi.org/10.1073/pnas.0811879106

Forstmann, B. U., Jahfari, S., Scholte, H. S., Wolfensteller, U., van den Wildenberg, W. P. M., & Ridderinkhof, K. R. (2008). Function and Structure of the Right Inferior Frontal Cortex Predict Individual Differences in Response Inhibition: A Model-Based Approach. *Journal of Neuroscience*, *28*(39), 9790–9796. https://doi.org/10.1523/JNEUROSCI.1465-08.2008

Fox, M. D., Snyder, A. Z., Vincent, J. L., Corbetta, M., Van Essen, D. C., & Raichle, M. E. (2005). From The Cover: The human brain is intrinsically organized into dynamic, anticorrelated functional networks. *Proceedings of the National Academy of Sciences*, *102*(27), 9673–9678. https://doi.org/10.1073/pnas.0504136102

Frank L.R. (2002). Characterization of anisotropy in high angular resolution diffusion-weighted MRI. *Magnetic Resonance in Medicine*. *47(6)*:1083-99. https://doi.org/ 10.1002/mrm.10156.

Friederici, A. D. (2017). *Language in our brain: The origins of a uniquely human capacity.* Retrieved from https://mitpress.mit.edu/books/language-our-brain

Friston, K. J., Holmes, A. P., Worsley, K. J., Poline, J.-P., Frith, C. D., & Frackowiak, R. S. J. (1994). Statistical parametric maps in functional imaging: A general linear approach. *Human Brain Mapping*, *2*(4), 189–210. https://doi.org/10.1002/hbm.460020402

Friston, K. J. (2011). Functional and Effective Connectivity: A Review. *Brain Connectivity*, *1*(1), 13–36. https://doi.org/10.1089/brain.2011.0008

Friston, K., Mattout, J., Trujillo-Barreto, N., Ashburner, J., & Penny, W. (2007). Variational free energy and the Laplace approximation. *NeuroImage*, *34*(1), 220–234. https://doi.org/10.1016/J.NEUROIMAGE.2006.08.035

Gallichan, D., Scholz, J., Bartsch, A., Behrens, T. E., Robson, M. D., & Miller, K. L. (2009). Addressing a systematic vibration artifact in diffusion-weighted MRI. *Human Brain Mapping*, *31*(2), NA-NA. https://doi.org/10.1002/hbm.20856

Gamerman, D. (1997). Sampling from the posterior distribution in generalized linear mixed models. *Statistics and Computing*, *7*(1), 57–68. https://doi.org/10.1023/A:1018509429360

Gilks, W R; Richardson, S., & Spiegelhalter, D. J. (1996). *Markov Chain Monte Carlo In Practice*. Chapman & Hall. Retrieved from https://books.google.it/books?hl=it&lr=&id=TRXrMWY_i2IC&oi=fnd&pg=PA1&dq=Gilks+et+al.,+1996+monte+carlo&ots=7iStvpNtru&sig=QitxEJ28_pbGiTH0h8V8TBjjCBg#v=onepage&q=Gilks et al.%2C 1996 monte carlo&f=false

Giménez, M., Junqué, C., Narberhaus, A., Botet, F., Bargalló, N., & Mercader, J. M. (2006). Correlations of thalamic reductions with verbal fluency impairment in those born prematurely. *NeuroReport*, *17*(5), 463–466. https://doi.org/10.1097/01.wnr.0000209008.93846.24

Glasser, M. F., Sotiropoulos, S. N., Wilson, J. A., Coalson, T. S., Fischl, B., Andersson, J. L., … WU-Minn HCP Consortium. (2013). The minimal preprocessing pipelines for the Human Connectome Project. *NeuroImage*, *80*, 105–124. https://doi.org/10.1016/j.neuroimage.2013.04.127

Glenn, O. A., Ludeman, N. A., Berman, J. I., Wu, Y. W., Lu, Y., Bartha, A. I., … Henry, R. G. (2007). Diffusion Tensor MR Imaging Tractography of the Pyramidal Tracts Correlates with Clinical Motor Function in Children with Congenital Hemiparesis. *American Journal of Neuroradiology*, *28*(9), 1796–1802. https://doi.org/10.3174/ajnr.A0676

Goebel, R. (2007). Localization of Brain Activity using Functional Magnetic Resonance Imaging. In *Clinical Functional MRI* (pp. 9–51). Berlin, Heidelberg: Springer Berlin Heidelberg. https://doi.org/10.1007/978-3-540-49976-3_2

Golestanirad, L., Das, S., Schweizer, T. A., & Graham, S. J. (2015). A preliminary fMRI study of a novel self-paced written fluency task: observation of left-hemispheric activation, and increased frontal activation in late vs. early task phases. *Frontiers in Human Neuroscience*, *9*(MAR), 113. https://doi.org/10.3389/fnhum.2015.00113

Grefkes, C., & Fink, G. R. (2011). Reorganization of cerebral networks after stroke: new insights from neuroimaging with connectivity approaches. *Brain*, *134*(5), 1264–1276. https://doi.org/10.1093/brain/awr033

Greicius, M. D., Krasnow, B., Reiss, A. L., & Menon, V. (2003). Functional connectivity in the resting brain: A network analysis of the default mode hypothesis. *Proceedings of the National Academy of Sciences*, *100*(1), 253–258. https://doi.org/10.1073/pnas.0135058100

Greicius, M. D., Supekar, K., Menon, V., & Dougherty, R. F. (2009). Resting-State Functional Connectivity Reflects Structural Connectivity in the Default Mode Network. *Cerebral Cortex*, *19*(1), 72–78. https://doi.org/10.1093/cercor/bhn059

Greve, D. N., & Fischl, B. (2009). Accurate and robust brain image alignment using boundary-based registration. *NeuroImage*, *48*(1), 63–72. https://doi.org/10.1016/j.neuroimage.2009.06.060

Griffanti, L., Salimi-Khorshidi, G., Beckmann, C. F., Auerbach, E. J., Douaud, G., Sexton, C. E., … Smith, S. M. (2014). ICA-based artefact removal and accelerated fMRI acquisition for improved resting state network imaging. *NeuroImage*, *95*, 232–247. https://doi.org/10.1016/J.NEUROIMAGE.2014.03.034

Gusnard, D. A., Akbudak, E., Shulman, G. L., & Raichle, M. E. (2001). Medial prefrontal cortex and self-referential mental activity: Relation to a default mode of brain function. *Proceedings of the National Academy of Sciences*, *98*(7), 4259–4264. https://doi.org/10.1073/pnas.071043098

Hagmann, P., Cammoun, L., Gigandet, X., Meuli, R., Honey, C. J., Wedeen, V. J., & Sporns, O. (2008). Mapping the Structural Core of Human Cerebral Cortex. *PLoS Biology*, *6*(7), e159. https://doi.org/10.1371/journal.pbio.0060159

Hagmann, P., Kurant, M., Gigandet, X., Thiran, P., Wedeen, V. J., Meuli, R., & Thiran, J.-P. (2007). Mapping Human Whole-Brain Structural Networks with Diffusion MRI. *PLoS ONE*, *2*(7), e597. https://doi.org/10.1371/journal.pone.0000597

Hess, C. P., Mukherjee, P., Han, E. T., Xu, D., & Vigneron, D. B. (2006). Q-ball reconstruction of multimodal fiber orientations using the spherical harmonic basis. *Magnetic Resonance in Medicine*, *56*(1), 104–117. https://doi.org/10.1002/mrm.20931

Honey, C. J., Sporns, O., Cammoun, L., Gigandet, X., Thiran, J. P., Meuli, R., & Hagmann, P. (2009). Predicting human resting-state functional connectivity from structural connectivity. *Proceedings of the National Academy of Sciences*, *106*(6), 2035–2040. https://doi.org/10.1073/pnas.0811168106

Hosey, T., Williams, G., & Ansorge, R. (2005). Inference of multiple fiber orientations in high angular resolution diffusion imaging. *Magnetic Resonance in Medicine*, *54*(6), 1480–1489. https://doi.org/10.1002/mrm.20723

Hua, K., Oishi, K., Zhang, J., Wakana, S., Yoshioka, T., Zhang, W., … Mori, S. (2009). Mapping of Functional Areas in the Human Cortex Based on Connectivity through Association Fibers. *Cerebral Cortex*, *19*(8), 1889–1895. https://doi.org/10.1093/cercor/bhn215

Hubbard, P. L., & Parker, G. J. M. (2014). Chapter 20 – Validation of Tractography. In *Diffusion MRI* (pp. 453–480). https://doi.org/10.1016/B978-0-12-396460-1.00020-2

Huettel, S. A. (2012). Event-related fMRI in cognition. *NeuroImage*, *62*(2), 1152–1156. https://doi.org/10.1016/j.neuroimage.2011.08.113

Hui, K. K. S., Liu, J., Marina, O., Napadow, V., Haselgrove, C., Kwong, K. K., … Makris, N. (2005). The integrated response of the human cerebro-cerebellar and limbic systems to acupuncture stimulation at ST 36 as evidenced by fMRI. *NeuroImage*, *27*(3), 479–496. https://doi.org/10.1016/j.neuroimage.2005.04.037

Irimia, A., Goh, S. Y., Torgerson, C. M., Vespa, P., & Van Horn, J. D. (2014). Structural and connectomic neuroimaging for the personalized study of longitudinal alterations in cortical shape, thickness and connectivity after traumatic brain injury. *Journal of Neurosurgical Sciences*, *58*(3), 129–144. Retrieved from http://www.ncbi.nlm.nih.gov/pubmed/24844173

Jackowski, M., Kao, C. Y., Qiu, M., Constable, R. T., & Staib, L. H. (2005). White matter tractography by anisotropic wavefront evolution and diffusion tensor imaging. *Medical Image Analysis*, *9*(5), 427–440. https://doi.org/10.1016/j.media.2005.05.008

Jbabdi, S. (2014). Chapter 25 – Imaging Structure and Function. In *Diffusion MRI* (pp. 585–605). https://doi.org/10.1016/B978-0-12-396460-1.00025-1

Jbabdi, S., & Johansen-Berg, H. (2011). Tractography: Where Do We Go from Here? *Brain Connectivity*, *1*(3), 169–183. https://doi.org/10.1089/brain.2011.0033

Jenkinson, M., & Smith, S. (2001). A global optimisation method for robust affine registration of brain images. *Medical Image Analysis*, *5*(2), 143–156. Retrieved from http://www.ncbi.nlm.nih.gov/pubmed/11516708

Jenkinson, M., Bannister, P., Brady, M., & Smith, S. (2002). Improved optimization for the robust and accurate linear registration and motion correction of brain images. *NeuroImage*, *17*(2), 825–841. Retrieved from http://www.ncbi.nlm.nih.gov/pubmed/12377157

Jenkinson, M., Beckmann, C. F., Behrens, T. E. J., Woolrich, M. W., & Smith, S. M. (2012). FSL. *NeuroImage*, *62*(2), 782–790. https://doi.org/10.1016/j.neuroimage.2011.09.015

Johansen-Berg, H., & Behrens, T. E. J. (n.d.). *Diffusion MRI : from quantitative measurement to in vivo neuroanatomy*.

Johansen-Berg, H., & Behrens, T. E. J. (2009). *Diffusion MRI: From quantitative measurement to in-vivo neuroanatomy*. *Diffusion MRI*. https://doi.org/10.1016/B978-0-12-374709-9.00002-X

Jones, D. K. (2008). Studying connections in the living human brain with diffusion MRI. *Cortex*, *44*(8), 936–952. https://doi.org/10.1016/j.cortex.2008.05.002

Jones, D. K. (2014). Chapter 5 – Gaussian Modeling of the Diffusion Signal. In *Diffusion MRI* (pp. 87–104). https://doi.org/10.1016/B978-0-12-396460-1.00005-6

Jones, D. K., Knösche, T. R., & Turner, R. (2013). White matter integrity, fiber count, and other fallacies: The do's and don'ts of diffusion MRI. *NeuroImage*, *73*, 239–254. https://doi.org/10.1016/J.NEUROIMAGE.2012.06.081

Jonsdottir, J., Cattaneo, D., Recalcati, M., Regola, A., Rabuffetti, M., Ferrarin, M., & Casiraghi, A. (2010). Task-Oriented Biofeedback to Improve Gait in Individuals With Chronic Stroke: Motor Learning Approach. *Neurorehabilitation and Neural Repair*, *24*(5), 478–485. https://doi.org/10.1177/1545968309355986

Khalsa, S., Mayhew, S. D., Chechlacz, M., Bagary, M., & Bagshaw, A. P. (2014). The structural and functional connectivity of the posterior cingulate cortex: Comparison between deterministic and probabilistic tractography for the investigation of structure–function relationships. *NeuroImage*, *102*, 118–127. https://doi.org/10.1016/j.neuroimage.2013.12.022

Klein, J. C. (2014). Chapter 21 – Connectivity Fingerprinting of Gray Matter. In *Diffusion MRI* (pp. 481–509). https://doi.org/10.1016/B978-0-12-396460-1.00021-4

Kleiser, R., Staempfli, P., Valavanis, A., Boesiger, P., & Kollias, S. (2010). Impact of fMRI-guided advanced DTI fiber tracking techniques on their clinical applications in patients with brain tumors. *Neuroradiology*, *52*(1), 37–46. https://doi.org/10.1007/s00234-009-0539-2

Kubicki, M., Westin, C.-F., Pasternak, O., & Shenton, M. E. (2014). Chapter 15 – Diffusion Tensor Imaging and its Application to Schizophrenia and Related Disorders. In *Diffusion MRI* (pp. 317–334). https://doi.org/10.1016/B978-0-12-396460-1.00015-9

Kubicki, M., Westin, C.-F., Maier, S. E., Mamata, H., Frumin, M., Ersner-Hershfield, H., … Shenton, M. E. (2002). Diffusion tensor imaging and its application to neuropsychiatric disorders. *Harv Rev Psychiatry*, *10*(6), 324–336. https://doi.org/10.1016/j.neuroimage.2008.10.054.Mathematical

Kundu, P., Inati, S. J., Evans, J. W., Luh, W.-M., & Bandettini, P. A. (2012). Differentiating BOLD and non-BOLD signals in fMRI time series using multi-echo EPI. *NeuroImage*, *60*(3), 1759–1770. https://doi.org/10.1016/j.neuroimage.2011.12.028

Kwong, K. K., Belliveau, J. W., Chesler, D. A., Goldberg, I. E., Weisskoff, R. M., Poncelet, B. P., … Turner, R. (1992). Dynamic magnetic resonance imaging of human brain activity during primary sensory stimulation. *Proceedings of the National Academy of Sciences of the United States of America*, *89*(12), 5675–5679. Retrieved from http://www.ncbi.nlm.nih.gov/pubmed/1608978

Laganà, M., Rovaris, M., Ceccarelli, A., Venturelli, C., Marini, S., & Baselli, G. (2010). DTI parameter optimisation for acquisition at 1.5T: SNR analysis and clinical application. *Computational Intelligence and Neuroscience*, *2010*, 254032. https://doi.org/10.1155/2010/254032

Landman, B. A., Wan, H., Bogovic, J. A., Bazin, P.-L., & Prince, J. L. (2010). Resolution of Crossing Fibers with Constrained Compressed Sensing using Traditional Diffusion Tensor MRI. *Proceedings of SPIE--the International Society for Optical Engineering*, *7623*, 76231H. https://doi.org/10.1117/12.844171

Le Bihan, D., Breton, E., Lallemand, D., Grenier, P., Cabanis, E., & Laval-Jeantet, M. (1986). MR imaging of intravoxel incoherent motions: application to diffusion and perfusion in neurologic disorders. *Radiology*, *161*(2), 401–407. https://doi.org/10.1148/radiology.161.2.3763909

Lee, G. R., Griswold, M. A., & Tkach, J. A. (2010). Rapid 3D radial multi-echo functional magnetic resonance imaging. *NeuroImage*, *52*(4), 1428–1443. https://doi.org/10.1016/j.neuroimage.2010.05.004

Leemans, A., Evans, C., & Jones, D. (2008). Quality Assessment through Analysis of REsiduals of Diffusion Image Fitting. *Proceedings 16th Scientific Meeting, International Society for Magnetic Resonance in Medicine*, *Toronto*, 3300. Retrieved from http://cds.ismrm.org/ismrm-2008/files/03300.pdf

Leemans, A., & Jones, D. K. (2009). The B-matrix must be rotated when correcting for subject motion in DTI data. *Magnetic Resonance in Medicine*, *61*(6), 1336–1349. https://doi.org/10.1002/mrm.21890

Lenglet, C., Campbell, J. S. W., Descoteaux, M., Haro, G., Savadjiev, P., Wassermann, D., … Thompson, P. M. (2009). Mathematical methods for diffusion MRI processing. *NeuroImage*, *45*(1), S111–S122. https://doi.org/10.1016/J.NEUROIMAGE.2008.10.054

Levin, H. S. (2003). Neuroplasticity following non-penetrating traumatic brain injury. *Brain Injury*, *17*(8), 665–674. https://doi.org/10.1080/0269905031000107151

Liu, Z., Bartsch, A. J., Berrocal, V. J., & Johnson, T. D. (2018). A mixed-effects, spatially varying coefficients model with application to multi-resolution functional magnetic resonance imaging data. *Statistical Methods in Medical Research*, 96228021775237. https://doi.org/10.1177/0962280217752378

Logothetis, N. K., Pauls, J., Augath, M., Trinath, T., & Oeltermann, A. (2001). Neurophysiological investigation of the basis of the fMRI signal. *Nature*, *412*(6843), 150–157. https://doi.org/10.1038/35084005

Lubrano, V., Filleron, T., Démonet, J. F., & Roux, F. E. (2014). Anatomical correlates for category-specific naming of objects and actions: A brain stimulation mapping study. *Human Brain Mapping*, *35*(2), 429–443. https://doi.org/10.1002/hbm.22189

Maier-Hein, K. H., Neher, P. F., Houde, J.-C., Côté, M.-A., Garyfallidis, E., Zhong, J., … Descoteaux, M. (2017). The challenge of mapping the human connectome based on diffusion tractography. *Nature Communications*, *8*(1), 1349. https://doi.org/10.1038/s41467-017-01285-x

Makris, N., Worth, A. J., Papadimitriou, G. M., Stakes, J. W., Caviness, V. S., Kennedy, D. N., … Davis, T. L. (1997). Morphometry of in vivo human white matter association pathways with diffusion-weighted magnetic resonance imaging. *Annals of Neurology*, *42*(6), 951–962. https://doi.org/10.1002/ana.410420617

Makris, N., Biederman, J., Monuteaux, M. C., & Seidman, L. J. (2009). Towards Conceptualizing a Neural Systems-Based Anatomy of Attention-Deficit/Hyperactivity Disorder. *Developmental Neuroscience*, *31*(1–2), 36–49. https://doi.org/10.1159/000207492

Makris, N., Kennedy, D. N., McInerney, S., Sorensen, A. G., Wang, R., Caviness, V. S., & Pandya, D. N. (2005). Segmentation of Subcomponents within the Superior Longitudinal Fascicle in Humans: A Quantitative, In Vivo, DT-MRI Study. *Cerebral Cortex*, *15*(6), 854–869. https://doi.org/10.1093/cercor/bhh186

Makris, N., Pandya, D. N., Normandin, J. J., Papadimitriou, G. M., Rauch, S. L., Caviness, V. S., & Kennedy, D. N. (2002). Quantitative DT-MRI Investigations of the Human Cingulum Bundle. *CNS Spectrums*, *7*(7), 522–528. https://doi.org/10.1017/S1092852900018071

Mangin, J.-F., Poupon, C., Clark, C., Le Bihan, D., & Bloch, I. (2002). Distortion correction and robust tensor estimation for MR diffusion imaging. *Medical Image Analysis*, *6*(3), 191–198. Retrieved from http://www.ncbi.nlm.nih.gov/pubmed/12270226

Mangin, J.-F., Poupon, C., Clark, C., Le Bihan, D., & Bloch, I. (2002). Distortion correction and robust tensor estimation for MR diffusion imaging. *Medical Image Analysis*, *6*(3), 191–198. Retrieved from http://www.ncbi.nlm.nih.gov/pubmed/12270226

Mayberg, H. S., Lozano, A. M., Voon, V., McNeely, H. E., Seminowicz, D., Hamani, C., … Kennedy, S. H. (2005). Deep Brain Stimulation for Treatment-Resistant Depression. *Neuron*, *45*(5), 651–660. https://doi.org/10.1016/j.neuron.2005.02.014

McDonald, C. R., Ahmadi, M. E., Hagler, D. J., Tecoma, E. S., Iragui, V. J., Gharapetian, L., … Halgren, E. (2008). Diffusion tensor imaging correlates of memory and language impairments in temporal lobe epilepsy. *Neurology*, *71*(23), 1869–1876. https://doi.org/10.1212/01.wnl.0000327824.05348.3b

McGrath, J., Johnson, K., O'Hanlon, E., Garavan, H., Leemans, A., & Gallagher, L. (2013). Abnormal functional connectivity during visuospatial processing is associated with disrupted organisation of white matter in autism. *Frontiers in Human Neuroscience*, *7*, 434. https://doi.org/10.3389/fnhum.2013.00434

McKeown, M. J., Makeig, S., Brown, G. G., Jung, T.-P., Kindermann, S. S., Bell, A. J., … McKeown, M. (1998). Analysis of fMRI Data by Blind Separation Into Independent Spatial Components. *Hum. Brain Mapping*, *6*, 160–188. Retrieved from https://pdfs.semanticscholar.org/e794/bac5ebb7d7b4e30881d78e86653929e3c4b1.pdf

McKiernan, K. A., Kaufman, J. N., Kucera-Thompson, J., & Binder, J. R. (2003). A Parametric Manipulation of Factors Affecting Task-induced Deactivation in Functional Neuroimaging. *Journal of Cognitive Neuroscience*, *15*(3), 394–408. https://doi.org/10.1162/089892903321593117

Meyer, M. C., Janssen, R. J., Van Oort, E. S. B., Beckmann, C. F., & Barth, M. (2013). The Quest for EEG Power Band Correlation with ICA Derived fMRI Resting State Networks. *Frontiers in Human Neuroscience*, *7*, 315. https://doi.org/10.3389/fnhum.2013.00315

Miller, K. L. (2014). Chapter 3 – Diffusion Acquisition: Pushing the Boundaries. In *Diffusion MRI* (pp. 35–61). https://doi.org/10.1016/B978-0-12-396460-1.00003-2

Morecraft, R. J., Ugolini, G., Lanciego, J. L., Wouterlood, F. G., & Pandya, D. N. (2014). Chapter 17 – Classic and Contemporary Neural Tract-Tracing Techniques. In *Diffusion MRI* (pp. 359–399). https://doi.org/10.1016/B978-0-12-396460-1.00017-2

Morgan, V. L., Mishra, A., Newton, A. T., Gore, J. C., & Ding, Z. (2009). Integrating Functional and Diffusion Magnetic Resonance Imaging for Analysis of Structure-Function Relationship in the Human Language Network. *PLoS ONE*, *4*(8), e6660. https://doi.org/10.1371/journal.pone.0006660

Mori, S., Kaufmann, W. E., Davatzikos, C., Stieltjes, B., Amodei, L., Fredericksen, K., … van Zijl, P. C. M. (2002). Imaging cortical association tracts in the human brain using diffusion-tensor-based axonal tracking. *Magnetic Resonance in Medicine*, *47*(2), 215–223. https://doi.org/10.1002/mrm.10074

Mori, S., Oishi, K., & Faria, A. V. (2009). White matter atlases based on diffusion tensor imaging. *Current Opinion in Neurology*, *22*(4), 362–369. https://doi.org/10.1097/WCO.0b013e32832d954b

Newton, J. M., Ward, N. S., Parker, G. J. M., Deichmann, R., Alexander, D. C., Friston, K. J., & Frackowiak, R. S. J. (2006). Non-invasive mapping of corticofugal fibres from multiple motor areas--relevance to stroke recovery. *Brain : A Journal of Neurology*, *129*(Pt 7), 1844–1858. https://doi.org/10.1093/brain/awl106

Nunes, R. G., Jezzard, P., Behrens, T. E. J., & Clare, S. (2005). Self-navigated multishot echo-planar pulse sequence for high-resolution diffusion-weighted imaging. *Magnetic Resonance in Medicine*, *53*(6), 1474–1478. https://doi.org/10.1002/mrm.20499

Ogawa, S., Lee, T. M., Kay, A. R., & Tank, D. W. (1990). Brain magnetic resonance imaging with contrast dependent on blood oxygenation. *Proceedings of the National Academy of Sciences of the United States of America*, *87*(24), 9868–9872. Retrieved from http://www.ncbi.nlm.nih.gov/pubmed/2124706

Pannek, K., Mathias, J. L., Bigler, E. D., Brown, G., Taylor, J. D., & Rose, S. E. (2011). The average pathlength map: A diffusion MRI tractography-derived index for studying brain pathology. *NeuroImage*, *55*(1), 133–141. https://doi.org/10.1016/j.neuroimage.2010.12.010

Pannek, K., Raffelt, D., Bell, C., Mathias, J. L., & Rose, S. E. (2012). HOMOR: Higher Order Model Outlier Rejection for high b-value MR diffusion data. *NeuroImage*, *63*(2), 835–842. https://doi.org/10.1016/j.neuroimage.2012.07.022

Parker, G. J. M., Haroon, H. A., & Wheeler-Kingshott, C. A. M. (2003). A framework for a streamline-based probabilistic index of connectivity (PICo) using a structural interpretation of MRI diffusion measurements. *Journal of Magnetic Resonance Imaging*, *18*(2), 242–254. https://doi.org/10.1002/jmri.10350

Passingham, R. (2014). Foreword. In *Diffusion MRI* (pp. ix–x). https://doi.org/10.1016/B978-0-12-396460-1.06001-7

Paulesu, E., Goldacre, B., Scifo, P., Cappa, S. F., Gilardi, M. C., Castiglioni, I., … Fazio, F. (1997). Functional heterogeneity of left inferior frontal cortex as revealed by fMRI. *Neuroreport*, *8*(8), 2011–2017. Retrieved from http://www.ncbi.nlm.nih.gov/pubmed/9223094

Perlbarg, V., Bellec, P., Anton, J.-L., Pélégrini-Issac, M., Doyon, J., & Benali, H. (2007). CORSICA: correction of structured noise in fMRI by automatic identification of ICA components. *Magnetic Resonance Imaging*, *25*(1), 35–46. https://doi.org/10.1016/j.mri.2006.09.042

Pestilli, F., Yeatman, J. D., Rokem, A., Kay, K. N., & Wandell, B. A. (2014). Evaluation and statistical inference for human connectomes. *Nature Methods*, *11*(10), 1058–1063. https://doi.org/10.1038/nmeth.3098

Pierpaoli, C., & Basser, P. J. (1996). Toward a quantitative assessment of diffusion anisotropy. *Magnetic Resonance in Medicine*, *36*(6), 893–906. https://doi.org/10.1002/mrm.1910360612

Pievani, M., Filippini, N., van den Heuvel, M. P., Cappa, S. F., & Frisoni, G. B. (2014). Brain connectivity in neurodegenerative diseases—from phenotype to proteinopathy. *Nature Reviews Neurology*, *10*(11), 620–633. https://doi.org/10.1038/nrneurol.2014.178

Pipe, J. (2014). Chapter 2 – Pulse Sequences for Diffusion-Weighted MRI. In *Diffusion MRI* (pp. 11–34). https://doi.org/10.1016/B978-0-12-396460-1.00002-0

Poldrack, R. A. (2012). The future of fMRI in cognitive neuroscience. *NeuroImage*, *62*(2), 1216–1220. https://doi.org/10.1016/j.neuroimage.2011.08.007

Poser, B. A., Koopmans, P. J., Witzel, T., Wald, L. L., & Barth, M. (2010). Three dimensional echo-planar imaging at 7 Tesla. *NeuroImage*, *51*(1), 261–266. https://doi.org/10.1016/j.neuroimage.2010.01.108

Preti, M. G., Makris, N., Papadimitriou, G., Laganà, M. M., Griffanti, L., Clerici, M., … Baglio, F. (2014). A Novel Approach of Groupwise fMRI-Guided Tractography Allowing to Characterize the Clinical Evolution of Alzheimer's Disease. *PLoS ONE*, *9*(3), e92026. https://doi.org/10.1371/journal.pone.0092026

Propper, R. E., O'Donnell, L. J., Whalen, S., Tie, Y., Norton, I. H., Suarez, R. O., … Golby, A. J. (2010). A combined fMRI and DTI examination of functional language lateralization and arcuate fasciculus structure: Effects of degree versus direction of hand preference. *Brain and Cognition*, *73*(2), 85–92. https://doi.org/10.1016/j.bandc.2010.03.004

Raichle, M. E., MacLeod, A. M., Snyder, A. Z., Powers, W. J., Gusnard, D. A., & Shulman, G. L. (2001). A default mode of brain function. *Proceedings of the National Academy of Sciences*, *98*(2), 676–682. https://doi.org/10.1073/pnas.98.2.676

Ramirez-Manzanares, A., Rivera, M., Vemuri, B. C., Carney, P., & Mareci, T. (2007). Diffusion Basis Functions Decomposition for Estimating White Matter Intravoxel Fiber Geometry. *IEEE Transactions on Medical Imaging*, *26*(8), 1091–1102. https://doi.org/10.1109/TMI.2007.900461

Rasmussen CE, & Williams CKI. (2006). *Gaussian Processes for Machine Learning*. MIT Press MIT Press. Retrieved from http://www.gaussianprocess.org/gpml/chapters/RW.pdf

Rehme, A. K., & Grefkes, C. (2013). Cerebral network disorders after stroke: evidence from imaging-based connectivity analyses of active and resting brain states in humans. *The Journal of Physiology*, *591*(1), 17–31. https://doi.org/10.1113/jphysiol.2012.243469

Reuter-Lorenz, P. A., & Park, D. C. (2014). How Does it STAC Up? Revisiting the Scaffolding Theory of Aging and Cognition. *Neuropsychology Review*, *24*(3), 355–370. https://doi.org/10.1007/s11065-014-9270-9

Rossi, S., Huang, S., Furtak, S. C., Belliveau, J. W., & Ahveninen, J. (2014). Functional connectivity of dorsal and ventral frontoparietal seed regions during auditory orienting. *Brain Research*, *1583*, 159–168. https://doi.org/10.1016/j.brainres.2014.08.002

Rushworth, M. F. S., Krams, M., & Passingham, R. E. (2001). The Attentional Role of the Left Parietal Cortex: The Distinct Lateralization and Localization of Motor Attention in the Human Brain. *Journal of Cognitive Neuroscience*, *13*(5), 698–710. https://doi.org/10.1162/089892901750363244

Rushworth, M. F. S., Sallet, J., Boorman, E. D., & Mars, R. B. (2014). Chapter 24 – Comparing Connections in the Brains of Humans and Other Primates Using Diffusion-Weighted Imaging. In *Diffusion MRI* (pp. 569–584). https://doi.org/10.1016/B978-0-12-396460-1.00024-X

Salat, D. H. (2014). Chapter 12 – Diffusion Tensor Imaging in the Study of Aging and Age-Associated Neural Disease. In *Diffusion MRI* (pp. 257–281). https://doi.org/10.1016/B978-0-12-396460-1.00012-3

Salimi-Khorshidi, G., Douaud, G., Beckmann, C. F., Glasser, M. F., Griffanti, L., & Smith, S. M. (2014). Automatic denoising of functional MRI data: Combining independent component analysis and hierarchical fusion of classifiers. *NeuroImage*, *90*, 449–468. https://doi.org/10.1016/j.neuroimage.2013.11.046

Salimi-Khorshidi, G., Douaud, G., Beckmann, C. F., Glasser, M. F., Griffanti, L., & Smith, S. M. (2014). Automatic denoising of functional MRI data: Combining independent component analysis and hierarchical fusion of classifiers. *NeuroImage*, *90*, 449–468. https://doi.org/10.1016/j.neuroimage.2013.11.046

Scaccianoce, E., Laganà, M. M., Baglio, F., Preti, M. G., Bergsland, N., Cecconi, P., … Makris, N. (2016). Combined DTI–fMRI Analysis for a Quantitative Assessment of Connections Between WM Bundles and Their Peripheral Cortical Fields in Verbal Fluency. *Brain Topography*, *29*(6), 814–823. https://doi.org/10.1007/s10548-016-0516-0

Schlösser, R. G. M., Nenadic, I., Wagner, G., Güllmar, D., von Consbruch, K., Köhler, S., … Sauer, H. (2007). White matter abnormalities and brain activation in schizophrenia: A combined DTI and fMRI study. *Schizophrenia Research*, *89*(1–3), 1–11. https://doi.org/10.1016/j.schres.2006.09.007

Scholz, J., & Tomassini, V. (2014). Chapter 14 – Individual Differences in White Matter Microstructure in the Healthy Brain. In *Diffusion MRI* (pp. 301–316). https://doi.org/10.1016/B978-0-12-396460-1.00014-7

Seunarine, K. K., & Alexander, D. C. (2014). Chapter 6 – Multiple Fibers: Beyond the Diffusion Tensor. In *Diffusion MRI* (pp. 105–123). https://doi.org/10.1016/B978-0-12-396460-1.00006-8

Shulman, G. L., Pope, D. L. W., Astafiev, S. V., McAvoy, M. P., Snyder, A. Z., & Corbetta, M. (2010). Right Hemisphere Dominance during Spatial Selective Attention and Target Detection Occurs Outside the Dorsal Frontoparietal Network. *Journal of Neuroscience*, *30*(10), 3640–3651. https://doi.org/10.1523/JNEUROSCI.4085-09.2010

Smith, R. E., Tournier, J.-D., Calamante, F., & Connelly, A. (2015). The effects of SIFT on the reproducibility and biological accuracy of the structural connectome. *NeuroImage*, *104*, 253–265. https://doi.org/10.1016/J.NEUROIMAGE.2014.10.004

Smith, S. M., Fox, P. T., Miller, K. L., Glahn, D. C., Fox, P. M., Mackay, C. E., … Beckmann, C. F. (2009). Correspondence of the brain's functional architecture during activation and rest. *Proceedings*

of the National Academy of Sciences, *106*(31), 13040–13045.
https://doi.org/10.1073/pnas.0905267106

Smith, S. M., Beckmann, C. F., Andersson, J., Auerbach, E. J., Bijsterbosch, J., Douaud, G., … WU-Minn
HCP Consortium. (2013). Resting-state fMRI in the Human Connectome Project. *NeuroImage*, *80*,
144–168. https://doi.org/10.1016/j.neuroimage.2013.05.039

Smith, S. M., Jenkinson, M., Woolrich, M. W., Beckmann, C. F., Behrens, T. E. J., Johansen-Berg, H., …
Matthews, P. M. (2004). Advances in functional and structural MR image analysis and
implementation as FSL. *NeuroImage*, *23*, S208–S219.
https://doi.org/10.1016/j.neuroimage.2004.07.051

Smith, S. M., Kindlmann, G., & Jbabdi, S. (2014). Chapter 10 – Cross-Subject Comparison of Local
Diffusion MRI Parameters. In *Diffusion MRI* (pp. 209–239). https://doi.org/10.1016/B978-0-12-
396460-1.00010-X

Soddu, A., Gómez, F., Heine, L., Di Perri, C., Bahri, M. A., Voss, H. U., … Laureys, S. (2016).
Correlation between resting state fMRI total neuronal activity and PET metabolism in healthy
controls and patients with disorders of consciousness. *Brain and Behavior*, *6*(1), n/a-n/a.
https://doi.org/10.1002/brb3.424

Sotiropoulos, S. N., & Jbabdi, S. (2014). Chapter 19 – MR Diffusion Tractography. In *Diffusion MRI* (pp.
429–451). https://doi.org/10.1016/B978-0-12-396460-1.00019-6

Sporns, O. (2014). Chapter 18 – The Human Connectome: Linking Structure and Function in the Human
Brain. In *Diffusion MRI* (pp. 401–428). https://doi.org/10.1016/B978-0-12-396460-1.00018-4

Sporns, O., Tononi, G., & Kötter, R. (2005). The Human Connectome: A Structural Description of the
Human Brain. *PLoS Computational Biology*, *1*(4), e42. https://doi.org/10.1371/journal.pcbi.0010042

Staempfli, P., Reischauer, C., Jaermann, T., Valavanis, A., Kollias, S., & Boesiger, P. (2008). Combining
fMRI and DTI: A framework for exploring the limits of fMRI-guided DTI fiber tracking and for
verifying DTI-based fiber tractography results. *NeuroImage*, *39*(1), 119–126.
https://doi.org/10.1016/j.neuroimage.2007.08.025

Stieltjes, B., Kaufmann, W. E., van Zijl, P. C. M., Fredericksen, K., Pearlson, G. D., Solaiyappan, M., &
Mori, S. (2001). Diffusion Tensor Imaging and Axonal Tracking in the Human Brainstem.
NeuroImage, *14*(3), 723–735. https://doi.org/10.1006/NIMG.2001.0861

Storti, S. F., Formaggio, E., Nordio, R., Manganotti, P., Fiaschi, A., Bertoldo, A., & Toffolo, G. M.
(2013). Automatic selection of resting-state networks with functional magnetic resonance imaging.
Frontiers in Neuroscience, *7*, 72. https://doi.org/10.3389/fnins.2013.00072

Sundararajan, S., & Keerthi, S. S. (2001). Predictive approaches for choosing hyperparameters in gaussian
processes. *Neural Computation*, *13*(5), 1103–1118. https://doi.org/10.1162/08997660151134343

Tax, C. M. W., Otte, W. M., Viergever, M. A., Dijkhuizen, R. M., & Leemans, A. (2015). REKINDLE:
Robust extraction of kurtosis INDices with linear estimation. *Magnetic Resonance in Medicine*,
73(2), 794–808. https://doi.org/10.1002/mrm.25165

Tohka, J., Foerde, K., Aron, A. R., Tom, S. M., Toga, A. W., & Poldrack, R. A. (2008). Automatic independent component labeling for artifact removal in fMRI. *NeuroImage*, *39*(3), 1227–1245. https://doi.org/10.1016/j.neuroimage.2007.10.013

Tournier, J.-D., Calamante, F., Gadian, D. G., & Connelly, A. (2004). Direct estimation of the fiber orientation density function from diffusion-weighted MRI data using spherical deconvolution. *NeuroImage*, *23*(3), 1176–1185. https://doi.org/10.1016/j.neuroimage.2004.07.037

Tournier, J.-D., Mori, S., & Leemans, A. (2011). Diffusion tensor imaging and beyond. *Magnetic Resonance in Medicine*, *65*(6), 1532–1556. https://doi.org/10.1002/mrm.22924

Tournier, J.-D., Calamante, F., & Connelly, A. (2007). Robust determination of the fibre orientation distribution in diffusion MRI: Non-negativity constrained super-resolved spherical deconvolution. *NeuroImage*, *35*(4), 1459–1472. https://doi.org/10.1016/j.neuroimage.2007.02.016

Tuch, D. S., Reese, T. G., Wiegell, M. R., Makris, N., Belliveau, J. W., & Wedeen, V. J. (2002). High angular resolution diffusion imaging reveals intravoxel white matter fiber heterogeneity. *Magnetic Resonance in Medicine*, *48*(4), 577–582. https://doi.org/10.1002/mrm.10268

Turken, U., Whitfield-Gabrieli, S., Bammer, R., Baldo, J. V., Dronkers, N. F., & Gabrieli, J. D. E. (2008). Cognitive processing speed and the structure of white matter pathways: Convergent evidence from normal variation and lesion studies. *NeuroImage*, *42*(2), 1032–1044. https://doi.org/10.1016/j.neuroimage.2008.03.057

Turner, R., Le Bihan, D., Maier, J., Vavrek, R., Hedges, L. K., & Pekar, J. (1990). Echo-planar imaging of intravoxel incoherent motion. *Radiology*, *177*(2), 407–414. https://doi.org/10.1148/radiology.177.2.2217777

Valk, J. (2011). A possible role of BA8 in pre-surgical fMRI: Homage to an exceptional neuroscientist. *Neuroradiology Journal*, *24*(3), 395–400. https://doi.org/10.1177/197140091102400308

van den Heuvel, M. P., & Hulshoff Pol, H. E. (2010). Exploring the brain network: A review on resting-state fMRI functional connectivity. *European Neuropsychopharmacology*, *20*(8), 519–534. https://doi.org/10.1016/j.euroneuro.2010.03.008

van der Kolk, A. G., Hendrikse, J., Zwanenburg, J. J. M., Visser, F., & Luijten, P. R. (2013). Clinical applications of 7T MRI in the brain. *European Journal of Radiology*, *82*(5), 708–718. https://doi.org/10.1016/j.ejrad.2011.07.007

van Eimeren, L., Niogi, S. N., McCandliss, B. D., Holloway, I. D., & Ansari, D. (2008). White matter microstructures underlying mathematical abilities in children. *NeuroReport*, *19*(11), 1117–1121. https://doi.org/10.1097/WNR.0b013e328307f5c1

Van Essen, D. C., Jbabdi, S., Sotiropoulos, S. N., Chen, C., Dikranian, K., Coalson, T., … Glasser, M. F. (2014). Chapter 16 – Mapping Connections in Humans and Non-Human Primates: Aspirations and Challenges for Diffusion Imaging. In *Diffusion MRI* (pp. 337–358). https://doi.org/10.1016/B978-0-12-396460-1.00016-0

Veer, I. M., Beckmann, C. F., van Tol, M.-J., Ferrarini, L., Milles, J., Veltman, D. J., … Rombouts, S. A. R. B. (2010). Whole brain resting-state analysis reveals decreased functional connectivity in major depression. *Frontiers in Systems Neuroscience*, *4*. https://doi.org/10.3389/fnsys.2010.00041

Vernooij, M. W., Smits, M., Wielopolski, P. A., Houston, G. C., Krestin, G. P., & van der Lugt, A. (2007). Fiber density asymmetry of the arcuate fasciculus in relation to functional hemispheric language lateralization in both right- and left-handed healthy subjects: A combined fMRI and DTI study. *NeuroImage*, *35*(3), 1064–1076. https://doi.org/10.1016/j.neuroimage.2006.12.041

Vidaurre, D., Smith, S. M., & Woolrich, M. W. (2017). Brain network dynamics are hierarchically organized in time. *Proceedings of the National Academy of Sciences*, *114*(48), 12827–12832. https://doi.org/10.1073/pnas.1705120114

Walker, L., Chang, L.-C., Koay, C. G., Sharma, N., Cohen, L., Verma, R., & Pierpaoli, C. (2011). Effects of physiological noise in population analysis of diffusion tensor MRI data. *NeuroImage*, *54*(2), 1168–1177. https://doi.org/10.1016/J.NEUROIMAGE.2010.08.048

Wittenberg, G. F. (2010). Experience, cortical remapping, and recovery in brain disease. *Neurobiology of Disease*, *37*(2), 252–258. https://doi.org/10.1016/j.nbd.2009.09.007

Worsley, K. J., Liao, C. H., Aston, J., Petre, V., Duncan, G. H., Morales, F., & Evans, A. C. (2002). A General Statistical Analysis for fMRI Data. *NeuroImage*, *15*(1), 1–15. https://doi.org/10.1006/NIMG.2001.0933

Xiaoxia Qu, X., Platisa, L., Despotovic, I., Kumcu, A., Tingzhu Bai, T., Deblaere, K., & Philips, W. (2014). Estimating blur at the brain gray-white matter boundary for FCD detection in MRI. In *2014 36th Annual International Conference of the IEEE Engineering in Medicine and Biology Society* (Vol. 2014, pp. 3321–3324). IEEE. https://doi.org/10.1109/EMBC.2014.6944333

Yo, T.-S., Anwander, A., Descoteaux, M., Fillard, P., Poupon, C., & Knösche, T. R. (2009). Quantifying brain connectivity: a comparative tractography study. *Medical Image Computing and Computer-Assisted Intervention : MICCAI ... International Conference on Medical Image Computing and Computer-Assisted Intervention*, *12*(Pt 1), 886–893. Retrieved from http://www.ncbi.nlm.nih.gov/pubmed/20426072

Zhang, H., Schneider, T., Wheeler-Kingshott, C. A., & Alexander, D. C. (2012). NODDI: Practical in vivo neurite orientation dispersion and density imaging of the human brain. *NeuroImage*, *61*(4), 1000–1016. https://doi.org/10.1016/J.NEUROIMAGE.2012.03.072

Zhang, K., Johnson, B., Pennell, D., Ray, W., Sebastianelli, W., & Slobounov, S. (2010). Are functional deficits in concussed individuals consistent with white matter structural alterations: combined FMRI & DTI study. *Experimental Brain Research*, *204*(1), 57–70. https://doi.org/10.1007/s00221-010-2294-3

Zhou, F., Zhuang, Y., Gong, H., Wang, B., Wang, X., Chen, Q., … Wan, H. (2014). Altered Inter-Subregion Connectivity of the Default Mode Network in Relapsing Remitting Multiple Sclerosis: A Functional and Structural Connectivity Study. *PLoS ONE*, *9*(7), e101198. https://doi.org/10.1371/journal.pone.0101198

Zwiers, M. P. (2010). Patching cardiac and head motion artefacts in diffusion-weighted images. *NeuroImage*, *53*(2), 565–575. https://doi.org/10.1016/J.NEUROIMAGE.2010.06.014